

National Library of Canada

Acquisitions and Bibliographic Services Branch

395 Wellington Street Ottawa, Ontario K1A 0N4 Bibliothèque nationale du Canada

Direction des acquisitions et des services bibliographiques

395, rue Wellington Ottawa (Ontario) K1A 0N4

Action has Aciden enterences

On the Notice reference

NOTICE

The quality of this microform is heavily dependent upon the quality of the original thesis submitted for microfilming. Every effort has been made to ensure the highest quality of reproduction possible.

dépend grandement de la qualité de la thèse soumise au microfilmage. Nous avons tout fait pour assurer une qualité supérieure de reproduction.

AVIS

La qualité de cette microforme

If pages are missing, contact the university which granted the degree.

S'il manque des pages, veuillez communiquer avec l'université qui a conféré le grade.

Some pages may have indistinct print especially if the original pages were typed with a poor typewriter ribbon or if the university sent us an inferior photocopy. La qualité d'impression de certaines pages peut laisser à désirer, surtout si les pages originales ont été dactylographiées à l'aide d'un ruban usé ou si l'université nous a fait parvenir une photocopie de qualité inférieure.

Reproduction in full or in part of this microform is governed by the Canadian Copyright Act, R.S.C. 1970, c. C-30, and subsequent amendments. La reproduction, même partielle, de cette microforme est soumise à la Loi canadienne sur le droit d'auteur, SRC 1970, c. C-30, et ses amendements subséquents.

Canadä

A UNIFIED THEORETICAL FRAMEWORK FOR THE SYNTHESIS OF CAM MECHANISMS

Max Antonio González-Palacios

B. Eng. Universidad Iberoamericana-León, 1986
 M. Eng. Universidad de Guanajuato, 1989
 Guanajuato, México

Department of Mechanical Engineering

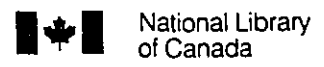
McGill University

Montreal, Quebec, Canada

A thesis submitted to the Faculty of Graduate Studies and Research in partial fulfillment of the requirements for the degree of Doctor of Philosophy

January 1993

(C) Max Antonio González-Palacios



Acquisitions and Bibliographic Services Branch

395 Wellington Street Ottawa, Ontario K1A 0N4 Bibliothèque nationale du Canada

Direction des acquisitions et des services bibliographiques

395, rue Wellington Ottawa (Ontario) K1A 0N4

Your No. Votre reference

Ou life Notice intercover

The author has granted an irrevocable non-exclusive licence allowing the National Library of Canada to reproduce, loan, distribute or sell copies of his/her thesis by any means and in any form or format, making this thesis available to interested persons.

L'auteur a accordé une licence irrévocable et non exclusive permettant à la Bibliothèque nationale du Canada reproduire, prêter, distribuer ou vendre des copies de sa thèse de quelque manière et sous quelque forme que ce soit pour mettre des exemplaires de cette thèse disposition à la des personnes intéressées.

The author retains ownership of the copyright in his/her thesis. Neither the thesis nor substantial extracts from it may be printed or otherwise reproduced without his/her permission. L'auteur conserve la propriété du droit d'auteur qui protège sa thèse. Ni la thèse ni des extraits substantiels de celle-ci ne doivent être imprimés ou autrement reproduits sans son autorisation.

ISBN 0-315-87648-4



Abstract

In this thesis, a unified formulation for the synthesis of cam mechanisms is presented, which allows the design of spatial, spherical and planar mechanisms within a single theoretical framework. This formulation has led to the design of novel cam mechanisms, as yet unknown.

We focus on mechanisms with three and four links containing one higher kinematic pair. The theory is first developed with the study of three-link mechanisms that are composed of a frame, a cam and a follower. The unified formulation is given in the dual space in which the three links are represented by three concentric unit dual spheres. In this space, the three instantaneous screw axes of the mechanism are mapped into three dual points or poles. Two of these poles, those arising from the frame-cam and frame-follower pairs, are fixed and lie on the sphere representing the frame, while the third pole, arising from the cam-follower pair, moves on the same sphere. The type of kinematic coupling, i.e., revolute or prismatic, for the frame-cam and cam-follower pairs, is specified by the location of the fixed poles. The polode, which is the dual curve defined by the moving pole, is mapped into the Cartesian space as the axode. The axode defines the contacting ruled surfaces of both cam and follower. Two basic theorems are stated as a result of this analysis.

The foregoing theory is then extended to the study of four-link cam mechanisms, where an intermediate element, namely, a roller, is placed between the cam and the follower. In general, the surface of the roller is shown to be a hyperboloid, which, for the planar case, becomes a regular cylinder, and, for the spherical case, a regular

cone. The two theorems stated for three-link cam mechanisms are then extended to four-link mechanisms. A general formulation is presented for the study of the pressure angle in both three- and four-link cam mechanisms. With this formulation, the general expression for the pressure angle of spherical mechanisms is derived as a particular case of the general expression for spatial cam mechanisms. Moreover, the pressure-angle expression corresponding to planar cam mechanisms is derived as a particular case of spherical cam mechanisms.

The unified formulation is then applied to the synthesis of planar cam mechanisms via graphical methods. Here, an innovative technique is introduced, which consists of finding contact points of the cam profile, in contrast to traditional graphical techniques that employ cam envelopes, and, hence, are prone to inaccuracies

Special attention is given to the synthesis of indexing cam mechanisms. In this context, a theorem is established for the determination of one of the design parameters that is used to avoid undercutting on the cam profile. A novel design of an indexing cam mechanism, called *PRICAM*, in which pure rolling and positive motion are achieved for planar and spherical mechanisms, is obtained using a combination of three- and four-link cam mechanisms.

The unified formulation is implemented in the software package *USYCAMS*, in which, with visualization aids, the user can design cam mechanisms of the three types and animate their motion, by providing the design parameters on-line. *USYCAMS* allowed the design of two versions of *PRICAM*, one planar and one spherical, and produced a database describing the contact surfaces, which served as input to the CNC machine tool used to cut actual prototypes of these mechanisms.

Résumé

L'objectif de la thèse est de présenter une formulation unifiée pour la synthèse des mécanismes à cames qui permet la conception de mécanismes pour les cas spatial, sphérique et planaire, dans un cadre théorique unifié. Cette formulation a ouvert la voie à la conception de nouveaux mécanismes à cames, inconnus jusqu'à maintenant.

Notre étude se concentre sur des mécanismes à trois et quatre maillons contenant un couple cinématique supérieur. En premier lieu, la théorie est développée par l'étude de mécanismes à trois maillons composés d'un bâti, d'une came et d'un récepteur de came. La formulation unifiée est donnée dans l'espace dual, dans lequel les trois maillons sont représentés par trois sphères duales concentriques à rayon unitaire. Dans cet espace, les trois axes de vissage instantané du mécanisme ont leurs images tracées en trois points duals ou pôles. Deux de ces pôles, ceux provenant des couples formés par l'ensemble bâti-came et l'ensemble bâti-récepteur, sont fixes et reposent sur la sphère représentant le bâti, tandis que le troisième pôle, provenant du couple came-récepteur, se déplace sur la même sphère. Le type de couple cinématique, c'est-à-dire rotoïde ou prismatique, pour les couples bâti-came et came-récepteur, est spécifié par la location des pôles fixes. Le poloïde, qui est la courbe duale définie par le pôle mobile, est tracé dans l'espace cartésien comme l'axoïde. L'axoïde détermine les surfaces réglées en contact de la came et de son récepteur. Comme résultat de cette analyse, deux théorèmes de base sont tirés.

Cette théorie est alors appliquée à l'étude des mécanismes de came à quatre maillons, alors qu'un élément intermédiaire, à savoir, un roulement, est placé entre la came et le récepteur. En général, la surface du roulement est hyperbolique, ce qui, dans le cas des mécanismes planaires, devient un cylindre régulier, et, pour les mécanismes sphériques, un cône régulier. Les deux théorèmes énoncés pour les mécanismes de came à trois maillons sont alors appliqués aux mécanismes à quatre maillons. Une formulation générale est présentée pour l'étude de l'angle de pression des mécanismes de came à trois et quatre maillons. Avec cette formulation, l'expression générale de l'angle de pression des mécanismes sphériques se conçoit comme un cas particulier de l'expression générale pour les mécanismes de came spatiaux.

La formulation unifiée est en outre appliquée à la synthèse des mécanismes de came planaires par le biais de méthodes graphiques. Ici, une technique innovatrice est introduite, laquelle consiste à trouver les points de contact du profil de la came, par opposition à des techniques graphiques plus traditionnelles qui emploient des enveloppes de came, et, de ce fait, sont sujet à des inexactitudes.

Une attention spéciale est apportée à la synthèse des mécanismes pas à pas. Dans ce contexte, on établi un théorème pour déterminer un des paramètres utilisé pour éviter le sous-cavage sur le profil de la came. Une conception nouvelle d'un mécanisme pas à pas appelé *PRICAM*, dans lequel des mouvements positifs de roulement pur sont obtenus pour les mécanismes planaires et sphériques, est réalisée en utilisant une combinaison de mécanismes de came à trois et quatre maillons.

La formulation unifiée est réalisée dans le logiciel USYCAMS, dans lequel, avec un support visuel, l'utilisateur peut concevoir des mécanismes de came des trois types, et animer leur mouvement en donnant au logiciel les paramètres du mécanisme en ligne. USYCAMS a permis la conception de deux versions de PRICAM, une planaire et l'autre sphérique, et a produit une base de données décrivant les surfaces de contact qui ont servi comme données d'entrée à la machine-outil à commande numérique assistée par ordinateur utilisée pour produire le profil des prototypes actuels de ces mécanismes.

Acknowledgements

I would like to extend my sincere thanks and gratitude to my advisor, Prof. Jorge Angeles, for his assistance and continuous guidance without which this thesis could not have been completed. His invaluable comments, full of knowledge, and suggestions, motivated me to improve the quality of this thesis.

I am grateful to the Consejo Nacional de Ciencia y Tecnología (National Council of Science and Technology), of Mexico, for its financial support through a scholarship and to the Quebec Government for the fee-waiver grant, without which this research work would have never been possible.

I would like to thank the faculty of the Department of Mechanical Engenieering of the Universidad de nanajuato from whom I have been motivated to continue with doctoral studies, particularly, Prof. Arturo Lara, for his support when I started considering high-level research work.

I am grateful to the Universidad Iberoamericana-Plantel León, in particular to Rev. Jorge Vértiz and to Profs. Otilio Gómez, Wenceslao Oñate, Miguel A. Arredondo and Roberto Ruelas, who inspired me to pursue doctoral studies.

The machine shop staff of the McGill Department of Mechanical Engineering and the Centre de recherche industrielle du Québec (CRIQ), particularly Mr. A. Clement and Mr. F. Picard, for their valuable suggestions to complete the final design and machining of the parts of the prototypes presented in this thesis.

I am indebted to the graduate students in my group for their fruitful comments. Special thanks to my fellow graduate student Robert Lucyshyn who unconditionally helped me in the preparation of the abstract and to Mrs. Irene Cartier, secretary of the McGill Department of Mechanical Engineering, for translating the abstract of my thesis in French. The valuable comments of Prof. Niky Kamran of the Department of Mathematics and Statistics, which helped to improve the quality of this thesis, are truly acknowledged.

The support I received from the Department of Mechanical Engineering and McGill Research Centre for Intelligent Machines is truly acknowledged.

I would like to thank my wife, Bertha Dávila, for her love and support throughout the time she missed my company along with our daughters while I was busy on my research work.

I thank God for His silent support in the moments in which I thought I would never finish this research work.

Claim of Originality

The research work reported here is original, the main contributions being listed below:

- (i) four basic theorems for three- and four-link cam mechanisms where either the input or the output contains a prismatic pair;
- (ii) a unified formulation for the definition of the pressure angle of three- and fourlink cam mechanisms;
- (iii) the method of synthesis of three-link cam mechanisms with constant pressure angle, better known as cam mechanisms with flat-face followers, including spherical mechanisms, that is based on the unified method pertaining to four-link cam mechanisms;
- (iv) the definition of positive action depending on the value of the pressure angle;
- (v) a novel design of planar and spherical indexing cam mechanisms with pure rolling and positive motion, called PRICAM;
- (vi) the software package USYCAMS, for the on-line design of spatial, spherical and planar cam mechanisms;
- (vii) the introduction of a novel semigraphical method for the synthesis of planar cam mechanisms.

The material presented in this thesis has been partially reported in (González-Palacios and Angeles, 1990; 1991; 1992a and 1992b).

Dedicated to:

the memory of my father;

my mother;

and my wife and daughters

Contents

A	bstra	ct							11
R	ésum	é							iv
A	ckno	wledge	ments						vi
Cl	laim	of Orig	ginality						viii
Li	st of	Figure	es						xiii
Li	st of	Tables							xvi
N	omei	ıclatur	e						xvii
1	Intr	oducti	on						1
	1.1	Genera	al Background and Motivation	 					1
	1.2	An Ov	erview of Previous Work	 					2
		1.2.1	Cam Mechanisms	 					3
		1.2.2	Screw Theory	 					7
	1.3	Scope	of the Thesis						8
	1.4	Thesis	Organization	 		•		٠	9
2	Kin	ematic	s of Three-Link Mechanisms						11
	2.1	Introd	uction	 			•	•	11
	2.2	Surfac	e Geometry			•			13
		2.2.1	Revolute-Higher-Revolute (RHR) Mechanisms						17
		2.2.2	Revolute-Higher-Prismatic (RHP) Mechanisms	 					19

		2.2.3	Prismatic-Higher-Revolute (PHR) Mechanisms	21
		2.2.4	Prismatic-Prismatic (PPP) Mechanisms	22
	2.3	Pressu	re Angle	24
		2.3.1	Pressure Angle of RHR Mechanisms	26
		2.3.2	Pressure Angle of RHP Mechanisms	31
		2.3.3	Pressure Angle of PHR Mechanisms	31
		2.3.4	Pressure Angle of PPP Mechanisms	31
3	Kin	ematio	cs of Four-Link Mechanisms	32
	3.1	Introd	luction	32
	3.2	Roller	-Followers	33
		3.2.1	Revolute-Higher-Cylindric-Revolute (RHCR) Mechanisms	-10
		3.2.2	Revolute-Higher-Cylindric-Prismatic (RHCP) Mechanisms	46
		3.2.3	Prismatic-Higher-Cylindric-Revolute (PHCR) Mechanisms	49
		3.2.4	Prismatic-Higher-Cylindric-Prismatic (PHCP) Mechanisms	53
	3.3	Pressu	re Angle	56
		3.3.1	Pressure Angle of RHCR Mechanisms	57
		3.3.2	Pressure Angle of RHCP Mechanisms	61
		3.3.3	Pressure Angle of PHRR Mechanisms	62
		3.3.4	Pressure Angle of PHRP Mechanisms	62
	3.4	Applie	cations to Three-Link Mechanisms with Constant Pressure Angle	63
		3.4.1	RHHR Mechanisms	64
		3.4.2	RHHP Mechanisms	67
		3.4.3	PHHR Mechanisms	68
		3.4.4	PHHP Mechanisms	69
4	Rea	alizatio	on of Indexing Motion with Higher Pairs	70
	4.l		luction	70
	4.2		Output Function of Indexing Cam Mechanisms (ICM)	71
	4.3	-	of RHR Type	71
	4.4		of RHCR Type	78
5	Pur	·e-Rall	ling Motion with ICM	82
-	5.1		duction	82
	5.2		ary and Secondary Mechanisms	
	0.2	1 111110	mi and accommentation of the electric terms	0,1

		5.2.1 Primary Mechanism	84
		5.2.2 Secondary Mechanism	85
	5.3	Positive Action and Positive Motion	89
6	Con	cluding Remarks	102
	6.1	Conclusions	102
	6.2	Considerations for Future Work	104
Re	efere	nces	106
Αį	ppen	dices	117
Λ	Dua	l Numbers	117
В	The	Aronhold-Kennedy Theorem	123
C	Rul	ed-Surface Geometry	125
D	Dis	placement Program Functions	128
	D.1	Generalized Input-Output Function	128
	D.2	Cycloidal Function	130
	D.3	Polynomial Functions	130
		D.3.1 3-4-5 Polynomial	130
		D.3.2 4-5-6-7 Polynomial	130
	D.4	Combined Functions	131
		D.4.1 Modified Trapezoidal Acceleration	131
E	CA	D-Based Methods. Planar Applications	133
	E.1	Introduction	133
	E.2	RHRR Mechanisms	135
	E.3	RHHR Mechanisms	139
	E.4	RHRP Mechanisms	142
	E 5	RHHP Mechanisms	144

List of Figures

1.1	Industrial applications of cam mechanisms	2
1.2	A pumping system	3
1.3	Primitive construction of a cam profile	4
2.1	Mapping from Euclidean to dual space	12
2.2	Graphical interpretation of the striction curve	26
3.1	Mapping of the geometry of four-link cam mechanisms, onto the dual sphere	33
3.2	ISAs of an RHCR cam mechanism	38
3.3	Ruled surfaces of the cam (\mathcal{R}_C) and roller (\mathcal{R}_R) of an RHCR cam mechanism	41
3.4	Three views of the RHCR cam mechanism obtained from the surfaces of Fig. 3.3	42
3.5	Spherical RHRR cam mechanism	43
3.6	Planar RHRR cam mechanism	44
3.7	RHCP cam mechanism	47
3.8	PHCR cam mechanism	50
3.9	PHRP cam mechanism	54
3.10	Graphical representation of the pressure angle	56
3.11	Spherical RHHR cam mechanism	65
3.12	Planar RHHR cam mechanism	66
3.13	RHHP cam mechanism	67
3.14	PHHR cam mechanism	68
3.15	PHHP cam mechanism	69
4.1	Motion function $\phi = \phi(\psi)$	72

4.2	Spatial RHR-ICM with $\Delta \psi = 120^{\circ}$, $a_1 = 1$, $\alpha_1 = 60^{\circ}$	74
4.3	Spatial RHR-ICM with $N=5$, $a_1=0.8$, $\alpha_1=45^{\circ}$	75
4.4	Transition from spatial to spherical RHR-ICM	76
4.5	Transition from internal to external RHR-ICM	77
4.6	Definition of ϕ_m for RHCR-ICM: a) internal; b) external	78
4.7	Transition from internal to external RHCR-ICM	80
4.8	Transition from spatial to spherical RHCR-ICM	81
5.1	The pitch curve and the corresponding plots of ρ and ρ'	87
5.2	Pressure angle distribution of PRICAM	90
5.3	Three cycles of the cam motion	91
5.4	Top and front views of planar PRICAM	92
5.5	Cam and follower of planar PRICAM	93
5.6	Front and lateral views of spherical PRICAM	94
5.7	Cam and follower of spherical PRICAM	95
5.8	Solid model of a planar PRICAM	96
5.9	Solid model of a spherical PRICAM	97
5.10	Front view of the planar PRICAM prototype	98
5.11	Top view of the planar PRICAM prototype	99
5.12	Front view of the spherical PRICAM prototype	100
5.13	Lateral view of the spherical PRICAM prototype	101
6.1	Maximum pressure angle between planar PRICAM and mirror-image	
	conjugate cam mechanisms	103
A.1	The common perpendicular to two parallel lines	121
B.1	The Aronhold-Kennedy Theorem	124
D.1	Normalized input-output function	129
E.1	RHRR mechanism layout	134
E.2	Difference between ϕ_g and ϕ_r	136
E.3	Plot of ξ_{max} vs. $\Delta \phi$	137
E.4	Contact point for $\psi = \psi_5$ of the RHRR mechanism	138
E 5	Cam profile of the RHRR mechanism	138

E.6	RHHR mechanism layout						139
E.7	Contact point for $\psi = \psi_5$ of the RHHR mechanism						140
E.8	Cam profile of the $R\overline{HH}R$ mechanism with $a_4=0$.						141
E.9	Cam profile of the R $\overline{\rm HH}$ R mechanism with $a_4 \neq 0$.			•			141
E.10	RHRP mechanism layout						142
E.11	Contact point for $\psi=\psi_5$ of the RHRP mechanism						143
E.12	Cam profile of the RHRP mechanism		•				143
E.13	RHHP mechanism layout						144
E.14	Contact point for $\psi = \psi_5$ of the RHHP mechanism						145
E.15	Cam profile of the RHHP mechanism						145

List of Tables

3.1	Notation used for the synthesis of four-link cam mechanisms		 34
D.1	Generalized Input-Output Function	 	 129

Nomenclature

```
a_1 =  distance between I_{21} and I_{31}
a_3 =  distance between I_{31} and I_{43}
a_4 =  distance between I_{43} and I_{42}
b_2 = distance between I_{21} and I_{32}
b_3 = distance between I_{32} and I_{43}
 c = \sqrt{\phi'^2 + 2\phi'\cos\alpha_1 + 1}
 d = b_2 - a_1
e_{ij} = unit vector in the direction of <math>I_{ij}
\hat{\mathbf{e}}_{ij} = \text{dual unit vector in the direction of } \hat{P}_{ij}
         unit vector
m =
         рхе
 n = unit normal
         position vector
 \mathbf{r}_i = \text{position vector of } \mathcal{R}_i
r_p = position vector of the pitch surface
r_c = position vector of the cam surface
 \hat{\mathbf{s}}_i = \text{position dual vector of polode } i
\hat{s}_p = position dual vector of the pitch surface
```

 $\hat{s}_c = position dual vector of the cam surface$

 $v_2 = -dz_2/dt$

 $v_3 = dz_3/dt$

 $v_{ij} = dz_{ij}/dt$

 $w = unit vector of the product \omega \times r$

 $z_2 = \text{displacement of the points of body 2 lying on } I_{21} \text{ with respect to body 1}$

 $z_3 =$ displacement of the points of body 3 lying on I_{31} with respect to body 1

 $z_{ij} =$ displacement of the points of body i lying on I_{ij} with respect to body j

 $C_{ijk} = \text{great circle containing poles } \hat{P}_{ij}, \hat{P}_{ik} \text{ and } \hat{P}_{jk}$

 $I_{ij} =$ instantaneous screw axis of bodies 1 and 2

 $\mathcal{L}_{ijk} = \text{Common perpendicular of } I_{ij}, I_{ik} \text{ and } I_{jk}$

N = indexing number

 $\hat{P}_{ij} = \text{pole of } S_i \text{ and } S_j$

 $\hat{\mathbf{Q}}(\hat{\nu}) = \text{dual rotation through } \hat{\nu} \text{ about } X\text{-axis}$

 $\hat{\mathbf{R}}(\hat{\nu}) = \text{dual rotation through } \hat{\nu} \text{ about } Y\text{-axis}$

 $\mathcal{R}_i = \text{ruled surface of body } i$

 $\hat{S}(\hat{\nu}) = \text{dual rotation through } \hat{\nu} \text{ about } Z\text{-axis}$

 $S_i = \text{dual sphere of body } i$

 $\alpha_1 = \text{ angle between } I_{21} \text{ and } I_{31}$

 $\hat{\alpha}_1 = \alpha_1 + \epsilon a_1$

 $\alpha_3 = \text{ angle between } I_{31} \text{ and } I_{43}$

 $\hat{\alpha}_3 = \alpha_3 + \epsilon a_3$

 $\alpha_4 =$ angle between I_{43} and I_{42}

 $\hat{\alpha}_4 = \alpha_4 + \epsilon a_4$

 $\beta = \theta_2 - \alpha_1$

 $\hat{\beta} = \beta + \epsilon d$

 $\delta=$ angle between \mathcal{L}_{123} and \mathcal{L}_{341}

 $\hat{\delta} = \delta + \epsilon z_{32}$

 $\theta_2 = \text{ angle between } I_{21} \text{ and } I_{32}$

 $\hat{\theta}_2 = \theta_2 + \epsilon b_2$

 $\theta_3 =$ angle between I_{21} and I_{32}

 $\hat{\theta}_3 = \theta_3 + \epsilon b_3$

 $\lambda = \text{real number}$

 $\mu = \text{pressure angle}$

 $\nu = \text{ angle between } \mathcal{L}_{341} \text{ and } \mathcal{L}_{234}$

 $\hat{\nu} = \nu + \epsilon z_{43}$

 $\xi_i = \omega_i \times \mathbf{r}_i$

 $\rho =$ radius of curvature

 $\hat{\rho} = \text{dual radius of curvature}$

 $\tau(x) =$ normalized function of x

 $\phi = -$ angle of rotation of the follower with respect to the frame

 $\dot{\phi} = d\phi/dt$

 $\phi' = d\phi/d\psi$

 $\hat{\phi} = \phi + \epsilon z_{31}$

 $\psi =$ angle of rotation of the cam with respect to the frame

 $\hat{\psi} = \psi + \epsilon z_{21}$

 $\omega_{ij} =$ angular velocity between bodies i and j

 $\hat{\omega}_{ij} = \omega_{ij} + \epsilon v_{ij}$

 $\hat{\omega}_{ij} = \hat{\omega}_{ij} \hat{\mathbf{e}}_{ij}$

Chapter 1

Introduction

1.1 General Background and Motivation

A mechanism, according to IFToMM's Commission A for Standardization of Terminology (1991), is a system of bodies designed to convert motion of, and forces on, one or several bodies into constrained motions of, and forces on, other bodies. The way these bodies are connected is defined by their kinematic pairs. Basically, there are two kinds of kinematic pairs, namely, higher and lower pairs. The former refer to the coupling of two bodies in point or line contact, while the latter refer to the same in surface contact. Moreover, according to the type of degree of freedom, lower kinematic pairs can be of six types, namely, revolute, prismatic, screw, cylindrical, spherical and planar (Angeles, 1988).

A cam mechanism is defined as that in which the motion is transmitted by a higher kinematic pair. The simplest cam mechanism is composed by three elements, namely, frame, cam and follower. The cam is the driver, while the follower is the driven element. Another type of cam mechanism contains a fourth element, a roller, which is usually connected to the follower by a revolute pair, the higher pair taking place between cam and roller. The coupling between frame and cam or between frame and follower can be done by revolute, prismatic, cylindric or screw pairs.

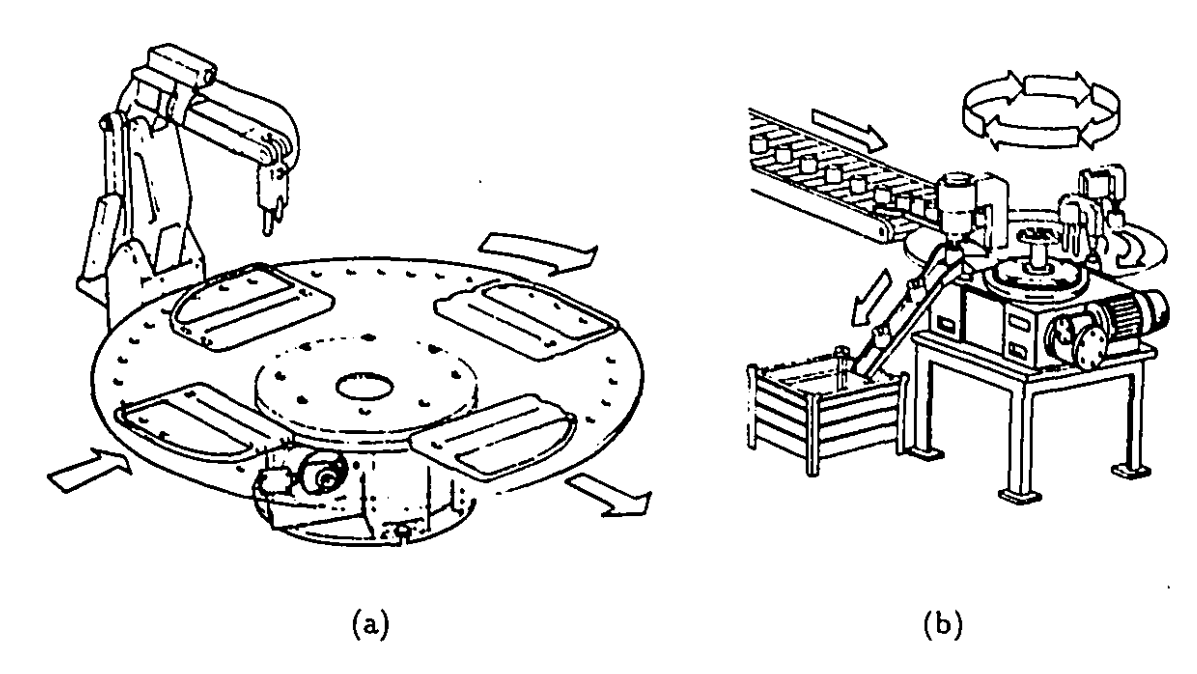


Figure 1.1 Industrial applications of cam mechanisms

Despite advances in robot technology whereby industrial manipulators may be effectively substituted for many mechanisms, cam mechanisms still find important industrial applications, such as in the textile, food-processing and manufacturing industries. Moreover, many applications of cam mechanisms, specifically indexing cam mechanisms, arise in conjunction with industrial robots. As shown in Fig. 1.1a, a robot is used to install fixtures on an automobile door, while an indexing cam mechanism rotates the circular table intermittently, allowing the process to be automated. In Fig. 1.1b a piece is presented to a cluster of machining stations by means of a table driven with an intermittent motion supplied by an indexing cam mechanism. Notice that this permits various machining operations to take place simultaneously.

1.2 An Overview of Previous Work

This subsection is divided in two main parts. The first part presents an overview of previous work on cam mechanisms, while the second deals with the mathematical

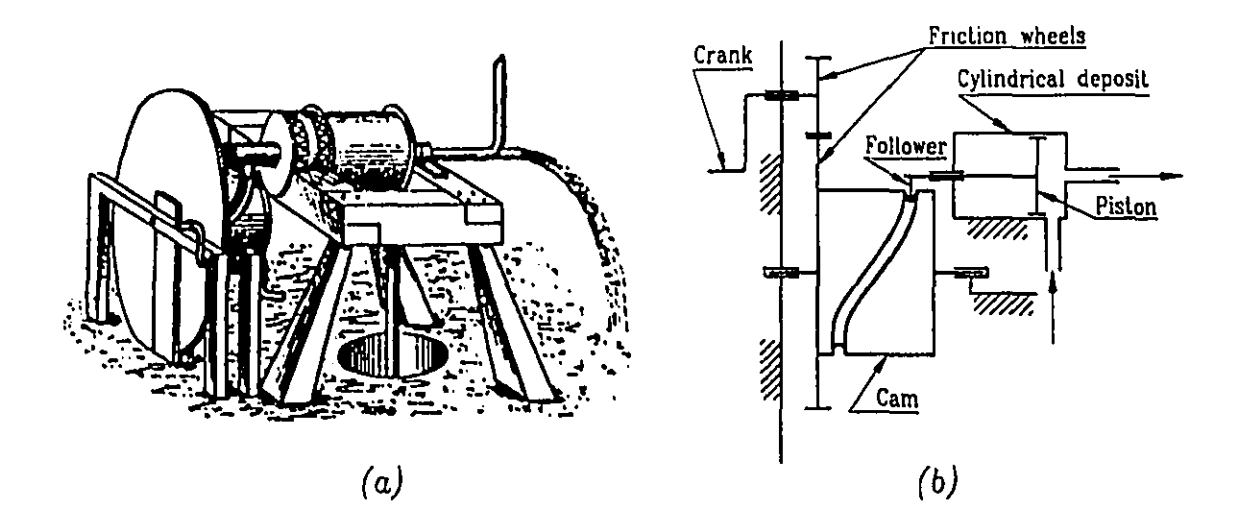


Figure 1.2 A pumping system

tools applied in this thesis.

1.2.1 Cam Mechanisms

The origin of cam mechanisms can be traced back to the Paleolithic age, as claimed by Müler and Mauersberger (1988), who present an account of the evolution of cam mechanisms, their applications and their contributors. Cam mechanisms seem to have their origin in one of the simple mechanisms of the ancient times (Müler, 1987), namely, the wedge. One of the most significant applications of cam mechanisms in the first half of the second millennium is in pumping systems, as shown in Fig. 1.2. The rotary motion of the crank is transmitted via friction wheels to the cam. The rotary motion of the cam is then transmitted to the lateral motion of the follower, which drives the piston. Morcover, the motion of the piston in one direction pulls water from the well and fills the cylindrical deposit, while motion in the other direction pushes water out. The modern design of cam mechanisms is considered to have been pioneered by Leonardo da Vinci. Since da Vinci's time and up to the XIX Century,

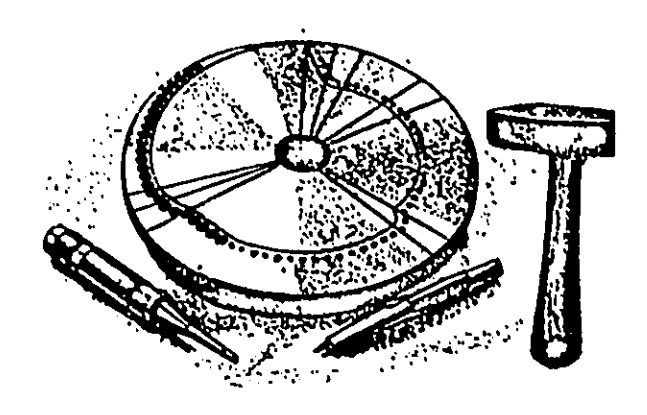


Figure 1.3 Primitive construction of a cam profile

important contributors to the development of cam mechanisms can be cited, e.g., A. Ramelli, L. Monge, J. Leupold, L. Bétancourt, Deparcieux, J. V. Poncelet, J. Borgnis, R. Willis, F. Reuleaux, etc.

The design of cam mechanisms in the first half of the XX Century was based on geometrical methods, while the cutting of the cam profile was done manually, as illustrated in Fig. 1.3. Below we present a survey of developments in the theory and practice of cam mechanisms, starting from the second half of the XX Century. This survey is divided in two main parts, namely, kinematics and dynamics.

Kinematics

In connection with kinematic synthesis, the method of finite differences was introduced by Johnson (1955) for the design of planar cam mechanisms. Later, this method was applied by the same author (Johnson, 1956c) to determine cam profiles with desired acceleration characteristics, while, with a different approach, Zigo (1967) derived an algorithm for the same purpose. Furthermore, some methods for the synthesis of

the cam profile from prescribed jerk patterns were proposed by Benedetto (1975), while Fenton (1966b) proposed to avoid noise in cams with a proper selection of camfollower offset for roller-follower radial cam mechanisms. A method of local analysis of the motion of mechanisms connected by a higher kinematic pair is discussed by Rosenberg and Křen (1987), while the theory of conjugate surfaces is applied to the synthesis of planar cam mechanisms by Zhong-Tang and Jing-Ping (1989).

The combination of linkages with cam mechanisms, in five-link mechanisms, was introduced by Hain (1970), who also proposed the optimization of these mechanisms (Hain, 1971). The same author later reported the optimization of a kinematic inversion of a five-link mechanism with a fixed cam (Hain, 1978). Furthermore, Amarnath and Gupta (1978) adopted the Hain's work to design cam-linkage mechanisms for multiple-dwell generation, whereas Sadler and Yang (1990), using a different approach, reported the optimal design of five-link cam mechanisms.

With the aim of improving the motion of cam mechanisms, the design of positive motion with single-disk planar cams and oscillating follower was presented by Jackowski and Dubil (1967) and Wunderlich (1971). Later, with a different approach but the same concept, Hunt (1973) presented a study of profiled-follower mechanisms.

It is well known that intermittent motion can be achieved with a kind of kinematic inversion of the slider-crank mechanism, i.e., the Geneva mechanism, which has been studied in the past to some extent (Bickford, 1965, 1972; Fenton, 1965, 1975a, 1975b; Oledzki and Szydlowski, 1975; Shadek et al., 1990). Intermittent motion has been produced with the aid of indexing cam mechanisms (Jacobs, 1949; Johnson, 1958; Makino, 1979). Moreover, the design of five-link cam mechanisms with multiple-dwell capability was reported by Amarnath and Gupta (1975).

The optimization of cam mechanisms can be considered from different points of view depending on the practical problem at hand. Thus, the minimization of the cam size for planar cam mechanisms was reported by Fenton (1966a, 1975c) and Loeff and Soni (1975). Moreover, the minimization of cam forces is reported by Jones (1978b),

while a comprehensive account on the optimization of planar cam mechanisms and an introduction to the optimization of spatial cam mechanisms is given by Angeles and López-Cajún (1991).

Experimental work to determine jump characteristics in planar cam-follower systems has been also reported (Rao and Raghavacharyulu, 1975), while experimental results on the changes of dynamic properties were presented by Bialkowicz et al. (1979). The problem of cutting the cam profile was studied by Jones (1978a); Norton et al. (1988) analyzed the effect of manufacturing methods on cam performance. Furthermore, the error due to manufacturing and assembly was studied by Dhande and Chakraborty (1975) from a probabilistic viewpoint, as pertaining to some planar and spatial cam mechanisms.

A method for the formula-based design of three-dimensional cams was reported by Raven (1959). Later, a unified approach to the design of this type of mechanisms was presented by Dhande et al. (1975). Furthermore, Dittrich and Zakel (1979) reported a study of three-dimensional cam mechanisms based on the values of the pressure angle, while a study of spherical cam mechanisms was discussed earlier by Dittrich (1966). Recently, envelope theory, which had been limited to planar mechanisms, was applied to spatial cam surface geometry, as reported by Backhouse and Jones (1990).

Dynamics

In the case of cams rotating at high speed, impact loads become crucial in the design. Thus, if force characteristics are considered in the synthesis of cam mechanisms, then we are referring to dynamic synthesis. A coordination of the polynomial equations of motion with the dynamic aspects of machine operation gives as a result the polydyne cam design, which was discussed by Stoddart (1953a, 1953b). Another approach onto dynamic synthesis was reported by Wiederrich and Roth (1975), who applied finite trigonometric series. Furthermore, a procedure for the dynamic analysis of a cam mechanism with bearing clearances was reported by Osman et al. (1987).

The optimization of cam and follower properties considering the dynamics of cam mechanisms has been reported by Johnson (1956a, 1956b) and Berzak and Freudenstein (1979), while the effects of cam profile error on the dynamic behaviour of follower cam systems was discussed by Grewal and Newcombe (1988).

In the realm of indexing cam mechanisms, the residual vibrations were studied by Takano and Toyama (1979). Moreover, the optimal configuration of planar external mechanisms of this kind is reported by Jones and Tsang (1987), and the optimal design of external and internal indexing cam mechanisms is reported by Gouxun et al. (1988).

Backlash, squeeze and impact of planar cam mechanisms are simulated in the work reported by Koster (1975) and Kass and Chace (1975), while different methods of cutting a plate cam are compared by Norton (1988).

1.2.2 Screw Theory

The approach to the kinematic synthesis of cam mechanisms introduced here is based on screw theory. While it is difficult to state the date of the origin of this theory, Ball (1900) includes a list of contributors to this theory. We based our study reported here on a number of references, namely, (Ball, 1875, 1900; Beggs, 1960; Veldkamp, 1967a, Roth, 1967; 1967b, 1976; Chen and Roth, 1969a; Waldron, 1972; Yang, 1974; Pandrea and Voiculescu, 1975; Rooney, 1975b; Ohwovoriole and Roth, 1981; De Sa and Roth, 1981a, 1981b; Hon-Cheung, 1987; McCarthy, 1987a; Agrawal, 1987; Kerr and Sanger, 1989; Sticher, 1989; Gibson and Hunt, 1990a, 1990b; Parkin, 1990).

Furthermore, ruled-surface theory has been considered an important tool for the study of screw theory. Along these lines, Yang et al. (1975) report applications of screw theory to spatial mechanisms. Moreover, differential properties of ruled surfaces in a form applicable to spatial kinematics are reported by McCarthy and Roth (1981), while a study of ruled surfaces in dual space is given in Köse (1982a, 1982b). The

geometry of axods is analyzed with the aid of ruled-surface theory by Dizioglu (1989), and a new dual integral invariant for a given closed ruled surface is introduced by Gürsoy (1990).

Contributions to the theory of mechanisms from the point of view of screw theory have been presented by different authors (Phillips and Hunt 1964; Yang and Freudenstein, 1964; Hunt, 1967a, 1967b; Chen and Roth, 1969b; Kohli and Soni, 1975; Rooney, 1975a; Vadasz and Soni, 1979; Sodh and Shoup, 1982; Sugimoto and Duffy, 1982; Sun and Waldron, 1982; Angeles, 1986a, 1986b; Xiao and Yang, 1989).

1.3 Scope of the Thesis

Cam mechanisms have been studied from different points of view, namely, kinematic synthesis, dynamic synthesis, analysis, design, optimization and manufacturing. This thesis is oriented to the kinematic synthesis of cam mechanisms in a unified framework. By this we mean that spatial, spherical and planar cam mechanisms are integrated in the same formulation. Traditionally, the synthesis of the three types of cam mechanisms has been approached using independent formulations. With a unified formulation, not only the well-known types of cam mechanisms, but also novel cam mechanisms can be synthesized, as shown in this thesis.

Moreover, since all the design parameters are considered in a unified framework, the optimization theory of cam mechanisms can be applied systematically, i.e., the criteria applied for the optimization of planar cam mechanisms, which can be found to some extent in the literature, can be complemented in order to provide general criteria for the optimization of spherical and spatial cam mechanisms.

The ideal solution in the design of cam mechanisms is that in which the actual output motion matches the prescribed one. However, the actual output motion is bound to be different due to deviation of certain parameters from their nominal values, such as manufacturing tolerances, clearances at the joints, misalignment errors, etc.

With the use of a proper design and machining facilities, namely, a CAD/CAM system, some of those errors can be minimized, but not totally eliminated. Therefore, an analysis of the error is an important topic to be considered whenever industrial production is required. Given that the stochastic analysis of errors in cams warrants a research program of its own, we did not address this issue here. Although this thesis does not discuss a stochastic error analysis, it is believed that the formulation presented here provides the basic information needed for the development of such a study, and is proposed as one of the items for future work.

1.4 Thesis Organization

ン

The unified synthesis of three-link mechanisms is presented in Chapter 2, where the geometry of contact surfaces and the pressure angle are discussed. Four types of threelink cam mechanisms are described, which are classified according to their kinematic pairs, namely, RHR, PHR, RHP and PPP. The first and last letters stand for the type of pair of the input and output axes, respectively, while the middle letter, for the camfollower pair. Moreover, R, P and H represent respectively, revolute, prismatic and higher pairs. The sliding velocity along the higher pair is minimized, and the contacting surfaces are obtained from this condition. In Chapter 3, the same philosophy as for Chapter 2 is applied for the unified synthesis of four-link cam mechanisms. Now, the four types are defined as RHCR, RHCP, PHCR and PHCP. Similarly, the first and last letters refer respectively, to the kinematic pair of the input and output axes. The second letter refers to the cam-roller coupling, while the third letter, to the roller-follower pair, where C stands for cylindric. A unified formulation for the pressure angle is introduced here. The concept of cam mechanisms with constant pressure angle and an auxiliary roller is applied to the synthesis of cam mechanisms with flat-face followers. Here, four types are discussed namely, RHHR, RHHP, PHHR and PHHP, where the symbol HH is explained in Section 3.4. In Chapter 4, the theory

presented in Chapters 2 and 3 is applied specifically to the synthesis of indexing cam mechanisms. The design of indexing cam mechanisms with pure rolling and positive motion is presented in Chapter 5. Chapter 6 concludes with a general discussion on the achievements in this thesis and suggestion for further research work.

Five appendices are included for completeness: A general review of dual numbers and a theorem which is considered a contribution to the theory of dual numbers are presented in Appendix A. In Appendix B, the Aronhold-Kennedy Theorem in dual-number notation is recalled. A general description of ruled-surface theory is presented in Appendix C. A few displacement functions applied for the synthesis of cam mechanisms are included in Appendix D. Finally, graphical methods, based on the theory presented in Chapters 2 and 3, are discussed in Appendix E, where the profile of the cam is obtained directly from the contact points between cam and follower

Chapter 2

Kinematics of Three-Link Mechanisms

2.1 Introduction

This chapter is confined to the study of cam mechanisms composed of three rigid links, namely, the fixed frame, the driving element or cam and the driven element or the follower. While the study is general, special attention is given to indexing cam mechanisms (ICM).

The synthesis of the profiles of both cam and follower as well as the quality of the transmission, quantified via pressure angle, are discussed in this chapter in a unified fashion. The profiles are designed as ruled surfaces, and motion is transmitted along a common line, which gives rise to a higher kinematic pair. Two more kinematic pairs arise, namely, the cam-frame and the follower-frame pairs, which belong to the class of lower kinematic pairs, and can be of any of three types, namely, revolute, prismatic or screw (Angeles, 1982). This generalization allows the analysis of those mechanisms not only with rotating but also with translating followers, i.e., if the output motion is attained via a prismatic pair.

Recalling the theorem on the existence of an instant screw axis (ISA) pertaining to the relative motion of two rigid bodies (Angeles, 1982), three ISAs arise within the kind of mechanisms under study. Moreover, the input and output pairs are represented by their instant screw axes I_{21} and I_{31} , where 1, 2 and 3 stand for frame, cam and follower, respectively. For a given input-output motion there is a unique pair of cam and follower surfaces that produce the given motion with a minimum sliding on the higher pair. This solution is achieved when the contact line coincides with the instant screw axis I_{32} . In some degenerate cases the surfaces may collapse into a line. Other solutions can be obtained if the contact line and I_{32} are not coincident, but parallel, e.g., in cam mechanisms with flat-face followers.

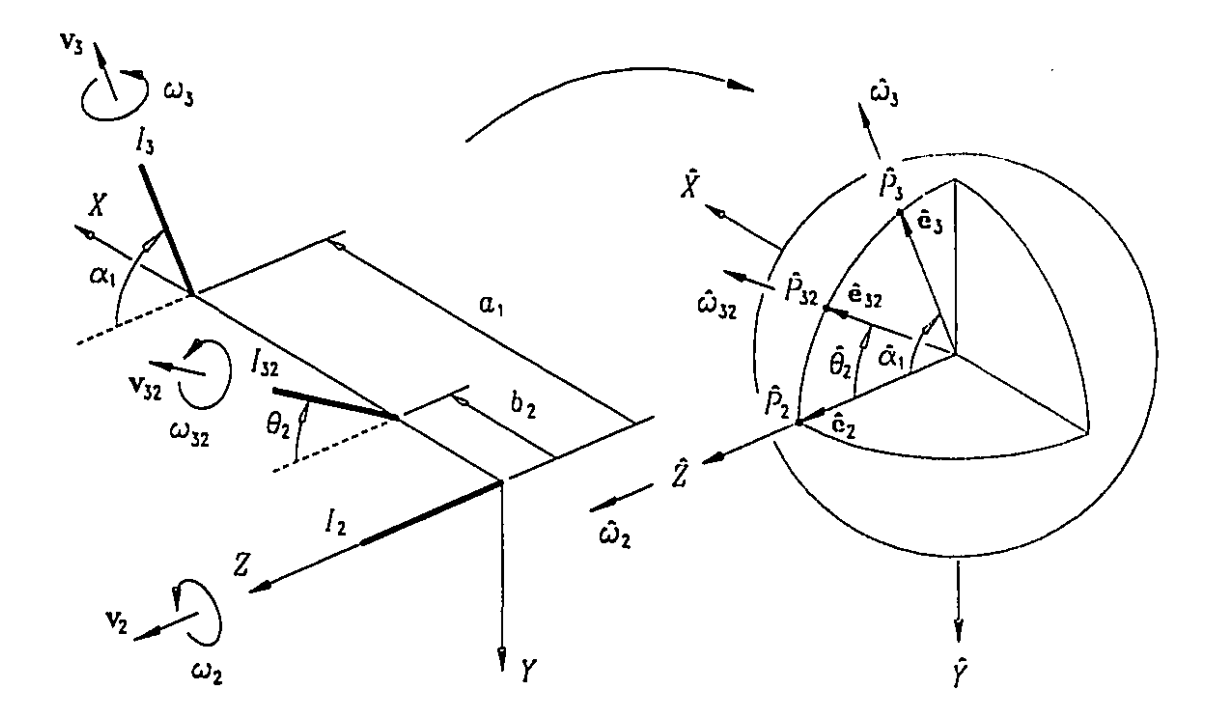


Figure 2.1 Mapping from Euclidean to dual space.

In this thesis, planar, spherical and spatial cam mechanisms are classified according to the relative location of their ISAs. Thus, the mechanism is planar if every ISA is either parallel to one direction or perpendicular to it; the mechanism is spherical

if all ISAs are concurrent; spatial, if none of the two foregoing conditions is met.

The contact line of the higher pair is an element of both surfaces, and is derived by application of the Aronhold-Kennedy Theorem, first proposed by Aronhold (1872) and Kennedy (1886) independently for planar motion and later extended to the three dimensional case by Beggs (1959) and Phillips and Hunt (1964). The formulation is based on a mapping of the motion onto the dual space, where the three bodies are considered as dual unit spheres S_1 , S_2 and S_3 in relative motion, and the poles \hat{P}_{ij} are the images of the axes I_{ij} under the aforementioned mapping. Appendix B includes an account of dual-number algebra for completeness, as the said mapping is based on this algebra.

2.2 Surface Geometry

As mentioned in Section 2.1, the surfaces of the cam and the follower are generated by the sweeping action of I_{32} onto each of the two bodies. The first part of this section is devoted to the derivation of the parameters defining I_{32} , the second to the definition of the surfaces.

Let S_1 , S_2 and S_3 be the dual unit spheres representing, in the dual space, the frame, cam and follower, respectively. We recall briefly here that dual quantities are denoted with a hat (^) and are composed of a primal part, usually a real scalar, vector or tensor, and a dual part, correspondingly a real scalar, vector or tensor, preceded by the dual unity ϵ with the property $\epsilon^2 \equiv 0$. The relative dual angular velocities of the foregoing dual spheres are related as in eq.(B.5), i.e.,

$$\hat{\omega}_{31}\hat{e}_{31} = \hat{\omega}_{32}\hat{e}_{32} + \hat{\omega}_{21}\hat{e}_{21}$$

In the above equation, the subscripts (ij) denote the dual angular velocity of the ith dual sphere with respect to jth sphere, but, in order to simplify the nomenclature, all dual angular velocities with respect to 1, i.e., the frame, will be indicated only with

the label of the other sphere, eq.(B.5) thus taking on the form

$$\hat{\omega}_3 \hat{\mathbf{e}}_3 = \hat{\omega}_{32} \hat{\mathbf{e}}_{32} + \hat{\omega}_2 \hat{\mathbf{e}}_2 \tag{2.1}$$

Now, three coordinate frames are defined so that their \hat{X} -axes are collinear and each of the \hat{Z} -axes is oriented towards one of the poles. Thus, the poles are locally represented by the dual unit vector

$$\hat{\mathbf{k}} = \begin{bmatrix} 0, & 0, & 1 \end{bmatrix}^T \tag{2.2}$$

with zero dual part.

Furthermore, \hat{a}_1 is the dual angle from \hat{e}_2 to \hat{e}_3 , whereas $\hat{\theta}_2$ is the dual angle from \hat{e}_2 to \hat{e}_{32} , both of which are defined as

$$\hat{\alpha}_1 = \alpha_1 + \epsilon a_1 \tag{2.3a}$$

$$\hat{\theta}_2 = \theta_2 + \epsilon b_2 \tag{2.3b}$$

The geometric representation of the foregoing mapping is shown in Fig. 2.1, where $\mathbf{v}_{ij} = v_{ij}\mathbf{e}_{ij}$, while v_{ij} and ω_{ij} are the components of $\hat{\omega}_{ij}$, as defined in eq.(B.6). Thus, the unit dual vectors of the poles are given as

$$\hat{\mathbf{e}}_3 = \hat{\mathbf{Q}}(\hat{\alpha}_1)\hat{\mathbf{k}} \tag{2.4a}$$

$$\hat{\mathbf{e}}_{32} = \hat{\mathbf{Q}}(\hat{\theta}_2)\hat{\mathbf{k}} \tag{2.4b}$$

$$\hat{\mathbf{e}}_2 = \hat{\mathbf{k}} \tag{2.4c}$$

where $\hat{\mathbf{Q}}$ is defined in eq.(A.11a).

Next, substituting the values of eqs.(2.4) into eq.(2.1), one obtains

$$\hat{\omega}_{3} \begin{bmatrix} 0 \\ -\sin \hat{\alpha}_{1} \\ \cos \hat{\alpha}_{1} \end{bmatrix} = \hat{\omega}_{32} \begin{bmatrix} 0 \\ -\sin \hat{\theta}_{2} \\ \cos \hat{\theta}_{2} \end{bmatrix} + \hat{\omega}_{2} \begin{bmatrix} 0 \\ 0 \\ 1 \end{bmatrix}$$
 (2.5)

Two dual equations are obtained from eq.(2.5), namely,

$$\hat{\omega}_{32} \sin \hat{\theta}_2 = \hat{\omega}_3 \sin \hat{\alpha}_1 \tag{2.6a}$$

$$\hat{\omega}_{32}\cos\hat{\theta}_2 = \hat{\omega}_3\cos\hat{\alpha}_1 - \hat{\omega}_2 \tag{2.6b}$$

Thus, the parameters of the pole \hat{P}_{32} can be written in terms of those of the poles \hat{P}_2 and \hat{P}_3 . Consequently, $\hat{\omega}_{32}$ is obtained by the addition of the squared terms of eqs.(2.6), while $\hat{\theta}_2$ is obtained upon dividing eq.(2.6a) by eq.(2.6b), namely,

$$\hat{\omega}_{32}^2 = \hat{\omega}_3^2 - 2\hat{\omega}_3\hat{\omega}_2\cos\hat{\alpha}_1 + \hat{\omega}_2^2 \tag{2.7}$$

$$\tan \hat{\theta}_2 = \frac{\hat{\omega}_3 \sin \hat{\alpha}_1}{\hat{\omega}_3 \cos \hat{\alpha}_1 - \hat{\omega}_2} \tag{2.8}$$

The discussion, as well as other operations with dual numbers, is outlined in Appendix Λ .

Moreover, we are interested in calculating the numerical values of the real angular velocity and the real sliding velocity of the follower with respect to the cam, ω_{32} and v_{32} , respectively. The former is the signed magnitude of the difference $\omega_3 - \omega_2$ while the latter is the minimum magnitude of the difference $\mathbf{v}_{P3} - \mathbf{v}_{P2}$, where \mathbf{v}_{P3} is the velocity of a point of the follower and \mathbf{v}_{P2} is the velocity of the same point of the cam. Now, in order to obtain the real angular velocity ω_{32} and the real sliding velocity v_{32} , one can expand eq.(2.7) considering eqs.(B.6 & 2.3) and the definitions given in eqs.(A.1 & A.10), which readily lead to

$$\omega_{32} = \pm \sqrt{\omega_3^2 - 2\omega_3\omega_2\cos\alpha_1 + \omega_2^2}$$
 (2.9a)

$$v_{32} = \frac{\omega_3 v_3 + \omega_3 \omega_2 a_1 \sin \alpha_1 - (\omega_3 v_2 + \omega_2 v_3) \cos \alpha_1 + \omega_2 v_2}{\omega_{32}}$$
(2.9b)

A similar procedure is followed to obtain θ_2 and θ_2 from eq.(2.8), namely,

$$\tan \theta_2 = \frac{\omega_3 \sin \alpha_1}{\omega_3 \cos \alpha_1 - \omega_2} \tag{2.10a}$$

$$b_2 = \frac{(\omega_3^2 - \omega_3\omega_2\cos\alpha_1)a_1 + (\omega_3v_2 - \omega_2v_3)\sin\alpha_1}{\omega_{32}^2}$$
 (2.10b)

In general, eqs. (2.9 & 2.10) provide all the necessary information to define I_{32} . Moreover, we claim that these are the general equations from which one can derive any type of the known cam mechanisms satisfying the condition of minimum sliding velocity at the contact line and new types depending of the combination used on the input and output screw parameters, namely, ω_2 , v_2 , ω_3 , v_3 , α_1 and a_4 . However, special treatment may be needed if both the input- and output-pairs are prismatic, as discussed in Subsection 2.2.4.

Now, if S_2 rotates with respect to S_1 through the dual angle $\hat{\psi} = \psi + \epsilon z_2$, where both ψ and z_2 are functions of time, \hat{P}_{32} will trace a curve on S_2 called the *polode*, which is given by the dual unit vector $\hat{s}_2(\hat{\psi})$ defined below:

$$\hat{\mathbf{s}}_2(\hat{\psi}) = \hat{\mathbf{S}}^T(\hat{\psi})\hat{\mathbf{Q}}(\hat{\theta}_2)\hat{\mathbf{k}}$$
 (2.11a)

where the dual rotation \hat{S} is defined in eq.(A.11c).

4

Similarly, if S_3 rotates with respect to S_1 through the dual angle $\hat{\phi} = \phi + \epsilon z_3$, where both ϕ and z_3 are functions of time t, \hat{P}_{32} will trace another polode on S_3 , which is given by the dual unit vector $\hat{s}_3(\hat{\phi})$, defined as

$$\hat{\mathbf{s}}_3(\hat{\boldsymbol{\phi}}) = \hat{\mathbf{S}}^T(\hat{\boldsymbol{\phi}})\hat{\mathbf{Q}}(\hat{\theta}_2 - \hat{\alpha}_1)\hat{\mathbf{k}}$$
 (2.11b)

Furthermore, the polodes defined by the dual unit vectors \hat{s}_2 and \hat{s}_3 are the images of the ruled surfaces \mathcal{R}_2 and \mathcal{R}_3 , the contact surfaces of cam and follower, respectively. Now, upon expansion, eqs.(2.11) take on the form

$$\hat{\mathbf{s}}_{2}(t) = \begin{bmatrix} -s\psi(t)s\theta_{2} \\ -c\psi(t)s\theta_{2} \\ c\theta_{2} \end{bmatrix} - \epsilon \begin{bmatrix} b_{2}s\psi(t)c\theta_{2} + z_{2}(t)c\psi(t)s\theta_{2} \\ b_{2}c\psi(t)c\theta_{2} - z_{2}(t)s\psi(t)s\theta_{2} \\ b_{2}s\theta_{2} \end{bmatrix}$$
(2.12a)

$$\hat{\mathbf{s}}_{3}(t) = \begin{bmatrix} -s\phi(t)s\beta \\ -c\phi(t)s\beta \\ c\beta \end{bmatrix} - \epsilon \begin{bmatrix} ds\phi(t)c\beta + z_{3}(t)c\phi(t)s\beta \\ dc\phi(t)c\beta - z_{3}(t)s\phi(t)s\beta \\ ds\beta \end{bmatrix}$$
(2.12b)

where $d \equiv b_2 - a_1$ and $\beta \equiv \theta_2 - \alpha_1$. Furthermore, $s \leftarrow \sin$ and $c \leftarrow \cos$.

By means of eq.(A.8), the point coordinates of \mathcal{R}_2 and \mathcal{R}_3 can be readily obtained from eqs.(2.12), namely,

$$\mathbf{r}_{2}(t,\lambda) = \begin{bmatrix} b_{2}c\psi(t) - z_{2}(t)s\psi(t)s\theta_{2}c\theta_{2} \\ -b_{2}s\psi(t) - z_{2}(t)c\psi(t)s\theta_{2}c\theta_{2} \\ -z_{2}(t)s^{2}\theta_{2} \end{bmatrix} + \lambda \begin{bmatrix} -s\psi(t)s\theta_{2} \\ -c\psi(t)s\theta_{2} \\ c\theta_{2} \end{bmatrix}$$
(2.13a)

and

$$\mathbf{r}_{3}(t,\lambda) = \begin{bmatrix} dc\phi(t) - z_{3}(t)s\phi(t)s\beta c\beta \\ -ds\phi(t) - z_{3}(t)c\phi(t)s\beta c\beta \\ -z_{3}(t)s^{2}\beta \end{bmatrix} + \lambda \begin{bmatrix} -s\phi(t)s\beta \\ -c\phi(t)s\beta \\ c\beta \end{bmatrix}$$
(2.13b)

2.2.1 Revolute-Higher-Revolute (RHR) Mechanisms

A cam mechanism with both input and output revolute pairs and with the contact line coinciding with I_{32} , is called a revolute-higher-revolute (RHR) mechanism. Its input-output function can be expressed as

$$\phi = \phi(\psi) \tag{2.14}$$

and, from the type of input and output pairs,

$$z_2 = v_2 = 0 (2.15a)$$

$$z_3 = v_3 = 0 (2.15b)$$

Next, from eq.(2.14), $\dot{\phi}$ can be expressed as

$$\dot{\phi} \equiv \frac{d\phi}{dt} = \frac{d\phi}{d\psi} \frac{d\psi}{dt} = \phi'\omega_2 \tag{2.15c}$$

Now, substituting the values of eqs. (2.15) into eqs. (2.9 & 2.10), the screw parameters of I_{32} are readily derived, namely,

$$\omega_{32} = \pm \omega_2 c \tag{2.16a}$$

$$v_{32} = \pm \frac{\phi' \sin \alpha_1}{c} a_1 \omega_2 \tag{2.16b}$$

$$\tan \beta_2 = \frac{\phi' \sin \alpha_1}{\phi' \cos \alpha_1 - 1} \tag{2.16c}$$

$$b_2 = \frac{\phi'^2 - \phi' \cos \alpha_1}{c^2} a_1 \tag{2.16d}$$

where

$$c = \sqrt{\phi'^2 - 2\phi' \cos \alpha_1 + 1} \tag{2.17}$$

Furthermore, combining eqs.(2.16) with eqs.(2.13), the cam and follower surfaces are derived from

$$\mathbf{r}_{2}(\psi,\lambda) = b_{2} \begin{bmatrix} \cos \psi \\ -\sin \psi \end{bmatrix} + \lambda \begin{bmatrix} -\sin \psi \sin \theta_{2} \\ -\cos \psi \sin \theta_{2} \\ \cos \theta_{2} \end{bmatrix}$$
(2.18a)

and

$$\mathbf{r}_{3}(\phi,\lambda) = (b_{2} - a_{1}) \begin{bmatrix} \cos \phi \\ -\sin \phi \end{bmatrix} + \lambda \begin{bmatrix} -\sin \phi \sin(\theta_{2} - \alpha_{1}) \\ -\cos \phi \sin(\theta_{2} - \alpha_{1}) \end{bmatrix}$$

$$\cos(\theta_{2} - \alpha_{1})$$

$$\cos(\theta_{2} - \alpha_{1})$$
(2.18b)

in agreement with the results presented in (González-Palacios and Angeles, 1990), using a more specific approach.

Now we can draw the conclusions below:

i) The surfaces generated by r_i correspond to any of the three classes of cam mechanisms. Thus, the classification below is given in terms of the values of a_1 and a_1 :

- Planar: $a_1 \neq 0$, $\alpha_1 = 0$.

- Spherical: $a_1 = 0$, $\alpha_1 \neq 0$.

- Spatial: $a_1 \neq 0$, $\alpha_1 \neq 0$.

ii) As expected, pure rolling is achieved in the first two cases mentioned above, which is apparent from eq.(2.16b), since v_{32} vanishes with the corresponding values of a_1 and a_1 .

2.2.2 Revolute-Higher-Prismatic (RHP) Mechanisms

A cam mechanism with a revolute pair as input and a prismatic pair as output, with line of contact I_{32} , is called a revolute-higher-prismatic (RHP) mechanism. Moreover, the output motion can be expressed as a function of the input motion, namely,

$$z_3 = z_3(\psi) (2.19)$$

From the types of input and output pairs, one concludes that

$$z_2 = v_2 = 0 (2.20a)$$

$$\phi = \omega_3 = 0 \tag{2.20b}$$

Now, considering eq. (2.19), v_3 can be expressed as

$$v_3 \equiv \frac{dz_3}{dt} = \frac{dz_3}{d\psi} \frac{d\psi}{dt} = z_3' \omega_2 \tag{2.20c}$$

Recalling eqs.(2.20), eqs.(2.9 & 2.10) take the form

$$\omega_{32} = -\omega_2 \tag{2.21a}$$

$$v_{32} = -z_3' \omega_2 \cos \alpha_1 \tag{2.21b}$$

$$an \theta_2 = 0 \tag{2.21c}$$

$$b_2 = -z_3' \sin \alpha_1 \tag{2.21d}$$

Furthermore, substituting eqs.(2.21) into eqs.(2.13), the cam and follower surfaces are readily derived in terms of the position vectors $\mathbf{r}_2(\psi, \lambda)$ and $\mathbf{r}_3(z_3, \lambda)$, namely,

$$\mathbf{r}_{2}(\psi,\lambda) = z_{3}' \sin \alpha_{1} \begin{bmatrix} -\cos \psi \\ \sin \psi \\ 0 \end{bmatrix} + \lambda \begin{bmatrix} 0 \\ 0 \\ 1 \end{bmatrix}$$
 (2.22a)

and

$$\mathbf{r}_{3}(z_{3},\lambda) = \begin{bmatrix} -(z_{3}' \sin \alpha_{1} + a_{1}) \\ z_{3} \sin \alpha_{1} \cos \alpha_{1} \\ -z_{3} \sin \alpha_{1} \end{bmatrix} + \lambda \begin{bmatrix} 0 \\ \sin \alpha_{1} \\ \cos \alpha_{1} \end{bmatrix}$$
(2.22b)

Equations (2.22) represent a family of cam mechanisms, characterized by specific values of α_1 . Because the output is a prismatic pair, a_1 can be arbitrarily defined without changing the geometry of the follower surface. In other words, a_1 only gives the position of the follower frame. Now, by looking at eq.(2.21b), v_{32} vanishes if $\alpha_1 = \pi/2$ or $3\pi/2$. Indeed, substitution of these values into eqs.(2.22), leads to the surfaces given below:

$$\mathbf{r}_{2}(\psi,\lambda) = \pm z_{3}' \begin{bmatrix} -\cos\psi\\ \sin\psi\\ 0 \end{bmatrix} + \lambda \begin{bmatrix} 0\\ 0\\ 1 \end{bmatrix}$$
 (2.23a)

and

$$\mathbf{r}_{3}(z_{3},\lambda) = \mp \begin{bmatrix} (z_{3}' + a_{1}) \\ 0 \\ z_{3} \end{bmatrix} \pm \lambda \begin{bmatrix} 0 \\ 1 \\ 0 \end{bmatrix}$$
 (2.23b)

the upper sign taking place when $\alpha_1 = \pi/2$.

From these results we can draw a few conclusions, namely,

- i) The surfaces are cylindrical.
- ii) The cam mechanism has a translating follower.
- iii) Because $\alpha_1 \neq 0$ and $b_2 \neq 0$, the ISAs are non-parallel and non-intersecting. Therefore, according to the given definition, these two mechanisms are spatial cams.

On the other hand, v_{32} of eq.(2.21b) is a maximum if $\alpha_1 = 0$ or π , the contacting surfaces being obtained by substituting either of the two values of α_1 into eqs.(2.22), namely,

$$\mathbf{r}(\lambda) = \pm \lambda \begin{bmatrix} 0 \\ 0 \\ 1 \end{bmatrix} \tag{2.24a}$$

and

$$\mathbf{f}(\lambda) = \begin{bmatrix} -a_1 \\ 0 \\ 0 \end{bmatrix} \pm \lambda \begin{bmatrix} 0 \\ 1 \\ 0 \end{bmatrix}$$
 (2.24b)

from which we can draw a few additional conclusions, namely,

- i) The surfaces degenerate into a common line, which is coincident with I_{32} .
- ii) The solution is ideally a cylindrical cam mechanism. In order to have a feasible mechanism, either the locus of the higher pair should be different from the locus of I_{32} or an intermediate rigid body should be included, e.g., a roller.
- iii) I_{32} is parallel to I_2 and I_3 , yielding a planar mechanism.

2.2.3 Prismatic-Higher-Revolute (PHR) Mechanisms

A prismatic-higher-revolute (PHR) mechanism is similar to an RHP mechanism, the only difference being that now the input has a prismatic pair and the output a revolute pair. The output motion is expressed as

$$\phi = \phi(z_2) \tag{2.25}$$

Now, considering the input and output pairs, one obtains

$$\psi = \omega_2 = 0 \tag{2.26a}$$

$$z_3 = v_3 = 0 (2.26b)$$

Furthermore, ω_3 is expressed as

$$\omega_3 \equiv \frac{d\phi}{dt} = \frac{d\phi}{dz_2} \frac{dz_2}{dt} = \phi' v_2 \tag{2.27}$$

Substitution of eqs. (2.26) into eqs. (2.9 & 2.10), one can readily obtain

$$\omega_{32} = \pm \phi' v_2 \tag{2.28a}$$

$$v_{32} = \mp v_2 \cos \alpha_1 \tag{2.28b}$$

$$\tan \theta_2 = \tan \alpha_1 \tag{2.28c}$$

$$b_2 = \frac{\phi' a_1 + \sin \alpha_1}{\phi'} \tag{2.28d}$$

Thus, the general surfaces for a PHR mechanism are obtained by substitution of eqs.(2.28) into eqs.(2.13), namely,

$$\mathbf{r}_{2}(z_{2},\lambda) = \begin{bmatrix} a_{1} + \sin \alpha_{1}/\phi' \\ -z_{2}sa_{1}\cos \alpha_{1} \\ -z_{2}\sin^{2}\alpha_{1} \end{bmatrix} + \lambda \begin{bmatrix} 0 \\ -\sin \alpha_{1} \\ \cos \alpha_{1} \end{bmatrix}$$
(2.29a)

$$\mathbf{r}_{3}(\phi,\lambda) = \frac{\sin\alpha_{1}}{\phi'} \begin{bmatrix} \cos\phi \\ -\sin\phi \\ 0 \end{bmatrix} + \lambda \begin{bmatrix} 0 \\ 0 \\ 1 \end{bmatrix}$$
 (2.29b)

Now, in order to have pure rolling, i.e., $v_{32} = 0$, α_1 must be $\pi/2$ or $3\pi/2$. Since the results are analogous to those of section 2.2.2, one obtains the same conclusions given there. According to the results presented in Sections 2.2.2 and 2.2.3, the theorems below are readily formulated:

Theorem 2.1: For RHP or PHR mechanisms, the contact line of minimum sliding velocity is parallel to the axis of the revolute pair.

Theorem 2.2: Pure rolling of RHP or PHR mechanisms is achieved if the axis of the prismatic pair is perpendicular to both the contact line and the axis of the revolute pair.

2.2.4 Prismatic-Prismatic-Prismatic (PPP) Mechanisms

If both the input and output pairs are prismatic in a cam mechanism, the third pair is also prismatic and so, the mechanism is termed prismatic-prismatic-prismatic (PPP).

The input-output function can be expressed as

$$z_3 = z_3(z_2) \tag{2.30}$$

This type of mechanism is the exception to the general formulation given in eqs. (2.9 & 2.10), where the screw parameters, except for ω_{32} , are undefined. Consequently, a particular derivation should be considered, i.e., instead of relative angular velocities, relative translational velocities of the contact point will be analyzed. These are related as

$$\hat{\mathbf{v}}_{31} = \hat{\mathbf{v}}_{32} + \hat{\mathbf{v}}_{21} \tag{B.4}$$

which can be rewritten as

$$v_3\hat{\mathbf{e}}_3 = v_{32}\hat{\mathbf{e}}_{32} + v_2\hat{\mathbf{e}}_2 \tag{2.31}$$

Comparing eq.(2.31) with eq.(2.1), one can apply a procedure similar to the one used to derive eqs.(2.7 & 2.8) to obtain

$$v_{32}^2 = v_3^2 - 2v_3v_2\cos\hat{\alpha}_1 + v_2^2 \tag{2.32a}$$

and

$$\tan \hat{\theta}_2 = \frac{v_3 \sin \hat{\alpha}_1}{v_3 \cos \hat{\alpha}_1 - v_2} \tag{2.32b}$$

Separating eqs.(2.32) into primal and dual parts, one can readily obtain

$$v_{32} = \pm \sqrt{v_3^2 - 2v_3v_2\cos\alpha_1 + v_2^2} + \epsilon v_3v_2a_1\sin\alpha_1$$
 (2.33a)

and

$$\tan \theta_2 + \epsilon b_2 (1 + \tan^2 \theta_2) = \frac{v_3 \sin \alpha_1}{v_3 \cos \alpha_1 - v_2} + \epsilon \left[\frac{v_3^2 - v_3 v_2 \cos \alpha_1}{(v_3 \cos \alpha_1 - v_2)^2} \right] a_1$$
 (2.33b)

The dual part of the left-hand side of eq.(2.33a) is zero, and hence,

$$v_3v_2a_1\sin\alpha_1=0$$

In general, $v_i \neq 0$, for i = 2, 3, and $\sin \alpha_1 \neq 0$. Thus, for the above equation to hold, a_1 must vanish. Consequently, from the dual part of eq.(2.33b), $b_2 = 0$.

Moreover, from eq.(2.30), one can define the relationship

$$v_3 \equiv \frac{dz_3}{dt} = \frac{dz_3}{dz_2} \frac{dz_2}{dt} = z_3' v_2 \tag{2.34}$$

Thus, with the aid of eq.(2.34), v_{32} and θ_2 can be written as

$$v_{32} = \pm \sqrt{z_3'^2 - 2z_3' \cos \alpha_1 + 1} v_2 \tag{2.35a}$$

$$\tan \theta_2 = \frac{z_3' \sin \alpha_1}{z_3' \cos \alpha_1 - 1} \tag{2.35b}$$

from which we can draw the conclusions below:

- i) The coupling between cam and follower is a prismatic pair.
- ii) Since $a_1 = b_2 = 0$, the three ISAs are concurrent.

2.3 Pressure Angle

In some cam mechanisms, as we will see in Chapter 5, the cam may play temporarily the role of the driven element; correspondingly, the follower may play temporarily the role of the driving element. For this reason, we distinguish here between direct and inverse operation of the mechanism. The direct operation is defined as that in which the cam is the driving element, the inverse operation being that in which the cam is the driven element.

Henceforth we assume that the cam and follower are bounded by the ruled surfaces \mathcal{R}_2 and \mathcal{R}_3 , respectively. The pressure angle μ_i is then defined as that subtended between the direction of the unit normal to \mathcal{R}_i and the direction of the velocity of the contact point as pertaining to the driven element, which is bounded by \mathcal{R}_i , for i=2,3. Since contact takes place along a line, μ_i is derived as a function of λ , which is a parameter defined along that line.

Let $\mathbf{r}_i(\psi, \lambda)$ be the position vector of a point of the ruled surface \mathcal{R}_i , defined as

$$\mathbf{r}_{i}(\psi,\lambda) = \mathbf{p}_{i}(\psi) + \lambda \mathbf{e}_{i}(\psi) \tag{2.36}$$

The normal vector \mathbf{n}_i of \mathcal{R}_i is determined as in eq.(C.3), namely,

$$\mathbf{n}_i(\psi, \lambda) = \frac{\mathbf{u}_i}{\|\mathbf{u}_i\|}; \ \mathbf{u}_i = \frac{\partial \mathbf{r}_i}{\partial \psi} \times \frac{\partial \mathbf{r}_i}{\partial \lambda}$$

In terms of eq. (2.36), $n_i(\psi, \lambda)$ becomes

$$\mathbf{n}_i = \frac{\mathbf{m}_i}{\parallel \mathbf{m}_i \parallel}; \qquad \mathbf{m}_i = (\mathbf{p}_i' + \lambda \mathbf{e}_i') \times \mathbf{e}_i \tag{2.37}$$

the prime denoting differentiation with respect to ψ .

Moreover, the unit vector \mathbf{w}_i , parallel to the follower velocity at the contact point, is obtained as

$$\mathbf{w}_{i} = \frac{\boldsymbol{\xi}_{i}}{\parallel \boldsymbol{\xi}_{i} \parallel}; \qquad \boldsymbol{\xi}_{i} = \boldsymbol{\omega}_{i} \times \mathbf{r}_{i}$$
 (2.38)

Once n; and w; are known, the pressure angle is derived from the relation

$$\tan \mu_i = \frac{\parallel \mathbf{n}_i \times \mathbf{w}_i \parallel}{\mathbf{n}_i \cdot \mathbf{w}_i} \tag{2.39}$$

The value of μ_i for the spatial mechanism changes at every point of the contact line. In order to derive a significant value of μ_i for this case, we define it along the striction curve (DoCarmo 1976), which is the curve of the central points of \mathcal{R}_i , at which λ attains the value λ_S given below:

$$\lambda_S = -\frac{\mathbf{p}_i' \cdot \mathbf{e}_i'}{\mathbf{e}_i' \cdot \mathbf{e}_i'} \tag{2.40}$$

and hence, μ_i is defined as

$$\mu_i \equiv \mu_i(\lambda_S) \tag{2.41}$$

The striction curve can be interpreted as follows: Given a ruled surface \mathcal{R} , consider two infinitesimally separated generators e and e' = e + de and their common perpendicular PP', as shown in Fig. 2.2. Then, point P is the central point of the generator e and the locus of the central points define the striction curve.

Thus, the central circle of an axially-symmetric hyperboloid \mathcal{H} is the striction curve of \mathcal{H} , whereas the striction curve is undetermined in cylindrical surfaces and reduces to a point in conical surfaces.

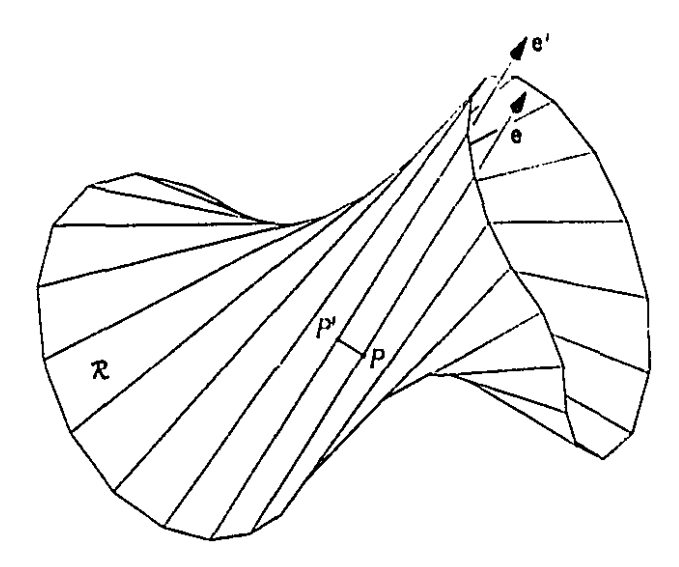


Figure 2.2 Graphical interpretation of the striction curve

2.3.1 Pressure Angle of RHR Mechanisms

General expressions of the pressure angle for both direct and inverse operations are derived using RHR cam mechanisms. The pressure angle for other types can be obtained following the same procedure presented here.

Direct Operation

The pressure angle is obtained in this case for i = 3. Following the procedure mentioned above, the unit normal is written as

$$n_3 = \frac{(p_3' + \lambda e_3') \times e_3}{\parallel m_3 \parallel}$$
 (2.42)

where the prime denotes differentiation with respect to ψ .

From eq. (2.18b), we obtain

$$\mathbf{p}_{3}' = \begin{bmatrix} -d\phi'\sin\phi + b_{2}'\cos\phi \\ -d\phi'\cos\phi - b_{2}'\sin\phi \\ 0 \end{bmatrix}$$
(2.43)

t:

Chapter 2. Kinematics of Three-Link Mechanisms

and

$$\mathbf{e}_{3}' = \begin{bmatrix} -\phi' \cos \phi \sin \beta - \theta_{2}' \sin \phi \cos \beta \\ \phi' \sin \phi \sin \beta - \theta_{2}' \cos \phi \cos \beta \\ -\theta_{2}' \sin \beta \end{bmatrix}$$
(2.44)

 θ_2' and θ_2' being derived from eqs. (2.16c & 2.16d), namely,

$$\theta_2' = -\frac{\phi'' \sin \alpha_1}{c} \tag{2.45a}$$

and

$$b_2' = \frac{2\phi' - (\phi'^2 + 1)\cos\alpha_1}{c^2}\phi''a_1 \tag{2.45b}$$

where c is defined as in eq. (2.17). Combining eqs. (2.42-2.44), we obtain the desired expression for n_3 , i.e.,

$$\mathbf{n}_{3} = \begin{bmatrix} -(d\phi'c\phi + b'_{2}s\phi)c\beta + \lambda(\phi's\phi s\beta c\beta - \theta'_{2}c\phi) \\ (d\phi's\phi - b'_{2}c\phi)c\beta + \lambda(\phi'c\phi s\beta c\beta + \theta'_{2}s\phi) \\ -b'_{2}s\beta + \lambda\phi's^{2}\beta \end{bmatrix} \frac{1}{\parallel \mathbf{m}_{3} \parallel}$$
(2.46)

Now, w₃ can be written as

$$\mathbf{w}_{3} = \begin{bmatrix} d\sin\phi + \lambda\cos\phi\sin\beta \\ d\cos\phi - \lambda\sin\phi\sin\beta \\ 0 \end{bmatrix} \frac{1}{\parallel \boldsymbol{\xi}_{3} \parallel}$$
 (2.47)

the cross product of the right-hand side of eq. (2.39) being computed as

$$\mathbf{n}_{3} \times \mathbf{w}_{3} = \begin{bmatrix} db'_{2}c\phi s\beta + \lambda s^{2}\beta(b'_{2}s\phi + \phi'dc\phi) - \lambda^{2}\phi's\phi s^{3}\beta \\ -db'_{2}s\phi s\beta - \lambda s^{2}\beta(b'_{2}c\phi - \phi'ds\phi) + \lambda^{2}\phi'c\phi s^{3}\beta \\ -d^{2}\phi'c\beta - \lambda(d\theta'_{2} - b'_{2}s\beta c\beta) - \lambda^{2}\phi's^{2}\beta c\beta \end{bmatrix} \frac{1}{\parallel \boldsymbol{\xi}_{3} \parallel \parallel \mathbf{m}_{3} \parallel}$$
(2.48)

whose magnitude is given by

$$\| \mathbf{n}_3 \times \mathbf{w}_3 \| = \frac{\sqrt{A\lambda^4 + B\lambda^3 + C\lambda^2 + D\lambda + E}}{\| \boldsymbol{\xi}_3 \| \| \mathbf{m}_3 \|}$$
 (2.49)

with the definitions shown below:

$$A = \phi'^2 s^4 \beta \tag{2.50a}$$

$$B = Fs^2\beta \tag{2.50b}$$

$$C = (b_2'^2 + {\phi'}^2 d^2) s^2 \beta + (\theta_2'^2 + {\phi'}^2 s^2 \beta c^2 \beta) d^2 - 2db_2' \theta_2' s \beta c \beta$$
 (2.50c)

$$D = Fd^2 \tag{2.50d}$$

$$E = d^2(b_2'^2 s^2 \beta + d^2 \phi'^2 c^2 \beta)$$
 (2.50e)

$$F = 2\phi'(d\theta_2'c\beta - b_2's\beta) \tag{2.50f}$$

Furthermore, the dot product of the right-hand side of eq. (2.39) is readily obtained as

$$\mathbf{n}_3 \cdot \mathbf{w}_3 = -\frac{db_2' \cos \beta + \lambda^2 \theta_2' \sin \beta}{\|\boldsymbol{\xi}_3\| \|\mathbf{m}_3\|}$$
 (2.51)

Finally, combining eqs. (2.39, 2.48 & 2.51), the tangent of the pressure angle takes on the form

$$\tan \mu_3 = -\frac{\sqrt{A\lambda^4 + B\lambda^3 + C\lambda^2 + D\lambda + E}}{db_2' \cos \beta + \lambda^2 \theta_2' \sin \beta}$$
 (2.52)

For the planar case, $\alpha_1=0$, and hence, $\theta_2=\beta=\theta_2'=0$, A=B=C=D=0, and $E=d^4\phi'^2$. Substituting all these values into eq. (2.52), $\tan\mu_3$ reduces to

$$\tan \mu_3 = -\frac{d}{b_2'}\phi' = \frac{\phi'(\phi'-1)}{\phi''} \tag{2.53}$$

For the spherical case, the pressure angle is obtained by taking the limit of $\tan \mu_3$ as λ tends to infinity (DoCarmo, 1976) in eq. (2.52), namely,

$$\tan \mu_3 = \lim_{\lambda \to \infty} -\frac{\sqrt{A\lambda^4 + B\lambda^3 + C\lambda^2 + D\lambda + E}}{db_2' \cos \beta + \lambda^2 \theta_2' \sin \beta} = -\frac{\phi' \sin \beta}{\theta_2'}$$
 (2.54)

Manipulating the expression for $\sin \beta$, eq. (2.54) can be readily rewritten as

$$\tan \mu_3 = \frac{\phi'}{\phi''} \sqrt{c} \tag{2.55}$$

with c defined as in eq. (2.17).

If c is evaluated for $\alpha_1 = 0$, $\sqrt{c} = \phi' - 1$. Therefore, eq. (2.53) is a particular case of eq. (2.55).

For the spatial case, eq. (2.52) is evaluated at the striction point, i.e., at λ_S as given by eq. (2.40), which, in terms of eqs. (2.43 & 2.44), becomes

$$\lambda_S = -\phi' \frac{\theta_2' d \cos \beta - b_2' \sin \beta}{\theta_2'^2 + \phi'^2 \sin^2 \beta}$$
 (2.56)

But,

$$\sin \beta \equiv \sin(\theta_2 - \alpha_1) = \frac{\sin \alpha_1}{\sqrt{c}} \tag{2.57a}$$

$$\cos \beta \equiv \cos(\theta_2 - \alpha_1) = \frac{\phi' - \cos \alpha_1}{\sqrt{c}} \tag{2.57b}$$

$$d \equiv b_2 - a_1 = \frac{\phi' \cos \alpha_1 - 1}{c} a_1 \tag{2.57c}$$

and now, substituting eqs.(2.45 and 2.57) into eq.(2.56), one obtains,

$$\lambda_S = \frac{\phi'^2 \phi'' \sin \alpha_1 \sqrt{c}}{(\phi'^2 c + \phi''^2)c} a_1 \tag{2.58}$$

which is the expression determining the point at which the pressure angle is evaluated.

Inverse operation

Here, the cam is considered as the driven element; therefore, we derive the expression for the pressure angle using i = 2. Following the same steps as those for the direct operation, one can readily obtain the expression for the pressure angle as

$$\tan \mu_2 = -\frac{\sqrt{\tilde{A}\lambda^4 + \tilde{B}\lambda^3 + \tilde{C}\lambda^2 + \tilde{D}\lambda + \tilde{E}}}{b_2 b_2' \cos \theta + \lambda^2 \theta_2' \sin \theta}$$
 (2.59)

where

$$\tilde{A} = s^4 \theta_2 \tag{2.60a}$$

$$\tilde{B} = \tilde{F}s^2\theta_2 \tag{2.60b}$$

$$\tilde{C} = (b_2'^2 + b_2^2)s^2\theta_2 + (\theta_2'^2 + s^2\theta_2c^2\theta_2)b_2^2 - 2b_2b_2'\theta_2's\theta_2c\theta_2$$
 (2.60c)

$$\tilde{D} = \tilde{F}b_2^2 \tag{2.60d}$$

$$\tilde{E} = b_2^2 (b_2'^2 s^2 \theta_2 + b_2^2 \cos^2 \theta_2) \tag{2.60e}$$

$$\tilde{F} = 2(b_2 \theta_2' \cos \theta_2 - b_2' \sin \theta_2) \tag{2.60f}$$

For the planar case, $\alpha_1=0$, and hence, $\theta_2=\theta_2'=0$, $\tilde{A}=\tilde{B}=\tilde{C}=\tilde{D}=0$ and $\tilde{E}=b_2^4$.

Substituting all these values into eq. (2.59), $\tan \mu_2$ reduces to

$$\tan \mu_2 = -\frac{b_2}{b_2'} = \frac{\phi'(\phi' - 1)}{\phi''} \tag{2.61}$$

For the spherical case, the pressure angle is obtained by taking the limit of $\tan \mu_2$ as λ tends to infinity in eq. (2.59), namely,

$$\tan \mu_2 = \lim_{\lambda \to \infty} -\frac{\sqrt{\tilde{A}\lambda^4 + \tilde{B}\lambda^3 + \tilde{C}\lambda^2 + \tilde{D}\lambda + \tilde{E}}}{b_2 b_2' \cos \theta + \lambda^2 \theta_2' \sin \theta} = -\frac{\sin \theta}{\theta_2'} \equiv \frac{\phi'}{\phi''} \sqrt{c}$$
 (2.62)

where c is defined as in eq.(2.17)

For the spatial case, eq. (2.52) is evaluated at the value of λ given by eq. (2.40), namely, at

$$\lambda_S = -\frac{b_2 \theta_2' \cos \theta_2 - b_2' \sin \theta_2}{\theta_2'^2 + \sin^2 \theta_2}$$
 (2.63)

But

$$\sin \theta_2 = \frac{\phi' \sin \alpha_1}{\sqrt{c}} \tag{2.64a}$$

$$\cos \theta_2 = \frac{\phi' \cos \alpha_1 - 1}{\sqrt{c}} \tag{2.64b}$$

Now, substituting eqs.(2.16d, 2.45 and 2.64) into eq.(2.63), one obtains,

$$\lambda_S = \frac{\phi'^2 \phi'' \sin \alpha \sqrt{c}}{(\phi'^2 c + \phi''^2)c} a_1 \tag{2.65}$$

Note that the results outlined above are apparent for spur, bevel and hypoid gears as well, in which the pressure angle on the pitch surfaces is 90°, and hence, no motion transmission is possible with the pitch surfaces. The tooth geometry makes this transmission possible at a constant pressure angle (Dudley, 1962). This result is easily obtained from either eq. (2.52) or eq. (2.59). In fact, for all these cases, eq. (2.14) takes on the form

$$\phi = k\psi, \qquad k = \text{constant}$$
 (2.66)

where k is the transmission ratio. From eq. (2.66), $\phi' = k$ and $\phi'' = 0$. Substitution of these two values into eqs. (2.45a & 2.45b) leads to $b_2' = 0$ and $\theta_2' = 0$. Consequently, the denominator of the right-hand side of either eq. (2.52) or eq. (2.59) vanishes, as expected.

2.3.2 Pressure Angle of RHP Mechanisms

The pressure angle of RHP mechanisms is also derived with the procedure presented in Section 2.3.1. Thus, from eqs. (2.22), the pressure angle for both direct and inverse operations can be readily obtained as,

$$\tan \mu_3 = \frac{\sqrt{(z_3'' s \alpha_1 c \alpha_1)^2 + z_3'^2 s^2 \alpha_1 (c^2 \alpha_1 + s \alpha_1)^2}}{-z_3'' s \alpha_1}$$

$$\tan \mu_2 = \frac{\sqrt{(z_3'' s \alpha_1 c \alpha_1)^2 + z_3'^2 s^2 \alpha_1 (c^2 \alpha_1 + 1)}}{-z_3'' s \alpha_1}$$
(2.67a)

$$\tan \mu_2 = \frac{\sqrt{(z_3'' s \alpha_1 c \alpha_1)^2 + z_3'^2 s^2 \alpha_1 (c^2 \alpha_1 + 1)}}{-z_3'' s \alpha_1}$$
(2.67b)

Notice that, for $\alpha_1 = \pm \pi/2$,

$$\tan \mu_3 = \tan \mu_2 = \frac{z_3'}{-z_3''} \tag{2.68}$$

Pressure Angle of PHR Mechanisms 2.3.3

The pressure angle for PHR mechanisms for direct and inverse operations is obtained from eqs.(2.29), namely,

$$\tan \mu_3 = \tan \mu_2 = \frac{\sqrt{\phi''^2 c^2 \alpha_1 + \phi'^4}}{s\alpha_1}$$
 (2.69)

Pressure Angle of PPP Mechanisms 2.3.4

From the results presented in Section 2.2.4, one can obtain the expressions for the contact surfaces of PPP mechanisms, and then, the pressure angle can be computed. Following this procedure, the pressure angle is found to be $\pi/2$ and no transmission is possible with this type of mechanisms. Nevertheless, with the introduction of a fourth body, i.e., a roller, a feasible mechanism is possible, as discussed in Chapter 3.

Chapter 3

Kinematics of Four-Link

Mechanisms

3.1 Introduction

This chapter is devoted to the study of cam mechanisms with four links. This study includes three-link mechanisms with a flat-face follower because these are synthesized with the aid of an auxiliary roller.

One fourth dual sphere S_4 , which represents the roller, is added to the three already considered in Chapter 2. Thus, a total of six ISAs arise now and, according to the Aronhold-Kennedy Theorem, there are four great circles having three poles each, namely, C_{123} : $\{\hat{P}_{21}, \hat{P}_{32}, \hat{P}_{31}\}$, C_{234} : $\{\hat{P}_{32}, \hat{P}_{42}, \hat{P}_{43}\}$, C_{341} : $\{\hat{P}_{43}, \hat{P}_{31}, \hat{P}_{41}\}$ and C_{412} : $\{\hat{P}_{41}, \hat{P}_{42}, \hat{P}_{21}\}$. The polodes generated by \hat{P}_{43} and \hat{P}_{42} over S_2 are the dual curves of the pitch and contact surfaces of the cam. The former is applied to derive the pressure angle.

Now, a great circle on a unit dual sphere can be defined with at least two points. Thus, C_{123} and C_{341} , shown in Fig. 3.1a, are defined by the given poles \hat{P}_{21} , \hat{P}_{31} and \hat{P}_{43} . Moreover, \hat{P}_{32} is computed according to the results obtained in Chapter 2. Once

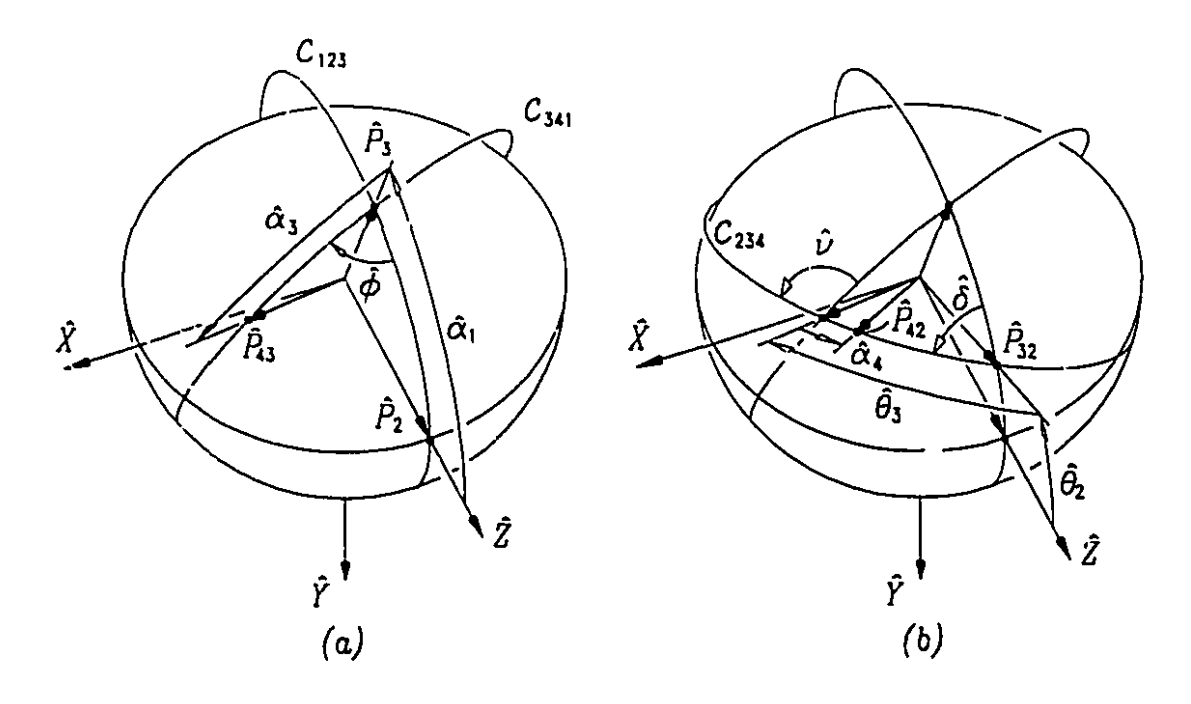


Figure 3.1 Mapping of the geometry of four-link cam mechanisms, onto the dual sphere.

 \hat{P}_{32} is obtained, both \hat{P}_{43} and \hat{P}_{32} define C_{234} , as shown in Fig. 3.1b. Finally, \hat{P}_{42} is located by the given dual radius of the roller, represented by $\hat{\alpha}_4$. The given parameters as well as the unknown variables for the synthesis of four-link cam mechanisms are shown in Table 3.1.

The components of the unit dual vector $\hat{\mathbf{e}}$ in the frame \mathcal{F}_i are represented by $[\hat{\mathbf{e}}]_i$. In order to simplify notation, the symbol $[\cdot]_i$ will be omitted for those vectors given in the frame fixed to \mathcal{S}_2 .

3.2 Roller-Followers

It was mentioned above that the dual curve generated by the motion of \hat{P}_{43} on S_2 represents the pitch surface of the cam, which is given by

$$\hat{\mathbf{s}}_p(t) \equiv \mathbf{e}_{43} + \epsilon \mathbf{m}_{43} = \mathbf{S}^T(\hat{\psi}) \mathbf{Q}(\hat{\alpha}_1) \mathbf{S}(\hat{\phi}) \mathbf{Q}(\hat{\alpha}_3) \mathbf{k}$$
(3.1)

Table 3.1 Notation used for the synthesis of four-link cam mechanisms

Given parameters:	
$\hat{\alpha}_1 = \alpha_1 + \epsilon a_1$	Dual angle between input and output axes
$\hat{\alpha}_3 = \alpha_3 + \epsilon a_3$	Dual angle between output and roller axes
$\hat{\alpha}_4 = \alpha_4 + \epsilon a_4$	Dual angle of the roller
$\hat{\psi} = \psi + \epsilon z_2$	Dual angle of rotation of the cam
$\hat{\phi} = \phi + \epsilon z_3$	Dual angle of rotation of the follower
Unknown variables:	
$\hat{\theta}_2 = \theta_2 + \epsilon b_2$	Dual arc $\hat{P}_2\hat{P}_{32}$
$\hat{\theta}_3 = \theta_3 + \epsilon b_3$	Dual arc $\hat{P}_{32}\hat{P}_{43}$
$\hat{\delta} = \delta + \epsilon z_{32}$	Dual angle between arc $\hat{P}_{32}\hat{P}_3$ and arc $\hat{P}_{32}\hat{P}_{43}$
$\hat{\nu} = . + \epsilon z_{43}$	Dual angle between arc $\hat{P}_3\hat{P}_{34}$ and arc $\hat{P}_{32}\hat{P}_{43}$

where $\hat{\mathbf{Q}}$, $\hat{\mathbf{S}}$ and \mathbf{k} are defined, respectively, in eqs.(A.11a, A.11c & 2.2).

From eq. (A.8), the point coordinates of the pitch ruled surface \mathcal{R}_p are defined as

$$\mathbf{r}_{p}(t,\lambda) = \mathbf{p}_{43}(t) + \lambda \mathbf{e}_{43}(t)$$
 (3.2)

where $p_{43} = e_{43} \times m_{43}$.

Thus, e_{43} , m_{43} and p_{43} can be readily computed as

$$\mathbf{e}_{43} = [-h_1, -h_2, k_1]^T$$
 (3.3a)

$$\mathbf{m}_{43} = \begin{bmatrix} -k_1 s \psi a_1 - k_3 a_3 - k_2 z_2 + k_5 s \alpha_3 z_3 \\ -k_1 c \psi a_1 - k_4 a_3 + k_1 z_2 - k_6 s \alpha_3 z_3 \\ -k_3 a_1 - k_4 a_3 + k_7 z_3 \end{bmatrix}$$
(3.3b)

$$p_{43} = \begin{bmatrix} (h_2k_3 + k_1^2c\psi)a_1 + (h_2k_4 + h_4k_1)a_3 \\ -k_1h_1z_2 + (k_1k_6s\alpha_3 - k_7h_2)z_3 \\ -(h_1k_3 + k_1^2s\psi)a_1 - (h_1k_4 + h_3k_1)a_3 \\ -k_1h_2z_2 + (k_1k_5s\alpha_3 + k_7h_1)z_3 \end{bmatrix}$$

$$(3.3c)$$

$$(h_1c\psi - h_2s\psi)k_1a_1 + (h_1h_4 - h_2h_3)a_3 \\ -(h_1^2 + h_2^2)z_2 + (h_2k_5 + h_1k_6)s\alpha_3z_3 \end{bmatrix}$$

where

$$k_1 = c\alpha_1 c\alpha_3 - s\alpha_1 s\alpha_3 c\phi \tag{3.4a}$$

$$k_2 = c\alpha_1 c\alpha_3 c\phi - s\alpha_1 s\alpha_3 \tag{3.4b}$$

$$k_3 = s\alpha_1 c\alpha_3 + c\alpha_1 s\alpha_3 c\phi \tag{3.4c}$$

$$k_4 = s\alpha_3 c\alpha_1 + c\alpha_3 s\alpha_1 c\phi \tag{3.4d}$$

$$k_5 = c\psi c\phi + s\psi s\phi c\alpha_1 \tag{3.4e}$$

$$k_6 = s\psi c\phi - c\psi s\phi c\alpha_1 \tag{3.4f}$$

$$k_7 = s\alpha_1 s\alpha_3 s\phi \tag{3.4g}$$

$$h_1 = k_3 s \psi - s \alpha_3 s \phi c \psi \tag{3.4h}$$

$$h_2 = k_3 c \psi + s \alpha_3 s \phi s \psi \tag{3.4i}$$

$$h_3 = k_2 s \psi - c \alpha_3 s \phi c \psi \tag{3.4j}$$

$$h_4 = k_2 c \psi + c \alpha_3 s \phi s \psi \tag{3.4k}$$

Now, the dual curve representing the surface of the cam is defined by the trajectory that \hat{P}_{42} traces on \mathcal{S}_2 , namely,

$$\hat{\mathbf{s}}_C(t) \equiv \mathbf{e}_{42} + \epsilon \mathbf{m}_{42} = \hat{\mathbf{S}}^T(\hat{\psi}) \hat{\mathbf{Q}}(\hat{\theta}_2) \hat{\mathbf{S}}(\hat{\delta}) \hat{\mathbf{Q}}(\hat{\eta}) \mathbf{k}$$
(3.5)

Furthermore, in order to completely define s_C , $\hat{\theta}_2$ is computed from eqs. (2.10). The derivation to obtain the dual angles $\hat{\eta}$ and $\hat{\delta}_2$ is presented below. The former is

defined as

$$\hat{\eta} \equiv \eta + \epsilon(b_3 - a_4) = \hat{\theta}_3 - \hat{\alpha}_4 \tag{3.6}$$

 $\hat{\alpha}_4$ representing the dual radius of the roller.

Moreover, $\hat{\theta}_3$ is obtained from the relation

$$\tan \hat{\theta}_3 = \frac{\hat{\mathbf{e}}_{32} \times \hat{\mathbf{e}}_{43} \cdot \hat{\mathbf{e}}_{234}}{\hat{\mathbf{e}}_{32} \cdot \hat{\mathbf{e}}_{43}} \tag{3.7}$$

where the vectors appearing in the right-hand side can be expressed in any frame, as long as all are in the same frame, for the cross and dot products are frame invariant. If these vectors are expressed in frame \mathcal{F}_1 , fixed to \mathcal{S}_1 , then,

$$[\hat{\mathbf{e}}_{32}]_1 = \hat{\mathbf{Q}}(\hat{\theta}_2)\mathbf{k} \tag{3.8a}$$

$$[\hat{\mathbf{e}}_{43}]_1 = \hat{\mathbf{Q}}(\hat{\alpha}_1)\hat{\mathbf{S}}(\hat{\phi})\hat{\mathbf{Q}}(\hat{\alpha}_3)\mathbf{k}$$
(3.8b)

and [ê234]1 is defined as

$$[\hat{\mathbf{e}}_{234}]_1 = \frac{[\hat{\mathbf{e}}_{32}]_1 \times [\hat{\mathbf{e}}_{43}]_1}{\|[\hat{\mathbf{e}}_{32}]_1 \times [\hat{\mathbf{e}}_{43}]_1\|}$$
(3.9)

On the other hand, the dual angle δ , shown in Figure 3.1, is obtained as

$$\tan \hat{\delta} = \frac{[\hat{\mathbf{e}}_{123}]_1 \times [\hat{\mathbf{e}}_{234}]_1 \cdot [\hat{\mathbf{e}}_{32}]_1}{[\hat{\mathbf{e}}_{123}]_1 \cdot [\hat{\mathbf{e}}_{234}]_1}$$
(3.10)

where

7.11 1.

$$[\hat{\mathbf{e}}_{123}]_1 = [1, 0, 0]^T$$
 (3.11)

From eqs. (A.8 & 3.5), the point coordinates of the ruled surface of the cam are given as

$$\mathbf{r}_{C}(t,\lambda) = \mathbf{p}_{42}(t) + \lambda \mathbf{e}_{42}(t)$$
 (3.12)

1

where $p_{42}(t) = e_{42} \times m_{42}$.

The transformation dual matrices in eq.(3.5) are the same as those in eq.(3.1), but with different arguments; therefore, the results given for e42, m42 and p42 are

1

11

37

Chapter 3. Kinematics of Four-Link Mechanisms

analogous to those of eqs.(3.3), namely,

$$\mathbf{e}_{42} = [-\tilde{h}_1, -\tilde{h}_2, \tilde{k}_1]^T \tag{3.13a}$$

$$\mathbf{m}_{42} = \begin{bmatrix} -\tilde{k}_1 s \psi b_2 - \tilde{h}_3 (b_3 - a_4) - \tilde{h}_2 z_2 + \tilde{k}_5 s \eta z_{32} \\ -\tilde{k}_1 c \psi b_2 - \tilde{h}_4 (b_3 - a_4) + \tilde{h}_1 z_2 - \tilde{k}_6 s \eta z_{32} \\ -\tilde{k}_3 b_2 - \tilde{k}_4 (b_3 - a_4) + \tilde{k}_7 z_{32} \end{bmatrix}$$
(3.13b)

$$\mathbf{p}_{42} = \begin{bmatrix} (\tilde{h}_{2}\tilde{k}_{3} + \tilde{k}_{1}^{2}c\psi)b_{2} + (\tilde{h}_{2}\tilde{k}_{4} + \tilde{h}_{4}\tilde{k}_{1})(b_{3} - a_{4}) \\ -\tilde{k}_{1}\tilde{h}_{1}z_{2} + (\tilde{k}_{1}\tilde{k}_{6}s\eta - \tilde{k}_{7}\tilde{h}_{2})z_{32} \end{bmatrix}$$

$$-(\tilde{h}_{1}\tilde{k}_{3} + \tilde{k}_{1}^{2}s\psi)b_{2} - (\tilde{h}_{1}\tilde{k}_{4} + \tilde{h}_{3}\tilde{k}_{1})(b_{3} - a_{4}) \\ -\tilde{k}_{1}\tilde{h}_{2}z_{2} + (\tilde{k}_{1}\tilde{k}_{5}s\eta + \tilde{k}_{7}\tilde{h}_{1})z_{32} \end{bmatrix}$$

$$(3.13c)$$

$$(\tilde{h}_{1}c\psi - \tilde{h}_{2}s\psi)\tilde{k}_{1}b_{2} + (\tilde{h}_{1}\tilde{h}_{4} - \tilde{h}_{2}\tilde{h}_{3})(b_{3} - a_{4}) \\ -(\tilde{h}_{1}^{2} + \tilde{h}_{2}^{2})z_{2} + (\tilde{h}_{2}\tilde{k}_{5} + \tilde{h}_{1}\tilde{k}_{6})s\eta z_{32} \end{bmatrix}$$

where

$$\tilde{k}_1 = c\theta_2 c\eta - s\theta_2 s\eta c\delta \tag{3.14a}$$

$$\tilde{k}_2 = c\theta_2 c\eta c\delta - s\theta_2 s\eta \tag{3.14b}$$

$$\tilde{k}_3 = s\theta_2 c\eta + c\theta_2 s\eta c\delta \tag{3.14c}$$

$$\tilde{k}_4 = s\eta c\theta_2 + c\eta s\theta_2 c\delta \tag{3.14d}$$

$$\tilde{k}_5 = c\psi c\delta + s\psi s\delta c\theta_2 \tag{3.14e}$$

$$\tilde{k}_6 = s\psi c\delta - c\psi s\delta c\theta_2 \tag{3.14f}$$

$$\tilde{k}_7 = s\theta_2 s\eta s\delta \tag{3.14g}$$

$$\tilde{h}_1 = \tilde{k}_3 s \psi - s \eta s \delta c \psi \tag{3.14h}$$

$$\tilde{h}_2 = \tilde{k}_3 c \psi + s \eta s \delta s \psi \tag{3.14i}$$

$$\tilde{h}_3 = \tilde{k}_2 s \psi - c \eta s \delta c \psi \tag{3.14j}$$

===-,

11

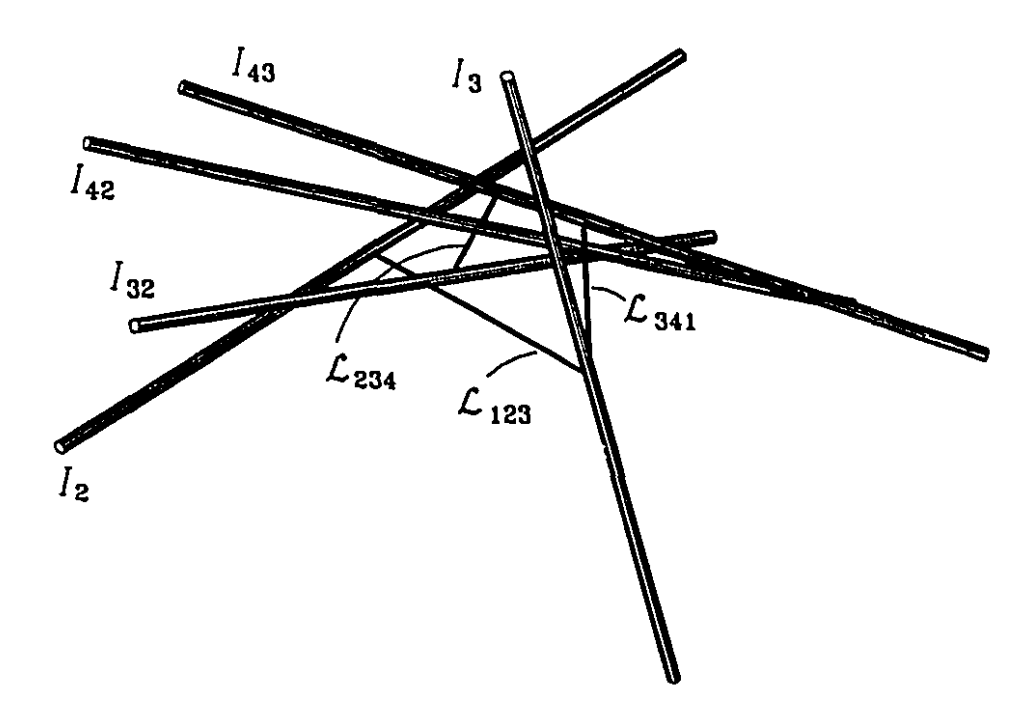


Figure 3.2 ISAs of an RHCR cam mechanism

$$\tilde{h}_4 = \tilde{k}_2 c \psi + c \eta s \delta s \psi \tag{3.14k}$$

In order to avoid undercutting, the dual angle $\hat{\alpha}_4$ must be constrained by

$$\hat{\alpha}_4 < \hat{\rho}_{min} \tag{3.15}$$

where $\hat{\rho}_{min}$ is the minimum value of the dual radius of curvature of the dual pitch curve of the cam, and is evaluated according to eq.(C.15).

Now, the dual angle $\hat{\nu} = \nu + \epsilon z_{43}$ can be computed as

$$\tan \hat{\nu} = \frac{\hat{e}_{341} \times \hat{e}_{234} \cdot \hat{e}_{43}}{\hat{e}_{341} \cdot \hat{e}_{234}}$$
(3.16)

where

$$\hat{\mathbf{e}}_{341} = \frac{\hat{\mathbf{e}}_{31} \times \hat{\mathbf{e}}_{43}}{\sin \hat{\alpha}_3} \tag{3.17}$$

The axial motion of the roller with respect to the follower is defined by z_{43} . In general, $z_{43} = z_{43}(t)$, the roller-follower pair being cylindrical; however, a revolute pair is present when z_{43} is constant.

Now, in order to derive the expressions for $\hat{\omega}_{42}$ and $\hat{\omega}_{43}$, the Aronhold-Kennedy Theorem, as defined in eq.(B.5), is applied to the poles of the great circle C_{234} , namely,

$$\hat{\omega}_{32}[\hat{\mathbf{e}}_{32}]_1 = \hat{\omega}_{42}[\hat{\mathbf{e}}_{42}]_1 + \hat{\omega}_{43}[\hat{\mathbf{e}}_{43}]_1 \tag{3.18}$$

with

$$[\hat{\mathbf{e}}_{32}]_1 = \hat{\mathbf{Q}}(\hat{\theta}_2)\mathbf{k} \tag{3.19a}$$

$$[\hat{\mathbf{e}}_{42}]_1 = \hat{\mathbf{Q}}(\hat{\alpha}_1)\hat{\mathbf{S}}(\hat{\phi})\hat{\mathbf{Q}}(\hat{\alpha}_3)\hat{\mathbf{S}}(\hat{\nu})\hat{\mathbf{Q}}(\hat{\alpha}_4)\mathbf{k}$$
(3.19b)

$$[\hat{\mathbf{e}}_{43}]_1 = \hat{\mathbf{Q}}(\hat{\alpha}_1)\hat{\mathbf{S}}(\hat{\phi})\hat{\mathbf{Q}}(\hat{\alpha}_3)\mathbf{k}$$
(3.19c)

Substituting eqs.(3.19) into eq.(3.18) and multiplying both sides by $\hat{\mathbf{Q}}^T(\hat{\theta}_2)$, one obtains

$$\hat{\omega}_{32}\mathbf{k} = \hat{\omega}_{42}\hat{\mathbf{Q}}(\hat{\boldsymbol{\beta}})\hat{\mathbf{S}}(\hat{\boldsymbol{\phi}})\hat{\mathbf{Q}}(\hat{\alpha}_3)\hat{\mathbf{S}}(\hat{\boldsymbol{\nu}})\hat{\mathbf{Q}}(\hat{\alpha}_4)\mathbf{k} + \hat{\omega}_{43}\hat{\mathbf{Q}}(\hat{\boldsymbol{\beta}})\hat{\mathbf{S}}(\hat{\boldsymbol{\phi}})\hat{\mathbf{Q}}(\hat{\alpha}_3)\mathbf{k}$$
(3.20)

Notice that $\hat{\mathbf{Q}}^T(\hat{\theta}_2)\hat{\mathbf{Q}}(\hat{\alpha}_1) = \hat{\mathbf{Q}}(\hat{\beta})$ and $\hat{\beta} = \hat{\alpha}_1 - \hat{\theta}_2$.

From the eq.(3.20), one can readily obtain the relations below:

$$\hat{\omega}_{42} \sin \hat{\alpha}_4 \sin \hat{\nu} = -\hat{\omega}_{32} \sin \hat{\beta} \sin \hat{\phi} \tag{3.21a}$$

$$\hat{\omega}_{42}\sin\hat{\alpha}_4\cos\hat{\nu} = -\hat{\omega}_{32}(\cos\hat{\beta}\sin\hat{\alpha}_3 + \cos\hat{\alpha}_3\cos\hat{\phi}\sin\hat{\beta}) \tag{3.21b}$$

$$\hat{\omega}_{42}\cos\hat{\alpha}_4 = \hat{\omega}_{43} - \hat{\omega}_{32}(\cos\hat{\beta}\cos\hat{\alpha}_3 - \sin\hat{\beta}\sin\hat{\alpha}_3\cos\hat{\phi}) \qquad (3.21c)$$

Thus, from eqs.(3.21a & 3.21c),

$$\hat{\omega}_{42} = -\frac{\sin \hat{\beta} \sin \hat{\phi}}{\sin \hat{\alpha}_4 \sin \hat{\nu}} \hat{\omega}_{32} \tag{3.22a}$$

$$\hat{\omega}_{43} = \hat{\omega}_{42} \cos \hat{\alpha}_4 + \hat{\omega}_{32} (\cos \hat{\beta} \cos \hat{\alpha}_3 - \sin \hat{\beta} \sin \hat{\alpha}_3 \cos \hat{\phi}) \tag{3.22b}$$

Moreover, the dual angle $\hat{\nu}$ can be computed following two approaches, one is based on eq.(3.16), the other consisting of forming the ratio of eq.(3.21a) with respect to eq.(3.21b), namely,

$$\tan \hat{\nu} = \frac{-\sin \hat{\beta} \sin \hat{\phi}}{\cos \hat{\beta} \sin \hat{\alpha}_3 + \cos \hat{\alpha}_3 \cos \hat{\phi} \sin \hat{\beta}}$$
(3.23)

It can thus be proven that both eq.(3.16) and eq.(3.23) lead to the same result. However, for planar mechanisms eq.(3.23) is undetermined. Nevertheless, if planar mechanisms are considered as particular cases of spherical mechanisms, eq.(3.23) can be applied as well, as shown in Subsubsection 3.2.1.

3.2.1 Revolute-Higher-Cylindric-Revolute (RHCR) Mechanisms

For the type of revolute-higher-cylindric-revolute (RHCR) mechanisms, the cam and follower are coupled to the frame via revolute pairs; therefore, $z_2 = z_3 = 0$. Moreover, $\phi = \phi(\psi)$, and eq.(3.2) can be written as

$$\mathbf{r}_{p}(\psi,\lambda) = \mathbf{p}_{43}(\psi) + \lambda \mathbf{e}_{43}(\psi) \tag{3.24}$$

with

$$\mathbf{e}_{43} = \begin{bmatrix} -h_1 \\ -h_2 \\ k_1 \end{bmatrix} \text{ and } \mathbf{p}_{43} = \begin{bmatrix} (h_2k_3 + k_1^2c\psi)a_1 + (h_2k_4 + h_4k_1)a_3 \\ -(h_1k_3 + k_1^2s\psi)a_1 - (h_1k_4 + h_3k_1)a_3 \\ (h_1c\psi - h_2s\psi)k_1a_1 + (h_1h_4 - h_2h_3)a_3 \end{bmatrix}$$
(3.25)

Similarly, eq.(3.12) is expressed as

$$\mathbf{r}_{C}(\psi, \lambda) = \mathbf{p}_{42}(\psi) + \lambda \mathbf{e}_{42}(\psi)$$
 (3.26)

with

$$\mathbf{e}_{42} = \begin{bmatrix} -\tilde{h}_1 \\ -\tilde{h}_2 \\ \tilde{k}_1 \end{bmatrix} \text{ and } \mathbf{p}_{42} = \begin{bmatrix} (\tilde{h}_2 \tilde{k}_3 + \tilde{k}_1^2 c \psi) b_2 + (\tilde{h}_2 \tilde{k}_4 + \tilde{h}_4 \tilde{k}_1) (b_3 - a_4) \\ -(\tilde{h}_1 \tilde{k}_3 + \tilde{k}_1^2 s \psi) b_2 - (\tilde{h}_1 \tilde{k}_4 + \tilde{h}_3 \tilde{k}_1) (b_3 - a_4) \\ (\tilde{h}_1 c \psi - \tilde{h}_2 s \psi) \tilde{k}_1 b_2 + (\tilde{h}_1 \tilde{h}_4 - \tilde{h}_2 \tilde{h}_3) (b_3 - a_4) \end{bmatrix}$$
(3.27)

where $\hat{\theta}_2$, $\hat{\eta}$ and $\hat{\delta}$ are evaluated with the aid of eqs.(2.16c, 2.16d, 3.6 & 3.10).

A geometric representation of the poles of Fig. 3.1 is shown in Fig. 3.2, where $\hat{P}_{ij} \rightarrow I_{ij}$ and $C_{ijk} \rightarrow \mathcal{L}_{ijk}$. Since I_{41} and \mathcal{L}_{412} are not needed for this derivation, they do not appear in Fig. 3.2. Moreover, if $\hat{\alpha}_4$ is a constant, the surface of the roller

8

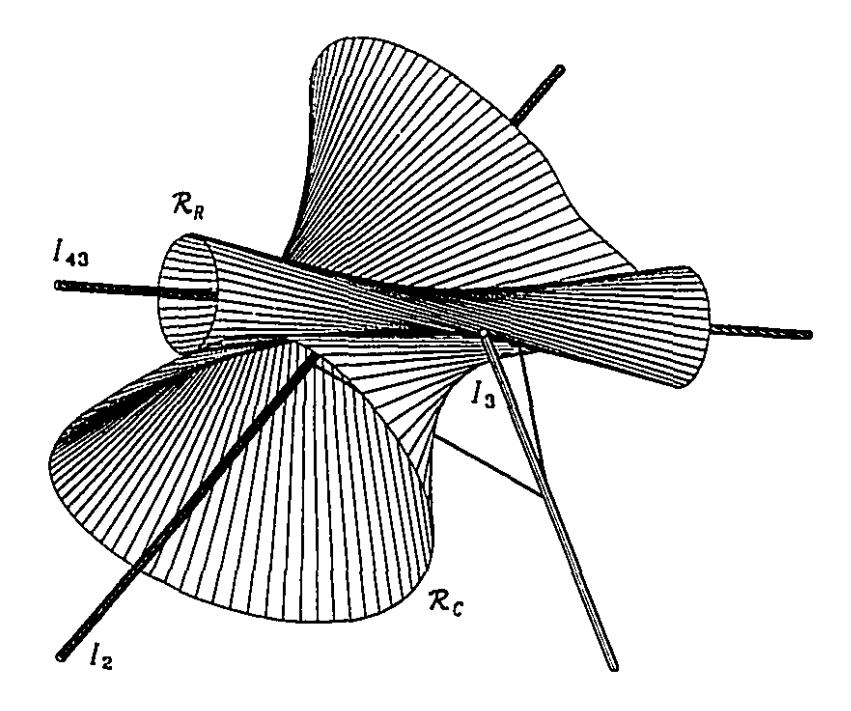


Figure 3.3 Ruled surfaces of the cam (\mathcal{R}_C) and roller (\mathcal{R}_R) of an RHCR cam mechanism

 \mathcal{R}_R , will be in general a hyperboloid. Under the assumption that $-\lambda_0 \leq \lambda \leq \lambda_0$ in eq.(3.26), where λ_0 is a design parameter, one obtains the surfaces shown in Fig. 3.3. On the other hand, if we bound λ as: $0.7\lambda_0 \leq \lambda \leq \lambda_0$, one can obtain the cam mechanism shown in Fig. 3.4 in various views.

For the cases when all axes are parallel or intersecting, z_{43} is always zero, and hence, the follower-roller pair becomes a revolute. These two cases are called RHRR mechanisms. The resulting surface geometry for RHRR mechanisms is rather simple and can be readily derived from the general formulation given above. However, a special treatment to compute dual cross products is needed for planar RHRR mechanisms, as discussed in Appendix A for the analysis pertaining to parallel dual vectors.

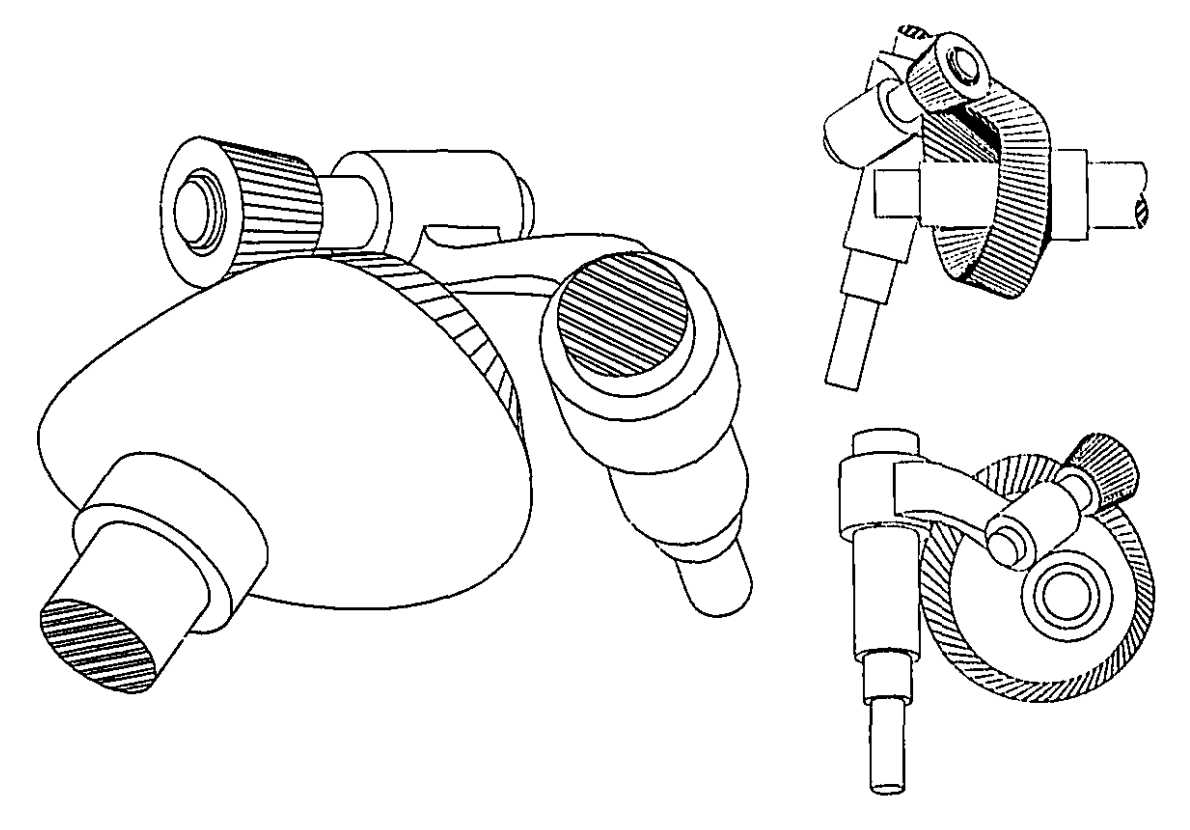


Figure 3.4 Three views of the RHCR cam mechanism obtained from the surfaces of Fig. 3.3

Spherical RHRR Mechanisms

For spherical RHRR mechanisms, the dual terms of the dual angles shown in Table 3.1 are all zero and, from eqs. (3.24 & 3.26), one can see that the pitch and contact surfaces of the cam reduce to conical surfaces, namely,

$$\mathbf{r}_{p}(\psi,\lambda) = \lambda \mathbf{e}_{43} \tag{3.28}$$

$$\mathbf{r}_{c}(\psi,\lambda) = \lambda \mathbf{e}_{42} \tag{3.29}$$

where e_{43} and e_{42} are defined in eqs.(3.25 & 3.27), respectively.

Now, θ_2 is computed from eq.(2.16c) and, from eqs.(3.7, 3.10 & 3.16), one can readily obtain

$$\tan \theta_3 = \frac{\sqrt{[c(\alpha_1 - \theta_2)c\phi s\alpha_3 + c\alpha_3 s(\alpha_1 - \theta_2)]^2 + s^2\alpha_3 s^2\phi}}{c\alpha_3 c(\alpha_1 - \theta_2) - c\phi s\alpha_3 s(\alpha_1 - \theta_2)}$$
(3.30)

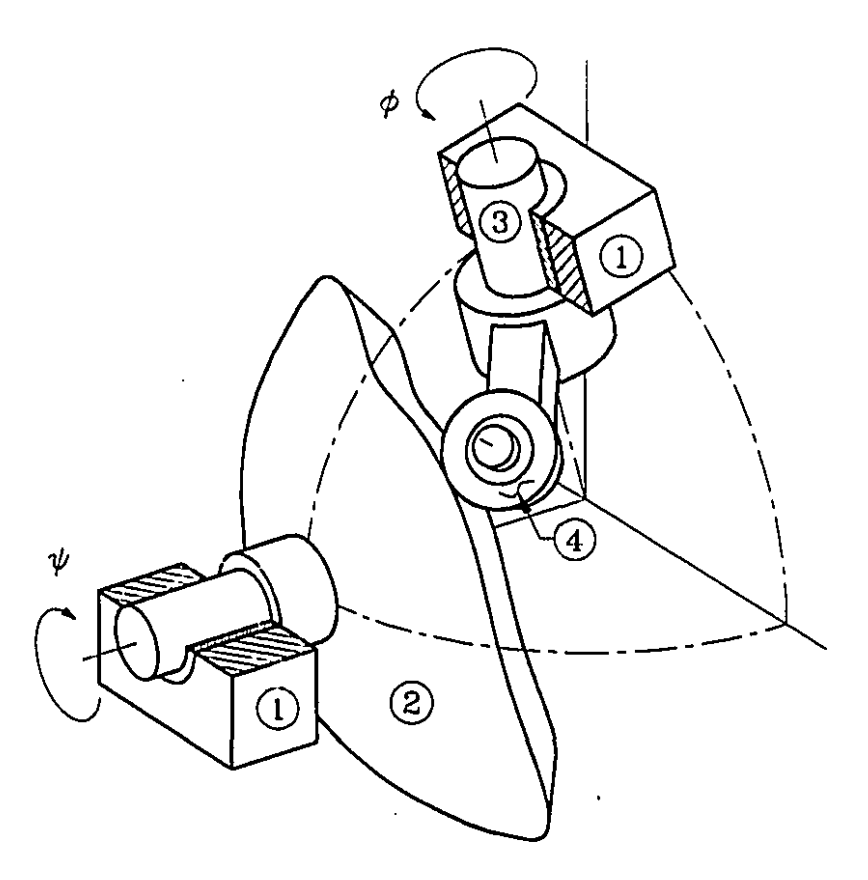


Figure 3.5 Spherical RHRR cam mechanism

$$\tan \delta = \frac{s\alpha_3 s\phi}{s\alpha_3 c(\alpha_1 - \theta_2)c\phi + c\alpha_3 s(\alpha_1 - \theta_2)}$$
(3.31)

$$\tan \nu = \frac{-s(\alpha_1 - \theta_2)s\phi}{c(\alpha_1 - \theta_2)s\alpha_3 + c\alpha_3 c\phi s(\alpha_1 - \theta_2)}$$
(3.32)

A typical design of a spherical RHRR cam mechanism is shown in Fig. 3.5.

Planar RHRR Mechanisms

The ISAs of planar RHRR mechanisms are all parallel, as shown in Fig. 3.6; consequently, the primal terms of $\hat{\alpha}_i$ and $\hat{\theta}_i$ shown in Table 3.1 are all zero and the

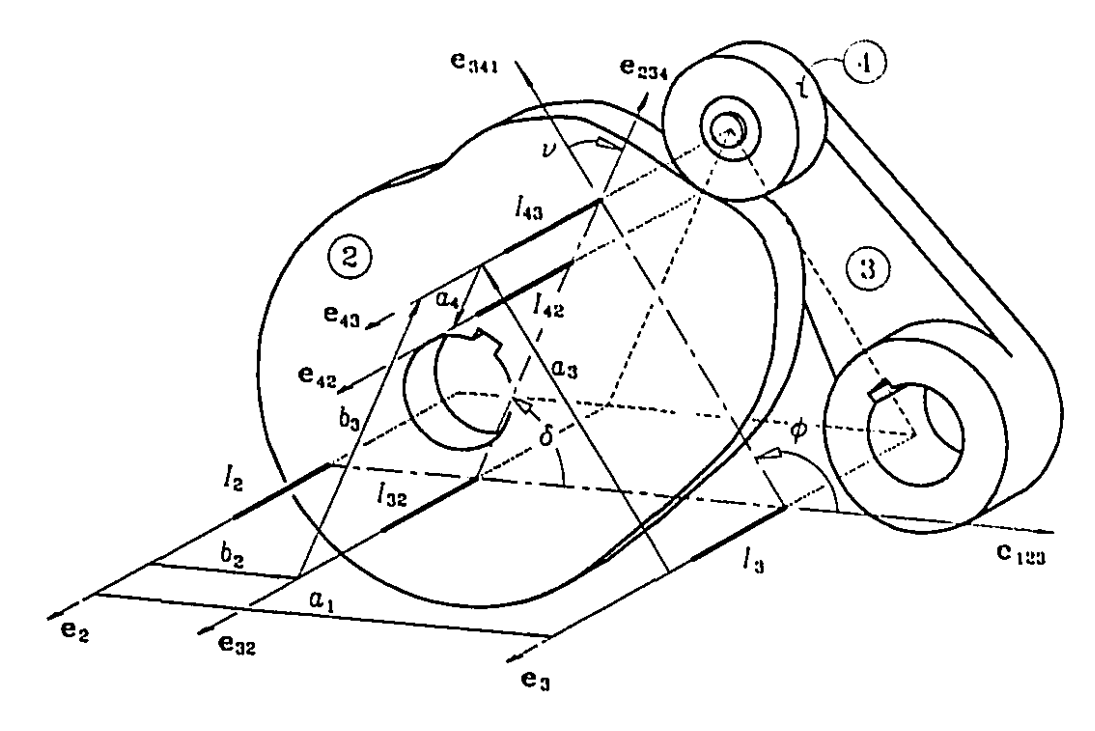


Figure 3.6 Planar RHRR cam mechanism

parameters k_i and h_i of eqs. (3.4) take on the values

$$k_1 = 1, k_2 = \cos \phi$$

 $k_3 = k_4 = k_7 = h_1 = h_2 = 0$
 $k_5 = h_4 = \cos(\psi - \phi)$
 $k_6 = h_3 = \sin(\psi - \phi)$

Similarly, parameters \tilde{k}_i and \tilde{h}_i of eqs.(3.14), take on the values

$$\tilde{k}_1 = 1, \ \tilde{k}_2 = \cos \delta$$

$$\tilde{k}_3 = \tilde{k}_4 = \tilde{k}_7 = \tilde{h}_1 = \tilde{h}_2 = 0$$

$$\tilde{k}_5 = \tilde{h}_4 = \cos(\psi - \delta)$$

$$\tilde{k}_6 = \tilde{h}_3 = \sin(\psi - \delta)$$

Now, the pitch and contact surfaces are defined as

$$\mathbf{r}_{p}(\psi,\lambda) = \mathbf{p}_{43} + \lambda \mathbf{e}_{43} \tag{3.33}$$

$$\mathbf{r}_{c}(\psi,\lambda) = \mathbf{p}_{42} + \lambda \mathbf{e}_{42} \tag{3.34}$$

with

$$\mathbf{e}_{43} = \mathbf{e}_{42} = \begin{bmatrix} 0, & 0, & 1 \end{bmatrix}^T$$
 (3.35)

and

$$\mathbf{p}_{43} = \begin{bmatrix} c\psi a_1 + c(\psi - \phi)a_3 \\ -s\psi a_1 - s(\psi - \phi)a_3 \\ 0 \end{bmatrix}$$
(3.36)

$$p_{42} = \begin{bmatrix} c\psi b_2 + c(\psi - \delta)(b_3 - a_4) \\ -s\psi b_2 - s(\psi - \delta)(b_3 - a_4) \\ 0 \end{bmatrix}$$
(3.37)

Here, the special theory for parallel dual vectors introduced in Appendix A is applied to derive b_3 and δ . From eqs.(3.8),

$$[\hat{\mathbf{e}}_{32}]_1 \equiv [\mathbf{e}_{32}]_1 + \epsilon [\mathbf{m}_{32}]_1 = \begin{bmatrix} 0 \\ 0 \\ 1 \end{bmatrix} + \epsilon \begin{bmatrix} 0 \\ -b_2 \\ 0 \end{bmatrix}$$
 (3.38a)

$$[\hat{\mathbf{e}}_{43}]_1 \equiv [\mathbf{e}_{43}]_1 + \epsilon [\mathbf{m}_{43}]_1 = \begin{bmatrix} 0 \\ 0 \\ 1 \end{bmatrix} + \epsilon \begin{bmatrix} a_3 s \phi \\ -a_3 c \phi - a_1 \\ 0 \end{bmatrix}$$
(3.38b)

Thus, the unit dual vector $\hat{\mathbf{e}}_{234}$ is defined by means of eq.(A.22), namely,

$$[\hat{\mathbf{e}}_{234}]_1 = \frac{[\mathbf{p}_{43}]_1 - [\mathbf{p}_{32}]_1}{b_3} + \epsilon \frac{[\mathbf{p}_{32}]_1 \times [\mathbf{p}_{43}]_1}{b_3}$$
(3.39)

where

$$[p_{32}]_1 \equiv [e_{32}]_1 \times [m_{32}]_1 = \begin{bmatrix} b_2 \\ 0 \\ 0 \end{bmatrix}$$
 (3.40a)

$$[p_{43}]_1 \equiv [e_{43}]_1 \times [m_{43}]_1 = \begin{bmatrix} a_3 c\phi + a_1 \\ a_3 c\phi \\ 0 \end{bmatrix}$$
 (3.40b)

and

$$b_3 \equiv \| [\mathbf{p}_{43}]_1 - [\mathbf{p}_{32}]_1 \| = \sqrt{(a_3 c\phi + a_1 - b_2)^2 + a_3^2 s^2 \phi}$$
 (3.41)

Combining eqs.(3.39-3.41) and substituting the dual vectors \mathbf{p}_{32} and $\hat{\mathbf{e}}_{234}$ into eq.(3.10), one can readily obtain

$$\tan \delta = \frac{a_3 s \phi}{a_3 c \phi + a_1 - b_2} \tag{3.42}$$

A similar procedure can be followed to derive the unit dual vector $[\dot{\mathbf{e}}_{341}]_1$ and evaluate ν from eq.(3.16) as

$$\tan \nu = \frac{-(a_1 - b_2)s\phi}{a_3 + (a_1 - b_2)c\phi} \tag{3.43}$$

Furthermore, b_2 is obtained from eq.(2.16d), namely,

$$b_2 = \frac{\phi'}{\phi' - 1} a_1 \tag{3.44}$$

It is apparent that eqs.(3.42, 3.43 & 3.44) can be derived directly from eqs.(3.31, 3.32 & 2.16c), respectively, under the assumption that, for small arcs on the unit sphere, $\sin \alpha_i \to a_i$; $\cos \alpha_i \to 1$; $\sin \theta_i \to b_i$ and $\cos \theta_i \to 1$, thereby concluding that planar mechanisms can be regarded as a special case of spherical mechanisms.

3.2.2 Revolute-Higher-Cylindric-Prismatic (RHCP) Mechanisms

Revolute-higher-cylindric-prismatic (RHCP) mechanisms have revolute and prismatic pairs as input and output, respectively, and an intermediate cylindrical pair, as shown in Fig. 3.7. Thus, $z_2 = \phi = 0$. The input-output function is given in eq.(2.19), as

$$z_3 = z_3(\psi) (2.19)$$

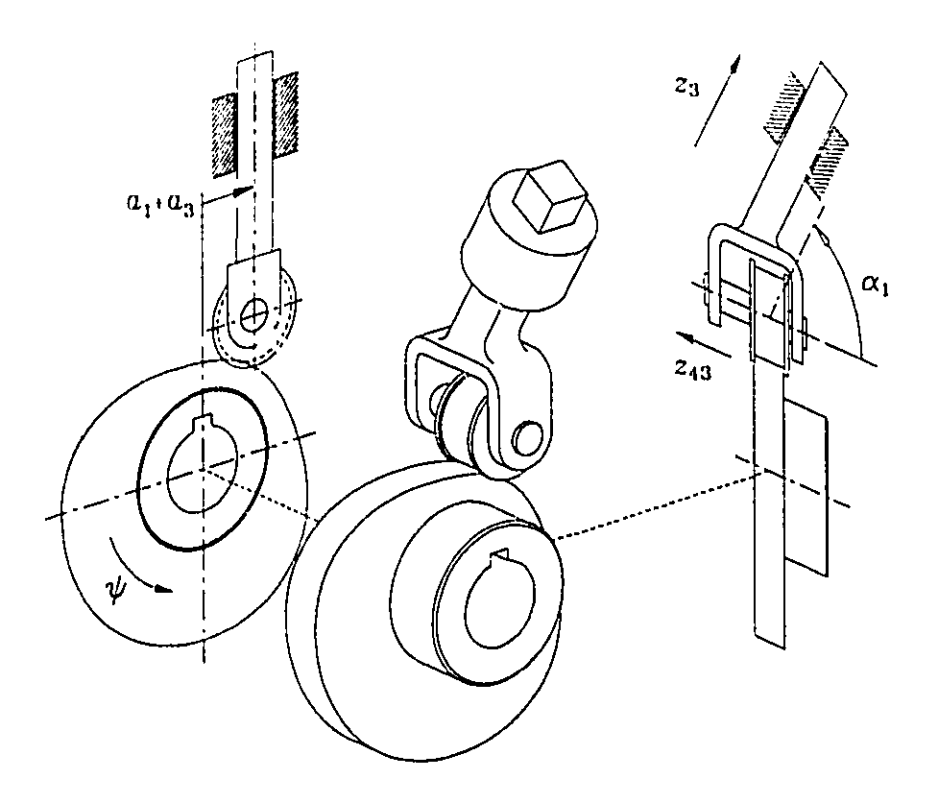


Figure 3.7 RHCP cam mechanism

Moreover, expanding eq.(3.21a) and knowing from eq.(2.21c) that $\theta_2=0$, one obtains

$$\omega_{42}s\alpha_4s\nu = 0 \tag{3.45a}$$

$$\omega_{42}(z_{43}s\alpha_4c\nu + a_4c\alpha_4s\nu) + v_{42}s\alpha_4s\nu = -\omega_{32}z_3s\beta$$
 (3.45b)

Now, considering that $\omega_{42} \neq 0$ and $\sin \nu \neq 0$, from eq.(3.45a), one concludes that α_4 must be zero, and from eq.(3.45b), one obtains

$$\omega_{42} = -\frac{z_3 \sin \alpha_1}{a_4 \sin \nu} \omega_{32} \tag{3.46}$$

Furthermore, expanding eq.(3.21b) with $\alpha_4 = 0$, one obtains from its primal part the relationship

$$0 = \omega_{32} \sin(\alpha_3 + \alpha_1) \tag{3.47}$$

Moreover, from eq.(2.21a), $\omega_{32} \neq 0$, and hence, $\alpha_3 = -\alpha_1$.

Now, substituting the corresponding values of α_3 and ϕ into eqs.(3.4), one obtains

$$k_1 = k_2 = 1$$

 $k_3 = k_4 = k_7 = h_1 = h_2 = 0$
 $k_5 = h_4 = \cos \psi$
 $k_6 = h_3 = \sin \psi$

With these values, the vectors of eqs. (3.3a & 3.3c) take on the form

$$\mathbf{e}_{43} = \begin{bmatrix} 0 \\ 0 \\ 1 \end{bmatrix}, \qquad \mathbf{p}_{43} = \begin{bmatrix} (a_1 + a_3)\cos\psi - z_3\sin\alpha_1\sin\psi \\ -(a_1 + a_3)\sin\psi - z_3\sin\alpha_1\cos\psi \\ 0 \end{bmatrix}$$
(3.48)

In order to derive the surface of the cam, dual vectors $[\hat{e}_{32}]_1$ and $[\hat{e}_{43}]_1$ are computed from eqs.(3.8), namely,

$$[\hat{\mathbf{e}}_{32}]_1 = \begin{bmatrix} 0 \\ 0 \\ 1 \end{bmatrix} + \epsilon \begin{bmatrix} 0 \\ -b_2 \\ 0 \end{bmatrix}$$
 (3.49a)

$$[\hat{\mathbf{e}}_{43}]_1 = \begin{bmatrix} 0 \\ 0 \\ 1 \end{bmatrix} + \epsilon \begin{bmatrix} -z_3 \sin \alpha_1 \\ -a_1 - a_3 \\ 0 \end{bmatrix}$$
 (3.49b)

It is clear that $[\hat{e}_{32}]_1$ and $[\hat{e}_{43}]_1$ are parallel, and hence, the theory of parallel dual vectors introduced in Appendix A is applied to obtain the expressions below:

$$\hat{\theta}_3 \equiv \theta_3 + \epsilon b_3 = 0 + \epsilon \sqrt{(a_3 + a_1 + z_3' \sin \alpha_1)^2 + z_3^2 \sin^2 \alpha_1}$$
 (3.50a)

$$\hat{\delta} \equiv \delta + \epsilon z_{32} = \arctan \frac{-z_3 \sin \alpha_1}{a_1 + a_3 + z_3' \sin \alpha_1} + \epsilon 0 \tag{3.50b}$$

$$\hat{\nu} \equiv \nu + \epsilon z_{43} = \arctan \frac{z_3 \sin \alpha_1}{-(a_1 + a_3 + z_3' \sin \alpha_1)} + \epsilon (-z_3 \cos \alpha_1) \qquad (3.50c)$$

Now, substituting $\theta_2 = 0$ and $\eta \equiv \theta_3 - \alpha_4 = 0$ into eqs.(3.14), one obtains

$$\tilde{k}_1 = 1, \ \tilde{k}_2 = \cos \delta$$

$$\hat{k}_3 = \tilde{k}_4 = \tilde{k}_7 = \tilde{h}_1 = \tilde{h}_2 = 0$$

$$\hat{k}_5 = \tilde{h}_4 = \cos(\psi - \delta)$$

$$\hat{k}_6 = \tilde{h}_3 = \sin(\psi - \delta)$$

Thus, vectors e_{42} and p_{42} of eqs.(3.13b & 3.13c) take on the form

$$\mathbf{e}_{42} = \begin{bmatrix} 0 \\ 0 \\ 1 \end{bmatrix} \text{ and } \mathbf{p}_{42} = \begin{bmatrix} b_2 \cos \psi + (b_3 - a_4) \cos(\delta - \psi) \\ -b_2 \sin \psi + (b_3 - a_4) \sin(\delta - \psi) \\ 0 \end{bmatrix}$$
(3.51)

RHRP Mechanisms

It was mentioned before that the condition of having a revolute pair between follower and roller is that $z_{43} = 0$. Moreover, from eq.(3.50c),

$$z_{43} = -z_3 \cos \alpha_1$$

Therefore, RHRP mechanisms can be obtained if $\alpha_1 = \pm \pi/2$.

Additionally, expanding and separating the primal and dual parts of eq.(3.21c), one obtains

$$\omega_{42} = \omega_{43} - \omega_{32} \tag{3.52a}$$

$$v_{42} = v_{43} - v_{32} \tag{3.52b}$$

Now, with $\alpha_1 = \pm \pi/2$, $v_{43} \equiv dz_{43}/dt = 0$ and, from eq.(2.21b), $v_{32} = 0$. Substitution of these two values into eq.(3.52b) reveals that v_{42} is zero and pure rolling between cam and roller is achieved.

3.2.3 Prismatic-Higher-Cylindric-Revolute (PHCR) Mechanisms

Shown in Fig. 3.8 is a prismatic-higher-cylindric-revolute (PHCR) mechanism, with prismatic and revolute pairs providing its input and output motions, respectively, and

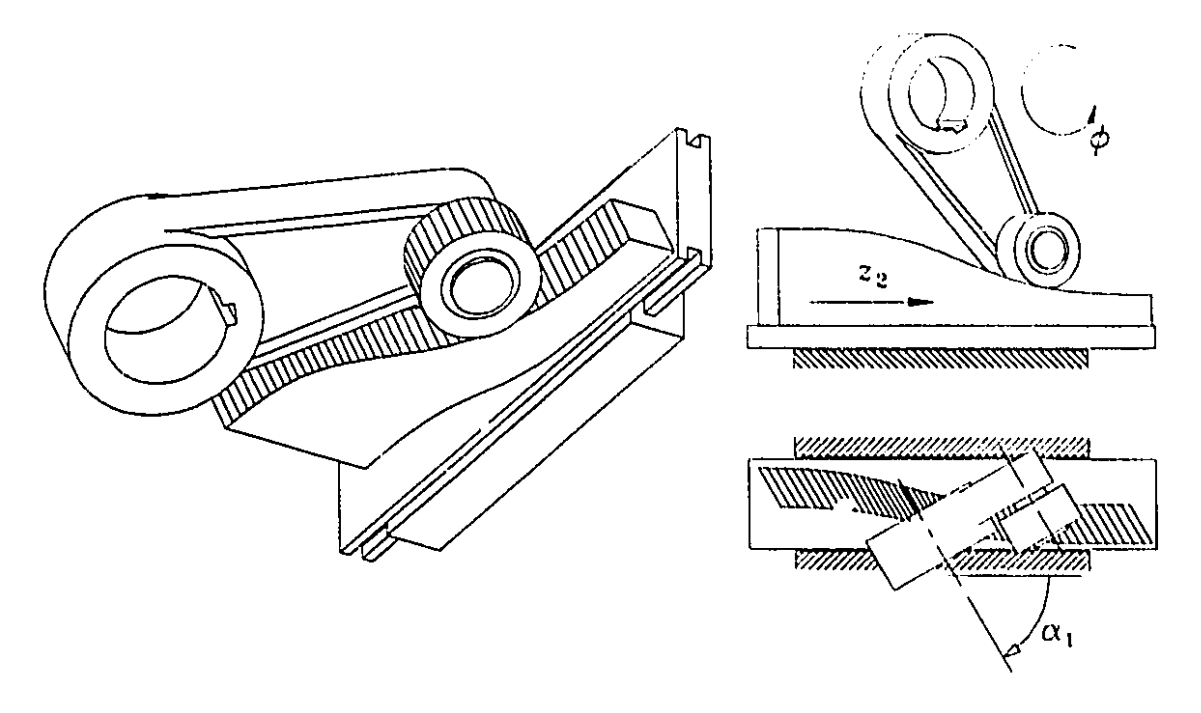


Figure 3.8 PHCR cam mechanism

an intermediate cylindrical pair. Thus, $\psi = 0$, $z_3 = 0$, and the input-output function is given as in eq.(2.25), namely,

$$\phi = \phi(z_2) \tag{2.25}$$

Furthermore, it is known from eq.(2.28c) that $\theta_2 = \alpha_1$, and substituting this value into eq.(3.21a), one can readily obtain the primal and dual parts of the expression thus resulting, namely,

$$\omega_{42}s\alpha_4s\nu = 0 \tag{3.53a}$$

$$\omega_{42}(z_{43}s\alpha_4c\nu + a_4s\nu c\alpha_4) + v_{42}s\alpha_4s\nu = -\omega_{32}(a_1 - b_2)s\phi$$
 (3.53b)

In general, $\omega_{42} \neq 0$ and $\nu \neq 0$, and hence, from eq.(3.53a), $\sin \alpha_4$ must be zero. Moreover, with $\sin \alpha_4 = 0$ the primal part of eq.(3.21b) takes on the form

$$0 = -\omega_{32} \sin \alpha_3 \tag{3.54}$$

Thus, from eq.(2.28a), $\omega_{32} = \pm \phi' v_2$, and one concludes that $\sin \alpha_3 = 0$.

Ō

Now, with $\psi = \sin \alpha_3 = 0$, eqs.(3.4) reduce to

$$k_1 = \cos \alpha_1$$

$$k_2 = h_4 = \cos \alpha_1 \cos \phi$$

$$k_3 = h_2 = \sin \alpha_1$$

$$k_4 = \sin \alpha_1 \cos \phi$$

$$k_5 = \cos \phi$$

$$k_6 = -\sin \phi \cos \alpha_1$$

$$k_7 = h_1 = 0$$

$$h_3 = -\sin \phi$$

and vectors e₄₃ and p₄₃ are obtained from eqs.(3.3a & 3.3c), namely,

$$\mathbf{e}_{43} = \begin{bmatrix} 0 \\ -\sin\alpha_1 \\ \cos\alpha_1 \end{bmatrix} \text{ and } \mathbf{p}_{43} = \begin{bmatrix} a_1 + a_3\cos\phi \\ \cos\alpha_1(a_3\sin\phi - z_2\sin\alpha_1) \\ \sin\alpha_1(a_3\sin\phi - z_2\sin\alpha_1) \end{bmatrix}$$
(3.55)

Next, the dual vectors $[\hat{\mathbf{e}}_{32}]_1$ and $[\hat{\mathbf{e}}_{43}]_1$ are computed from eqs.(3.8) as

$$[\hat{\mathbf{e}}_{32}]_1 = \begin{bmatrix} 0 \\ -\sin\alpha_1 \\ \cos\alpha_1 \end{bmatrix} + \epsilon b_2 \begin{bmatrix} 0 \\ -\cos\alpha_1 \\ \sin\alpha_1 \end{bmatrix}$$
 (3.56a)

$$[\hat{\mathbf{e}}_{43}]_1 = \begin{bmatrix} 0 \\ -\sin\alpha_1 \\ \cos\alpha_1 \end{bmatrix} + \epsilon \begin{bmatrix} a_3\sin\phi \\ -(a_1 + a_3\cos\phi)\cos\alpha_1 \\ -(a_1 + a_3\cos\phi)\sin\alpha_1 \end{bmatrix}$$
(3.56b)

With application of the theory of parallel dual vectors of Appendix A, one can obtain, from eqs. (3.7, 3.10 & 3.16), the expressions below:

$$\hat{\theta}_{3} \equiv \theta_{3} + \epsilon b_{3} = 0 + \epsilon \frac{\sqrt{(a_{3}\phi'\cos\phi - \sin\alpha_{1})^{2} + (a_{3}\phi'\sin\phi)^{2}}}{\phi'}$$

$$\hat{\delta} \equiv \delta + \epsilon z_{32} = \arctan\frac{a_{3}\phi'\sin\phi}{a_{3}\phi'\cos\phi - \sin\alpha_{1}} + \epsilon 0$$

$$\hat{\nu} \equiv \nu + \epsilon z_{43} = \arctan\frac{\sin\alpha_{1}\sin\phi}{a_{3}\phi' + \sin\alpha_{1}\cos\phi} + \epsilon 0$$
(3.57c)

$$\hat{\delta} \equiv \delta + \epsilon z_{32} = \arctan \frac{a_3 \phi' \sin \phi}{a_3 \phi' \cos \phi - \sin \alpha_1} + \epsilon 0 \tag{3.57b}$$

$$\hat{\nu} \equiv \nu + \epsilon z_{43} = \arctan \frac{\sin \alpha_1 \sin \phi}{a_3 \phi' + \sin \alpha_1 \cos \phi} + \epsilon 0 \tag{3.57c}$$

According to eq.(3.57b), $z_{43} = 0$, which means that the follower-roller pair is a revolute; therefore, a PHCR mechanism is, in fact, a PHRR mechanism.

In order to find expressions for e_{42} and p_{42} , values of $\theta_2 = \alpha_1$ and $\eta \equiv \theta_3 - \alpha_4 = 0$ are substituted into eqs.(3.14) to obtain

$$\tilde{k}_1 = \cos \alpha_1$$

$$\tilde{k}_2 = \tilde{h}_4 = \cos \alpha_1 \cos \delta$$

$$\tilde{k}_3 = \tilde{h}_2 = \sin \alpha_1$$

$$\tilde{k}_4 = \sin \alpha_1 \cos \delta$$

$$\tilde{k}_5 = \cos \delta$$

$$\tilde{k}_6 = -\sin \delta \cos \alpha_1$$

$$\tilde{k}_7 = \tilde{h}_1 = 0$$

$$\tilde{h}_3 = -\sin \delta$$

Thus, substituting these values into eqs.(3.13b & 3.13c),

$$\mathbf{e}_{42} = \begin{bmatrix} 0 \\ -\sin\alpha_1 \\ \cos\alpha_1 \end{bmatrix} \text{ and } \mathbf{p}_{42} = \begin{bmatrix} a_1 + \sin\alpha_1/\phi' + (b_3 - a_4)\cos\delta \\ [(b_3 - a_4)\sin\delta - z_2\sin\alpha_1]\cos\alpha_1 \\ [(b_3 - a_4)\sin\delta - z_2\sin\alpha_1]\sin\alpha_1 \end{bmatrix}$$
(3.58)

Further analysis of eq.(3.21c) leads to the relations

$$\omega_{42} = \omega_{43} - \omega_{32} \tag{3.59a}$$

$$v_{42} = v_{32} \tag{3.59b}$$

Now, from eq.(2.28b) $v_{32} = \pm v_2 \cos \alpha_1$, and hence, pure rolling between cam and roller is achieved if $\alpha_1 = \pm \pi/2$.

According to the results pertaining to RHCP and PHRR mechanisms, similar theorems to those for RHP and PHR mechanisms can be stated, namely:

Theorem 3.1: All ISAs of RHCP and PHRR mechanisms, except for the one associated with the prismatic pair, are parallel.

10

form

Theorem 3.2: Pure rolling between cam and roller on RHCP and PHRR mechanisms is achieved if the axis of the prismatic pair is perpendicular to all other ISAs.

3.2.4 Prismatic-Higher-Cylindric-Prismatic (PHCP) Mechanisms

A prismatic-higher-cylindric-prismatic (PHCP) mechanism is defined with prismatic pairs in both input and output motions, and an intermediate cylindrical pair. Thus, $\psi = 0$ and ϕ is constant, and the input-output function is given as in eq.(2.30), namely,

$$z_3 = z_3(z_2) \tag{2.30}$$

Furthermore, it is known from Subsubsection 2.2.4 that $a_1 = b_2 = 0$. Substituting this value into eq.(3.21a), one can readily obtain the primal and dual parts of this equation as

$$\omega_{42} s \alpha_4 s \nu = 0 \tag{3.60a}$$

$$\omega_{42}(z_{43}s\alpha_4c\nu + a_4s\nu c\alpha_4) + v_{42}s\alpha_4s\nu = -v_{32}s\beta s\phi$$
 (3.60b)

In general, $\omega_{42} \neq 0$ and $\nu \neq 0$; therefore, from eq.(3.60a), $\sin \alpha_4$ must be zero. Moreover, with $\sin \alpha_4 = 0$, the primal and dual parts of eq.(3.21c) take on the

 $\omega_{42} = \omega_{43} \tag{3.61a}$

$$v_{42} = v_{43} - v_{32}(c\beta c\alpha_3 - s\beta s\alpha_3 c\phi)$$
 (3.61b)

The desirable PHCP mechanism is one with pure rolling between cam and roller. Thus, v_{42} must be zero, and from eq.(3.61b), v_{43} is given as

$$v_{43} = v_{32}(c\beta c\alpha_3 - s\beta s\alpha_3 c\phi) \tag{3.62}$$

Pitch and contact surfaces are derived with application of eqs. (3.3 & 3.13).

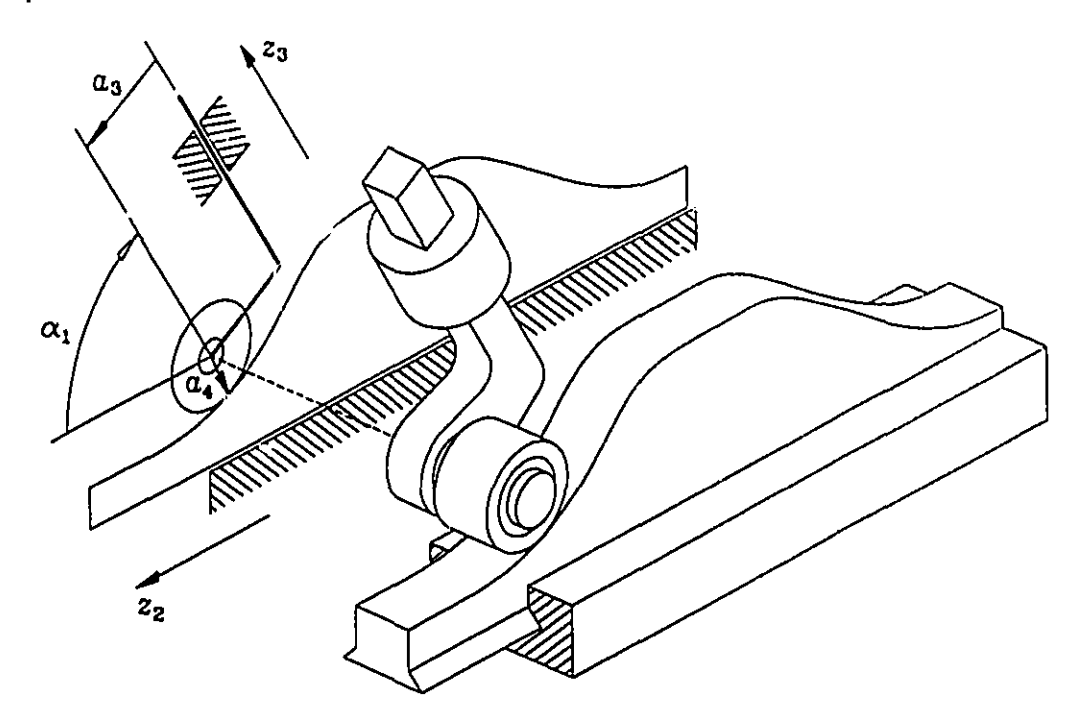


Figure 3.9 PHRP cam mechanism

PHRP mechanisms

The cylindrical pair becomes a revolute pair if v_{43} vanishes. Thus, from eq.(3.62), the coefficient of v_{32} must be zero, i.e.,

$$c\beta c\alpha_3 - s\beta s\alpha_3 c\phi = 0 \tag{3.63}$$

Since β is a variable and α_3 and ϕ are constants, the only solution of eq.(3.63) is that in which each term vanishes independently, i.e., $\alpha_3 = \pm \pi/2$ and $\phi = \pm \pi/2$.

Now, with $\psi=0,\,\alpha_3=\pi/2$ and $\phi=\pi/2,\,{\rm eqs.}(3.4)$ reduce to

$$k_1 = k_3 = h_2 = h_3 = 0$$

 $k_2 = -k_7 = h_4 = -\sin \alpha_1$
 $k_4 = -k_6 = \cos \alpha_1$

and vectors e_{43} and p_{43} are obtained from eqs.(3.3a & 3.3c), namely,

$$\mathbf{e}_{43} = \begin{bmatrix} 1 \\ 0 \\ 0 \end{bmatrix} \text{ and } \mathbf{p}_{43} = \begin{bmatrix} 0 \\ a_3 \cos \alpha_1 - z_3 \sin \alpha_1 \\ a_3 \sin \alpha_1 + z_3 \cos \alpha_1 - z_2 \end{bmatrix}$$
(3.64)

Moreover, the dual vectors $[\hat{\mathbf{e}}_{32}]_1$ and $[\hat{\mathbf{e}}_{43}]_1$ are computed from eqs.(3.8), namely,

$$[\hat{\mathbf{e}}_{32}]_1 = \begin{bmatrix} 0 \\ -\sin\theta_2 \\ \cos\theta_2 \end{bmatrix} + \epsilon 0 \tag{3.65a}$$

$$[\hat{\mathbf{e}}_{43}]_1 = \begin{bmatrix} 1 \\ 0 \\ 0 \end{bmatrix} + \epsilon \begin{bmatrix} 0 \\ z_3 \cos \alpha_1 + a_3 \sin \alpha_1 \\ z_3 \sin \alpha_1 - a_3 \cos \alpha_1 \end{bmatrix}$$
(3.65b)

Now, from eqs.(3.7, 3.10 & 3.16), one can readily obtain the expressions below:

$$\hat{\theta}_3 \equiv \theta_3 + \epsilon b_3 = \pi/2 + \epsilon [a_3 \cos(\alpha_1 - \theta_2) - z_3 \sin(\alpha_1 - \theta_2)] \tag{3.66a}$$

$$\hat{\delta} \equiv \delta + \epsilon z_{32} = \pi/2 + \epsilon [a_3 \sin(\alpha_1 - \theta_2) + z_3 \cos(\alpha_1 - \theta_2)] \tag{3.66b}$$

$$\hat{\nu} \equiv \nu + \epsilon z_{43} = \arctan \frac{-\sin(\alpha_1 - \theta_2)}{\cos(\alpha_1 - \theta_2)} + \epsilon 0 \tag{3.66c}$$

Moreover, combining eqs. (2.35b & 3.66c),

$$\tan \nu = \frac{\sin \alpha_1}{z_3' - \cos \alpha_1} \tag{3.66d}$$

In order to find expressions for e_{42} and p_{42} , values $\delta_2 = \pi/2$, $\eta \equiv \theta_3 - \alpha_4 = \pi/2$ and $\psi = 0$ are substituted into eqs.(3.14) to obtain

$$\tilde{k}_1 = \tilde{k}_3 = \tilde{h}_2 = \tilde{h}_3 = 0$$

$$\tilde{k}_2 = -\tilde{k}_7 = \tilde{h}_4 = -\sin\theta_2$$

$$\tilde{k}_4 = -\tilde{k}_6 = \cos\theta_2\cos\delta$$

4.5

Thus, substituting these values into eqs. (3.13b & 3.13c), one obtains

$$\mathbf{e}_{42} = \begin{bmatrix} 1\\0\\0 \end{bmatrix} \text{ and } \mathbf{p}_{42} = \begin{bmatrix} 0\\(b_3 - a_4)\cos\theta_2 - z_{32}\sin\theta_2\\(b_3 - a_4)\sin\theta_2 + z_{32}\cos\theta_2 - z_2 \end{bmatrix}$$
(3.67)

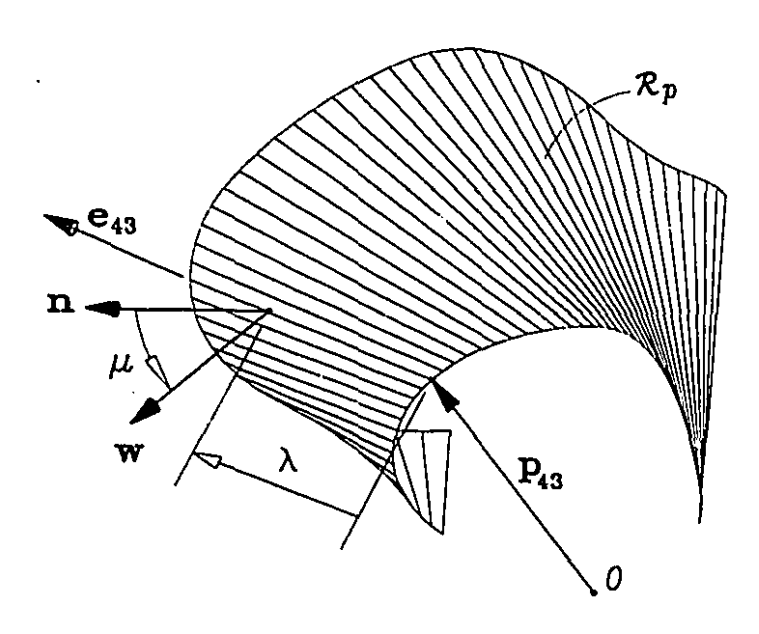


Figure 3.10 Graphical representation of the pressure angle

3.3 Pressure Angle

The pressure angle is defined as that comprised between the direction of the unit normal to the pitch surface \mathcal{R}_p and the direction of the velocity of the follower at the contact point. Thus, the unit normal defined in eq. (C.5) is written as

$$\mathbf{n} = \frac{\mathbf{u}}{\parallel \mathbf{u} \parallel}; \qquad \mathbf{u} \equiv \frac{\partial \mathbf{r}_p}{\partial \psi} \times \frac{\partial \mathbf{r}_p}{\partial \lambda}$$
 (3.68)

On the other hand, the unit vector w parallel to the follower velocity at points on

 I_{43} is obtained as

$$\mathbf{w} = \frac{\boldsymbol{\xi}}{\parallel \boldsymbol{\xi} \parallel}; \qquad \boldsymbol{\xi} \equiv \boldsymbol{\omega} \times \mathbf{r}_{p} \tag{3.69}$$

where ω is the angular velocity of the follower.

Thus, the pressure angle is derived as

$$\tan \mu = \frac{\parallel \mathbf{n} \times \mathbf{w} \parallel}{\mathbf{n} \cdot \mathbf{w}} \tag{3.70}$$

A graphical representation of this definition is shown in Figure 3.10.

3.3.1 Pressure Angle of RHCR Mechanisms

The unit normal of RHCR mechanisms is computed from application of eq.(C.5), with the aid of eq.(3.24). Thus, the three components of u of eq.(3.68) in frame \mathcal{F}_1 , are given as

$$u_{1} = a_{1}k_{1} - a_{3}\cos\phi h_{5} - \lambda\sin\alpha_{3}\sin\phi h_{5}$$

$$u_{2} = -a_{3}\cos\alpha_{1}\sin\phi h_{5} + \lambda[\cos\alpha_{1}\cos\phi\sin\alpha_{3}h_{5}$$

$$+\sin\alpha_{1}(\phi' + \cos\alpha_{3}h_{5})]$$

$$u_{3} = \sin\phi(a_{1}\sin\alpha_{3} - a_{3}\sin\alpha_{1}h_{5}) + \lambda(1 - k_{1}h_{5} - \phi'\cos\alpha_{1})$$

and

$$h_5 = k_1 - \phi' \cos \alpha_3 \tag{3.71a}$$

$$h_6 = k_4 - \phi' \sin \alpha_3 \tag{3.71b}$$

Furthermore, from eq.(3.69), w can be written as

$$\mathbf{w} = \frac{1}{\parallel \boldsymbol{\xi} \parallel} \begin{bmatrix} -a_3 \sin \phi + \lambda \sin \alpha_3 \cos \phi \\ a_3 \cos \alpha_1 \cos \phi + \lambda \sin \alpha_3 \cos \alpha_1 \sin \phi \\ a_3 \sin \alpha_1 \cos \phi + \lambda \sin \alpha_1 \sin \phi \sin \alpha_3 \end{bmatrix}$$
(3.72)

Moreover, the cross product of eq. (3.70) is computed as

$$\mathbf{n} \times \mathbf{w} = \frac{\lambda^2 \mathbf{d} + \lambda \mathbf{f} + \mathbf{g}}{\|\boldsymbol{\xi}\| \|\mathbf{u}\|}$$
(3.73)

11/1

where the components of vectors \mathbf{d} , \mathbf{f} and \mathbf{g} , in frame \mathcal{F}_1 , are given below:

$$d_{1} = -\sin^{2} \alpha_{3} \sin \phi h_{6}$$

$$f_{1} = -\sin \alpha_{3} (a_{1} \cos \alpha_{1} \sin \alpha_{3} \sin^{2} \phi + a_{3} \cos \phi h_{6})$$

$$g_{1} = -a_{1} a_{3} \cos \alpha_{1} \cos \phi \sin \alpha_{3} \sin \phi$$

$$d_{2} = \sin \alpha_{3} [\sin \alpha_{1} \sin \alpha_{3} h_{5} + \cos \phi (\cos \alpha_{1} \sin \alpha_{3} h_{6} + \sin^{2} \alpha_{1})$$

$$f_{2} = \sin \phi [a_{1} \cos \alpha_{1} \sin \alpha_{3} k_{3} - a_{3} (1 - \phi' \cos \alpha_{1} - \cos \alpha_{1} \cos \alpha_{3} h_{5})]$$

$$g_{2} = a_{3} [-a_{1} (\sin \alpha_{3} - \cos \phi \cos \alpha_{1} k_{3}) + a_{3} \sin \alpha_{1} h_{5}]$$

$$d_{3} = \sin \alpha_{3} [\sin \alpha_{3} (\cos \phi \sin \alpha_{1} h_{6} - \cos \alpha_{1} h_{5}) - \cos \alpha_{1} \cos \phi \sin \alpha_{1}]$$

$$f_{3} = -\sin \phi [a_{1} \cos \alpha_{1} \sin \alpha_{3} k_{1} - a_{3} (\phi' \sin \alpha_{1} + \sin \alpha_{1} \cos \alpha_{3} h_{5})]$$

$$g_{3} = a_{3} \cos \alpha_{1} (-a_{1} \cos \phi k_{1} - a_{3} h_{5})$$

Then, $|| n \times w ||$ can be written as

$$\parallel \mathbf{n} \times \mathbf{w} \parallel = \frac{\sqrt{A\lambda^4 + B\lambda^3 + C\lambda^2 + D\lambda + E}}{\parallel \boldsymbol{\xi} \parallel \parallel \mathbf{u} \parallel}$$
(3.75)

where

$$A = d_1^2 + d_2^2 + d_3^2$$

$$B = 2(d_1f_1 + d_2f_2 + d_3f_3)$$

$$C = f_1^2 + f_2^2 + f_3^2 + 2(d_1g_1 + d_2g_2 + d_3g_3)$$

$$D = 2(f_1g_1 + f_2g_2 + f_3g_3)$$

$$E = g_1^2 + g_2^2 + g_3^2$$
(3.76)

Furthermore, the denominator of the right-hand side of the eq. (3.70) can be written as

$$\mathbf{n} \cdot \mathbf{w} = \frac{F\lambda^2 + G\lambda + H}{\parallel \boldsymbol{\xi} \parallel \parallel \mathbf{u} \parallel} \tag{3.77}$$

where

 $F = \sin \alpha_1 \sin \alpha_3 \sin \phi$

$$G = a_1 \sin \alpha_3 (\sin \alpha_1 \sin \alpha_3 - \cos \alpha_1 \cos \alpha_3 \cos \phi) + a_3 \cos \phi \sin \alpha_1$$
 (3.78)

$$H = a_1 a_3 \cos \alpha_1 \cos \alpha_3 \sin \phi$$

Thus, the general expression for the pressure angle is given by

$$\tan \mu = \frac{\sqrt{A\lambda^4 + B\lambda^3 + C\lambda^2 + D\lambda + E}}{F\lambda^2 + G\lambda + H}$$
(3.79)

Spherical Cam Mechanisms

The pressure angle for spherical cams is derived from eq. (3.73) by taking the limit of $\tan \mu$ as $\lambda \to \infty$ (González-Palacios and Angeles, 1991), i.e.,

$$\tan \mu = \lim_{\lambda \to \infty} \frac{\sqrt{A\lambda^4 + B\lambda^3 + C\lambda^2 + D\lambda + E}}{F\lambda^2 + G\lambda + H} = \frac{\sqrt{A}}{F}$$
(3.80)

Thus, from eqs. (3.74, 3.76 & 3.78), one can readily obtain the desired general expression for spherical cam mechanisms, namely,

$$\tan \mu = \frac{(\phi' - \cos \alpha_1) \sin \alpha_3 - \sin \alpha_1 \cos \alpha_3 \cos \phi}{\sin \alpha_1 \sin \phi}$$
(3.81)

Comparing eq.(3.81) with eq.(3.32) one can find a similitude. In fact, one can eliminate θ_2 from eq.(3.32) with the aid of eq.(2.16c). Thus, upon reduction, eq.(3.32) takes on the form

$$\tan \nu = \frac{-(\sin \alpha_1 - \cos \alpha_1 \tan \theta_2) \sin \phi}{(\cos \alpha_1 - \sin \alpha_1 \tan \theta_2) \sin \alpha_3 + (\sin \alpha_1 - \cos \alpha_1 \tan \theta_2) \cos \alpha_3 \cos \phi}$$
(3.82)

which, with the aid of eq.(2.16c), becomes

$$\tan \nu = \frac{\sin \alpha_1 \sin \phi}{(\phi' - 1) \sin \alpha_3 - \sin \alpha_1 \cos \alpha_3 \cos \phi}$$
 (3.83)

Consequently, it is clear that

$$\tan \mu = \frac{1}{\tan \nu} \tag{3.84}$$

Planar Cam Mechanisms

The pressure angle for planar cam mechanisms is obtained from eq. (3.79) as indicated below. Since all the ISAs are parallel, $\alpha_1 = \alpha_3 = 0$. Moreover, variables k_1 , k_3 , k_5 and k_6 , appearing in eqs. (3.4a), (3.4c), (3.71a) and (3.71b), respectively, take on the values

$$k_1 = 1$$

$$k_3 = 0$$

$$h_5 = 1 - \phi'$$

$$h_6 = 0$$

Moreover, all components appearing in eq. (3.74) become zero, except for g_3 , which reduces to

$$g_3 = a_3[a_3(\phi' - 1) - a_1 \cos \phi] \tag{3.85}$$

Consequently,

$$A = B = C = D = 0$$

$$E = a_3^2 [a_3(\phi' - 1) - a_1 \cos \phi]^2$$

$$F = G = 0$$

$$H = a_1 a_3 \sin \phi$$

and the expression for the pressure angle takes on the form

$$\tan \mu = \frac{a_3(\phi' - 1) - a_1 \cos \phi}{a_1 \sin \phi} \tag{3.86}$$

in agreement with results available in the literature (Rothbart, 1956; Tesar, 1976; Angeles and López-Cajún, 1991).

Here, it can also be proven that $\tan \mu = 1/\tan \nu$ if eq.(3.44) is substituted into eq.(3.43).

Spatial Cam Mechanisms

We have shown that eq. (3.79) represents the pressure angle for all planar, spherical and spatial cam mechanisms. In fact, planar and spherical cam mechanisms are particular cases in which the expressions for the pressure angle are independent of λ . Here we present two more cases as examples of spatial cam mechanisms in order to show the influence of λ , namely, cylindrical and globoidal cam mechanisms.

The pressure angle of cylindrical cam mechanisms is derived taking into account that $\alpha_1 = \pi/2$ and $\alpha_3 = 0$. Consequently, the expression for the pressure angle can be readily obtained from eq. (3.79) as

$$\tan \mu = \frac{\lambda \sin \phi + a_3 \phi'}{\lambda \cos \phi} \tag{3.87}$$

On the other hand, $\alpha_1 = \alpha_3 = \pi/2$ and $a_3 = 0$ for globoidal cam mechanisms, and eq. (3.79) reduces to

$$\tan \mu = \frac{\lambda \phi'}{a_1 + \lambda \sin \phi} \tag{3.88}$$

3.3.2 Pressure Angle of RHCP Mechanisms

The unit normal of the cam surface of RHCP mechanisms is computed from application of eq.(C.5) and with the aid of eqs.(3.48). Thus, $e'_{43} = 0$ and p'_{43} is expressed as

$$\mathbf{p}'_{43} = \begin{bmatrix} -(a_1 + a_3)\sin\psi - z_3\sin\alpha_1\cos\psi - z_3'\sin\alpha_1\cos\psi \\ -(a_1 + a_3)\cos\psi + z_3\sin\alpha_1\sin\psi - z_3'\sin\alpha_1\cos\psi \end{bmatrix}$$
(3.89)

where the prime denotes differentiation with respect to ψ .

Now, n is given as in eq.(3.68) with u defined as

$$\mathbf{u} \equiv [-(a_1 + a_3) - z_3' \sin \alpha_1, \quad z_3 \sin \alpha_1, \quad 0]^T \tag{3.90}$$

Moreover, the unit vector in the direction of the velocity of the follower on I_{43} is given as

$$\mathbf{w} = [0, 1, 0]^T$$

15

From eq.(3.70), one can readily obtain

$$\tan \mu = \frac{-(a_1 + a_3 + z_3')}{z_3 \sin \alpha_1} \tag{3.91}$$

3.3.3 Pressure Angle of PHRR Mechanisms

The unit normal of the contact surface of PHRR mechanisms is computed from application of eq.(C.5) and with the aid of eqs.(3.55). Thus, $\mathbf{e}'_{43} = \mathbf{0}$ and \mathbf{p}'_{43} is expressed as

$$\mathbf{p}_{43}' = \begin{bmatrix} -\phi' a_3 \sin \phi \\ \cos \gamma & a_3 \phi' \cos \phi - \sin \alpha_1 \end{pmatrix}$$

$$\begin{bmatrix} \sin \alpha_1 (a_3 \phi' \cos \phi - \sin \alpha_1) \end{bmatrix}$$
(3.92)

where the prime denotes differentiation with respect to z_2 . Now, n is given as in eq.(3.68) with u defined as

$$\mathbf{u} \equiv \begin{bmatrix} a_3 \phi' \cos \phi - \sin \alpha_1 \\ a_3 \phi' \sin \phi \cos \alpha_1 \\ a_3 \phi' \sin \phi \sin \alpha_1 \end{bmatrix}$$
(3.93)

Moreover, the unit vector in the direction of the velocity of the follower on I_{43} is given as

$$\mathbf{w} = \begin{bmatrix} -\sin\phi \\ \cos\alpha_1\cos\phi \\ \sin\alpha_1\cos\phi \end{bmatrix}$$

From eq.(3.70), one obtains

$$\tan \mu = \frac{a_3 \phi' - \sin \alpha_1 \cos \phi}{\sin \phi \sin \alpha_1} \tag{3.94}$$

3.3.4 Pressure Angle of PHRP Mechanisms

The unit normal of the cam surface of PHRP mechanisms is computed from application of eq.(C.5) and with the aid of eqs.(3.64). Thus, $e'_{43} = 0$ and p'_{43} is expressed

as

$$\mathbf{p}_{43}' = \begin{bmatrix} 0 \\ -z_3' \sin \alpha_1 \\ z_3' \cos \alpha_1 - 1 \end{bmatrix}$$
 (3.95)

where the prime denotes differentiation with respect to z_2 .

Now, n is given, again, as in eq.(3.68), with u defined as

$$\mathbf{u} \equiv \begin{bmatrix} 0 \\ z_3' \cos \alpha_1 - 1 \\ z_3' \sin \alpha_1 \end{bmatrix}$$
 (3.96)

Furthermore, the unit vector in the direction of the velocity of the follower on I_{43} is given as

$$\mathbf{w} = [0, -\sin \alpha_1, \cos \alpha_1]^T$$

From eq.(3.70), one obtains

١,

$$\tan \mu = \frac{z_3' - \cos \alpha_1}{\sin \alpha_1} \tag{3.97}$$

3.4 Applications to Three-Link Mechanisms with Constant Pressure Angle

Cam mechanisms with a constant pressure angle are attractive because they involve rather simple follower shapes. Planar cam mechanisms with a flat-face follower are good examples of this kind, their followers containing planar surfaces at the camfollower interface. Here we study the synthesis of these mechanisms and their spherical counterparts. However, when dealing with the latter, one cannot speak in general of flat-face but rather of conical-face followers, as we will show presently.

The approach presented here for the synthesis of the mechanisms under study is based on the introduction of an auxiliary roller in contact with the cam and the follower, which gives rise to a four-link mechanism, although the mechanism under

study is, in fact of the three-link type. The lines of contact of the roller with the came and the follower are, respectively, the ISAs I_{42} and I_{43} , and hence, two higher pairs arise at the cam-follower interface. A nomenclature is adopted here to distinguish the aforementioned four-link mechanisms from the three-link mechanisms analyzed in Chapter 2, namely, the two higher pairs of the roller are indicated as $\overline{1111}$ in order to emphasize that these two higher pairs replace a single one. The synthesis of came mechanisms with a constant pressure angle is thus rendered similar to the synthesis of came mechanisms with roller-followers, the difference here being that the dual angle $\hat{\alpha}_3$ is unknown. On the other hand, it was proven in Section 3.3 that $\tan \nu = 1/\tan \mu$, i.e., $\nu = \pi/2 - \mu$. Thus, the dual curve of the cam is given as

$$\mathbf{s}_{c} \equiv \mathbf{e}_{42} + \epsilon \mathbf{m}_{42} = \hat{\mathbf{S}}^{T}(\hat{\psi})\hat{\mathbf{Q}}(\hat{\alpha}_{1})\hat{\mathbf{S}}(\hat{\phi})\hat{\mathbf{Q}}(\hat{\alpha}_{3})\hat{\mathbf{S}}(\hat{\nu})\hat{\mathbf{Q}}(\hat{\alpha}_{4})\mathbf{k}$$
(3.98)

and the surface of the cam is expressed as

$$\mathbf{r}_{c} \equiv \mathbf{e}_{42} \times \mathbf{m}_{42} + \lambda \mathbf{e}_{42} = \mathbf{p}_{42} + \lambda \mathbf{e}_{42}$$
 (3.99)

This approach is applied to those cases in which pure rolling between the cam and the roller is achieved, and hence, conical and cylindrical surfaces are considered. The envelopes of the roller on the follower give rise to a regular cone for spherical RHHR mechanisms and a plane for planar RHHR, RHHP, PHHR and PHHP mechanisms. The latter are the well-known planar mechanisms with a flat-face follower. The input-output functions are the same as for the related RHR, RHP, PHR and PPP mechanisms discussed in Chapter 2.

3.4.1 $R\overline{H}R$ Mechanisms

Figures 3.11 and 3.12 show the two cases of RHHR mechanisms with $\mu=0$. For the spherical RHHR, the dual terms of the angles of the eq.(3.98) are zero, while, for planar RHHR, the primal terms of the angles $\hat{\alpha}_i$ and the dual terms of the angles $\hat{\psi}$, $\hat{\phi}$ and $\hat{\nu}$ are zero.

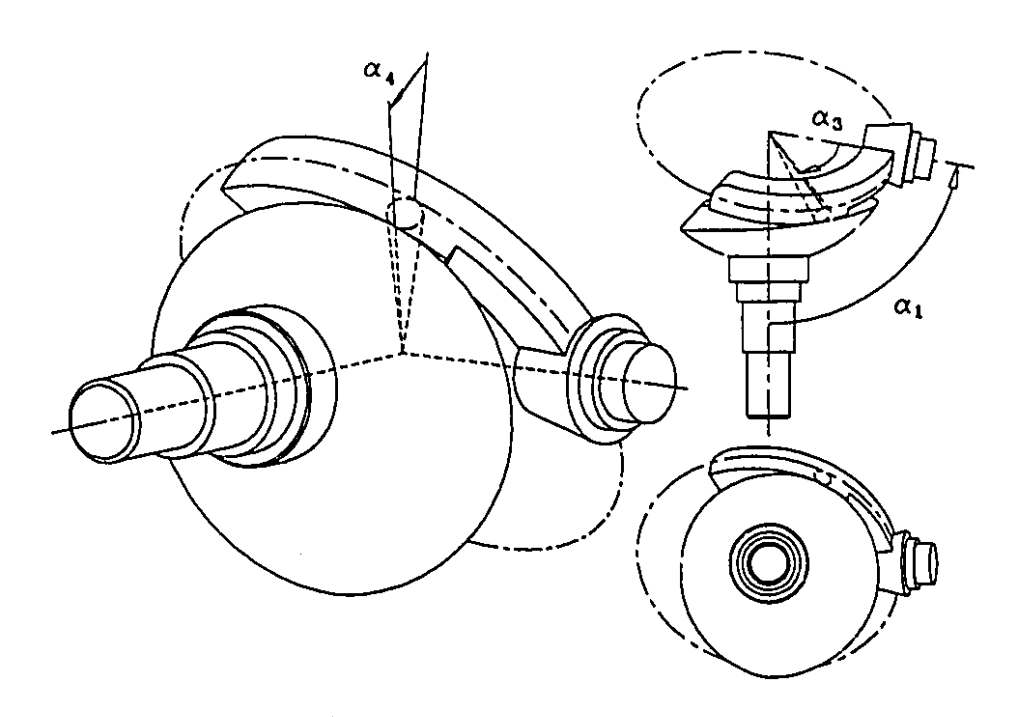


Figure 3.11 Spherical RHHR cam mechanism

Spherical RHHR mechanisms

With application of eq.(3.98), the surface of the cam is given via vector \mathbf{r}_c defined as

$$\mathbf{r}_{c} \equiv \lambda \mathbf{e}_{42} = \lambda \begin{bmatrix} k_{5} \sin \alpha_{4} - h_{1} \cos \alpha_{4} \\ -k_{6} \sin \alpha_{4} - h_{2} \cos \alpha_{4} \\ \sin \alpha_{1} \sin \phi \sin \alpha_{4} + k_{1} \cos \alpha_{4} \end{bmatrix}$$
(3.100)

where k_i and h_i are defined in eqs.(3.4) and, from eq.(3.80), it is clear that $\mu = 0$ if α_3 takes the value

$$\tan \alpha_3 = \frac{\sin \alpha_1 \cos \phi}{\phi' - \cos \alpha_1} \tag{3.101}$$

Note that spherical mechanisms with a constant pressure angle and zero offset, i.e., with $\alpha_4 = 0$, give rise to a flat-face follower.

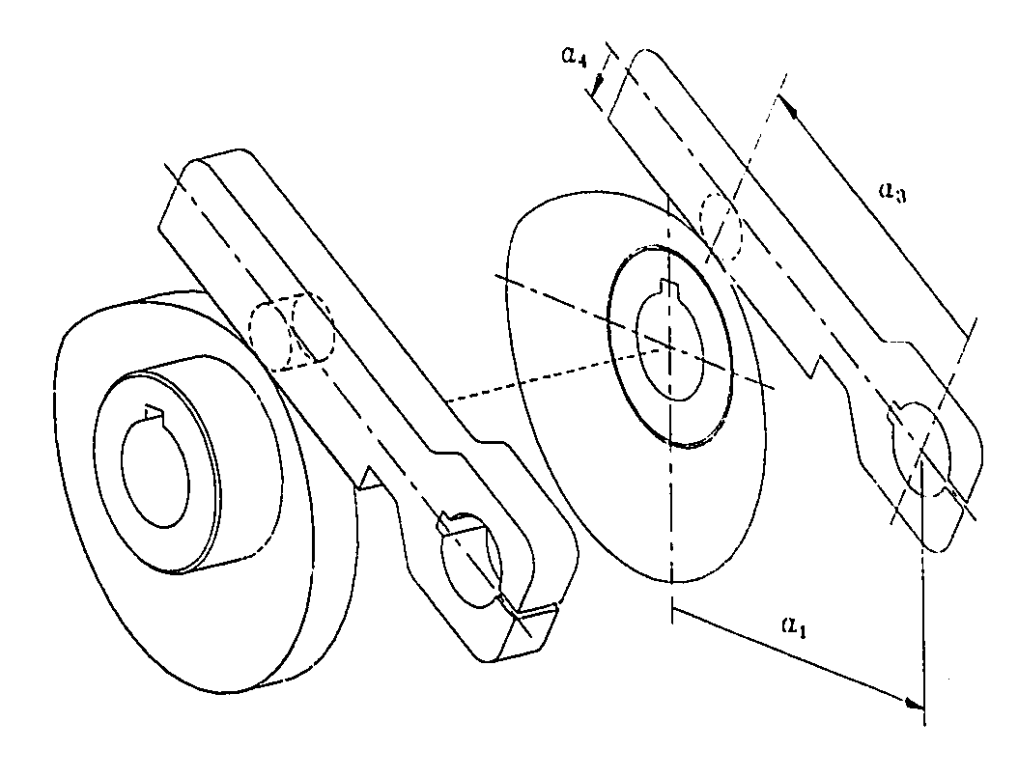


Figure 3.12 Planar RHHR cam mechanism

Planar RHHR mechanisms

Vectors e₄₂ and p₄₂ for planar RHHR mechanisms are readily obtained from eqs.(3.98 & 3.99) as

$$\mathbf{e_{42}} = \begin{bmatrix} 0 \\ 0 \\ 1 \end{bmatrix} \text{ and } \mathbf{p_{42}} = \begin{bmatrix} a_1 \cos \psi + a_3 \cos(\psi - \phi) + a_4 \sin(\psi - \phi) \\ -a_1 \sin \psi - a_3 \sin(\psi - \phi) + a_4 \cos(\psi - \phi) \\ 0 \end{bmatrix}$$
(3.102)

Now, from eq.(3.86) one obtains the value of a_3 in which $\mu = 0$, namely,

$$a_3 = \frac{a_1 \cos \phi}{\phi' - 1} \tag{3.103}$$

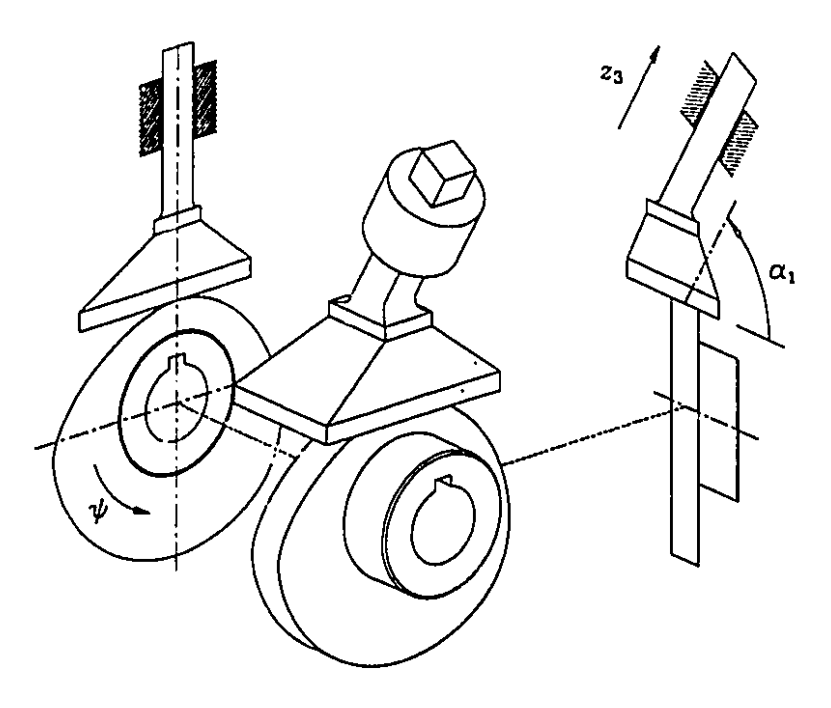


Figure 3.13 RHHP cam mechanism

3.4.2 RHHP Mechanisms

Considering that, from eq.(3.91), $a_3 = -a_1 - z_3' \sin \alpha_1$, vectors e_{42} and p_{42} of the surface of the cam are given as

$$\mathbf{e}_{42} = \begin{bmatrix} 0 \\ 0 \\ 1 \end{bmatrix} \text{ and } \mathbf{p}_{42} = \begin{bmatrix} -z_3' \sin \alpha_1 \cos \psi + (a_4 - z_3 \sin \alpha_1) \sin \psi \\ z_3' \sin \alpha_1 \sin \psi + (a_4 - z_3 \sin \alpha_1) \cos \psi \\ 0 \end{bmatrix}$$
(3.104)

Figure 3.13 shows a general case of an RHHP mechanism.

Comparing the size of a cam obtained with $\alpha_1 \neq \pi/2$ with that of the cam obtained with $\alpha_1 = \pi/2$, for the same displacement program, the former is of smaller size, henceforth, the angle α_1 should be considered as design parameter in optimization procedures which objective is minimize the cam size. However, as the angle α_1 decreases, the sliding between cam and follower increases. For the same displacement program, the size of the cam with $\alpha_1 = \pi/2$.

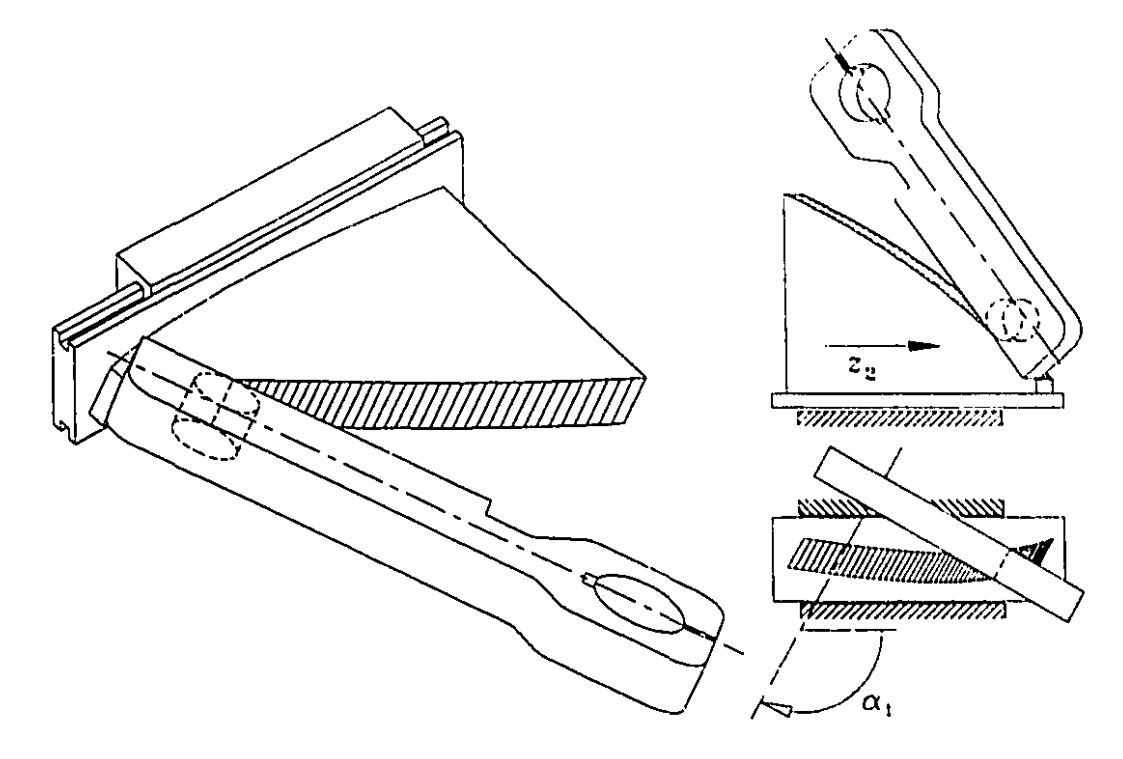


Figure 3.14 PHHR cam mechanism

3.4.3 PHHR Mechanisms

Figure 3.14 shows a PHHR mechanism. Vectors e_{42} and p_{42} , for the cam of this mechanism, are obtained from eqs. (3.98 & 3.99), namely,

$$\mathbf{e_{42}} = \begin{bmatrix} 0 \\ -\sin\alpha_1 \\ \cos\alpha_1 \end{bmatrix} \text{ and } \mathbf{p_{42}} = \begin{bmatrix} a_1 + a_3\cos\phi - a_4\sin\phi \\ a_3\cos\alpha_1\sin\phi + a_4\cos\alpha_1\cos\phi - z_2\cos\alpha_1\sin\alpha_1 \\ a_3\sin\alpha_1\sin\phi + a_4\cos\phi\sin\alpha_1 - z_2\sin^2\alpha_1 \end{bmatrix}$$
(3.105)

with a_3 obtained from eq.(3.94) as

$$a_3 = \frac{\sin \alpha_1 \cos \phi}{\phi'} \tag{3.106}$$

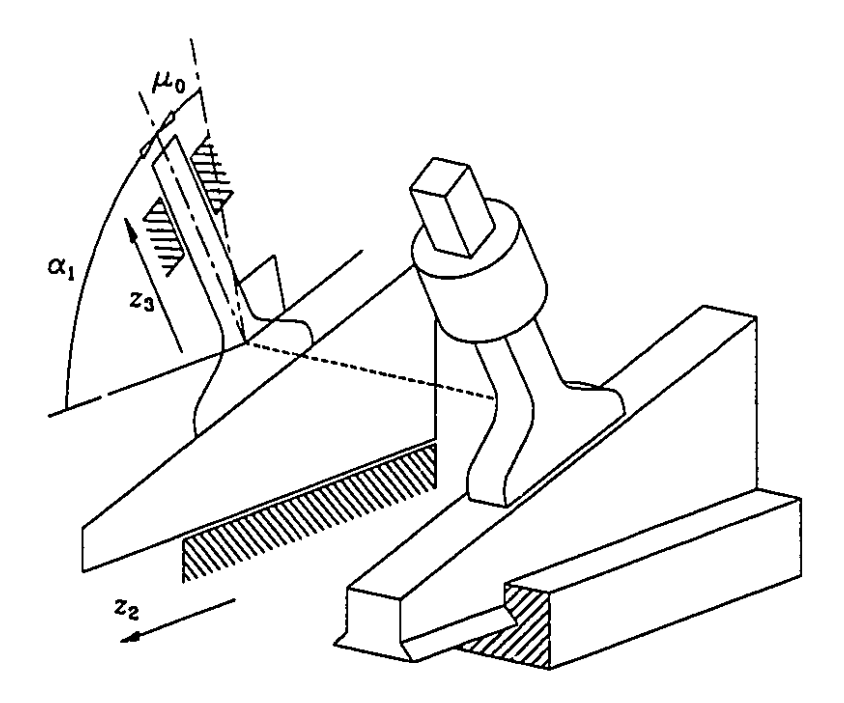


Figure 3.15 PHHP cam mechanism

3.4.4 PHHP Mechanisms

For the case of the PHHP mechanism, μ is independent of a_5 . Moreover, one can consider a given value of μ , namely, $\mu = \mu_0$, and hence, from eq.(3.97) one obtains

$$\tan \mu_0 = \frac{z_3' - \cos \alpha_1}{\sin \alpha_1} \tag{3.107}$$

10

Therefore, z_3' must be constant and, consequently, both surfaces will have flat faces, which thus gives rise to wedge cam mechanisms.

Considering that $\nu = \pi/2 - \mu_0$, one can readily obtain the vectors below:

$$\mathbf{e}_{42} = \begin{bmatrix} 1 \\ 0 \\ 0 \end{bmatrix} \text{ and } \mathbf{p}_{42} = \begin{bmatrix} 0 \\ a_3 \cos \alpha_1 - a_4 \sin(\alpha_1 - \mu_0) - z_3 \sin \alpha_1 \\ a_3 \sin \alpha_1 + a_4 \cos(\alpha_1 - \mu_0) + z_3 \cos \alpha_1 - z_2 \end{bmatrix}$$
(3.108)

Figure 3.15 illustrates a PHHP mechanism. Notice that the contact between cam and follower is a surface, giving as result a PPP mechanism.

Chapter 4

Realization of Indexing Motion with Higher Pairs

4.1 Introduction

Indexing mechanisms for motion and force transmission between parallel axes, such as the Geneva mechanism and external and internal parallel indexing cam mechanisms, have been studied in the past (Guoxun, Zhengyang and Huimin 1988), as well as indexing mechanisms for skew axes, such as the Ferguson indexing cam mechanism. Indexing cam mechanisms (ICM) have been used extensively, but the optimization of the cam contour for minimum friction losses, under various functionality conditions, has not been given due attention. Although the kinematics of spatial cams has been studied in the past (Jensen 1965; Chakraborty and Dhande 1977; Koloc and Václavík 1988), to our knowledge no work has been reported in connection with the minimization of power losses in the synthesis of spatial ICM. Here we propose a unified approach to the synthesis of cam and follower profiles, when motion is transmitted either through direct contact (RHR mechanisms) or through an intermediate roller (RHCR mechanisms), while power losses due to sliding are minimized.

These surfaces are generated with the application of the theory presented in Chapters 2 and 3, since this approach satisfies the condition that the relative velocity at the contact points is of minimum magnitude.

The method presented here can be applied to the synthesis of the contact surfaces of both the cam and the follower for a prescribed indexing output motion of the latter when the input cam rotates at a constant speed, assuming that the position of the axes of both the cam and the follower is given.

4.2 Input-Output Function of Indexing Cam Mechanisms (ICM)

As shown in Fig. 4.1, a full rotation of the cam is divided into two intervals, of lengths $\Delta \psi$ and $2\pi - \Delta \psi$. When the cam rotates in the second interval, ϕ is a constant, N being the number of indexing steps for one full rotation of the follower. Moreover, $\phi(\psi)$ is defined in the first interval as

$$\phi(\psi) = \frac{2\pi}{N} \tau \left(\frac{\psi}{\Delta \psi}\right) \tag{4.1}$$

where $\tau(x)$ is a normalized function, namely,

$$\tau = \tau(x), \quad 0 \le \tau \le 1, \quad 0 \le x \le 1$$
 (4.2)

The function $\tau(x)$ as discussed in Appendix D. Cycloidal motion is applied here for concreteness, but the ensuing analysis is not limited to this type of motion.

4.3 ICM of RHR Type

It was shown in Chapter 2 that, with the application of eqs. (2.16 & 2.18), it is possible to generate the shapes of two rigid bodies in contact, when transmitting a motion

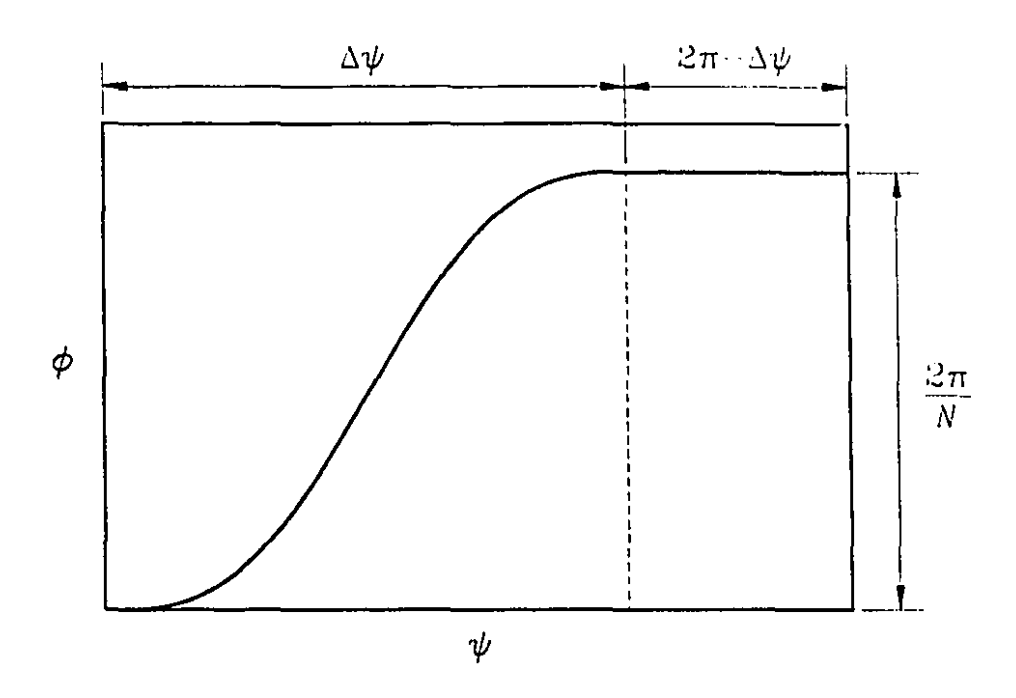


Figure 4.1 Motion function $\phi = \phi(\psi)$

given by the functional relation $\phi = \phi(\psi)$. Now, with $\phi(\psi)$ defined as in eq.(4.1), one can readily obtain the surfaces of an ICM of the type RHR mechanism (RHR-ICM) by prescribing the values: N; $\Delta \psi$; a_1 ; and a_1 .

Thus, ϕ and its first and second derivatives with respect to ψ are readily defined with the values of N and $\Delta\psi$, namely,

$$\phi = \frac{2\pi}{N} \left(\frac{\psi}{\Delta \psi} - \frac{1}{2\pi} \sin \frac{2\pi}{\Delta \psi} \right) \tag{4.3a}$$

$$\phi' = \frac{2\pi}{N\Delta\psi} \left(1 - \cos\frac{2\pi\psi}{\Delta\psi} \right) \tag{4.3b}$$

$$\phi'' = \frac{4\pi^2}{N\Delta^2\psi}\sin\frac{2\pi}{\Delta\psi} \tag{4.3c}$$

Equations (4.3) are valid in the range $0 \le \psi \le \Delta \psi$. For $\Delta \psi < \psi \le 2\pi$, $\phi = 2\pi/N$ and $\phi' = \phi'' = 0$.

The cam and follower surfaces are now defined, as in eqs. (2.18), by the vectors r₂

Chapter 4. Realization of Indexing Motion with Higher Pairs and \mathbf{r}_3 , respectively, as indicated below:

$$\mathbf{r}_{2} = b_{2} \begin{bmatrix} \cos \psi \\ -\sin \psi \end{bmatrix} + \lambda \begin{bmatrix} -\sin \psi \sin \theta_{2} \\ -\cos \psi \sin \theta_{2} \\ \cos \theta_{2} \end{bmatrix}$$

$$\mathbf{r}_{3} = (b_{2} - a_{1}) \begin{bmatrix} \cos \phi \\ -\sin \phi \end{bmatrix} + \lambda \begin{bmatrix} -\sin \phi \sin(\theta_{2} - \alpha_{1}) \\ -\cos \phi \sin(\theta_{2} - \alpha_{1}) \\ \cos(\theta_{2} - \alpha_{1}) \end{bmatrix}$$

where λ defines the thickness of the surfaces, while $\tan \theta_2$ and b_2 are computed as in eqs.(2.16c & 2.16d), namely,

$$\tan \theta_2 = \frac{\phi' \sin \alpha_1}{\phi' \cos \alpha_1 - 1}$$

$$b_2 = \frac{\phi'^2 - \phi' \cos \alpha_1}{\phi'^2 - 2\phi' \cos \alpha_1 + 1} a_1$$

A solid model of the surfaces defined above was implemented on a Silicon Graphics Power Series Workstation (IRIS 4D/420VGX). Moreover, the motion is simulated for any value of the four parameters defining the RHR-ICM. Thus, fixing three of them, the changes of the profile can be appreciated according to the variation of the fourth parameter.

In order to give a better idea of the software implemented for the above-mentioned purpose, we present four figures with six still frames each, so that the changes can be appreciated. Thus, in Fig. 4.2 six RHR-ICM are shown with different values of N, while in Fig 4.3, $\Delta \psi$ changes. Furthermore, the transition from spatial to spherical RHR-ICM, when a_1 varies from 1 to 0, is shown in Fig.4.4. Moreover, with $\alpha_1 = 0$ in Fig. 4.5, the cam and the follower have parallel axes and rotate in the same direction. In this configuration, the mechanism is an internal RHR-ICM. As α_1 increases, the input and output axes are skew until they become parallel again with $\alpha_1 = \pi$. At this value, the cam and the follower rotate in opposite directions, thus giving rise to an external RHR-ICM. The transition from internal to external RHR-ICM is shown with four intermediate configurations.

.

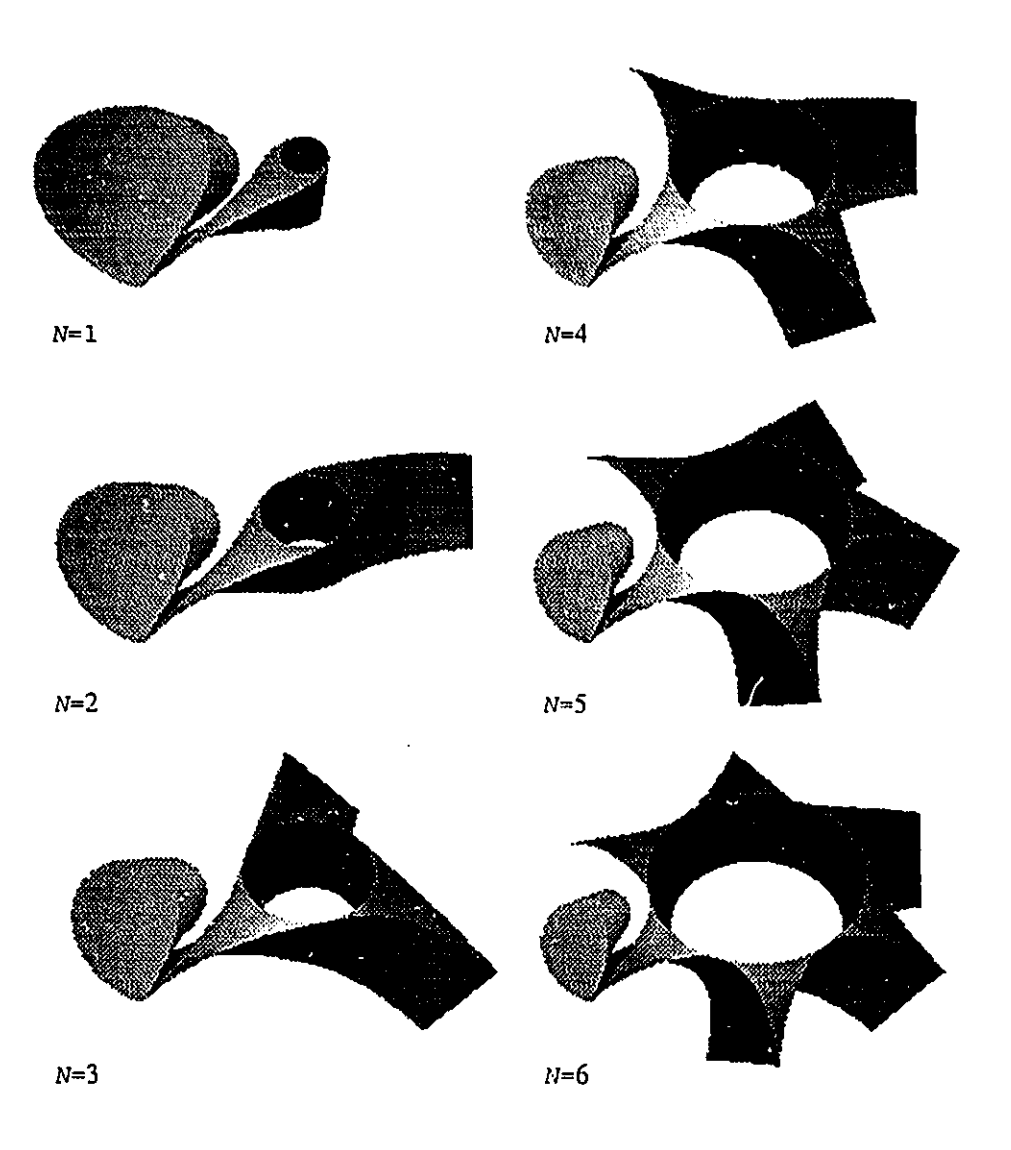


Figure 4.2 Spatial RHR-ICM with $\Delta \psi = 120^{\circ}$, $a_1 = 1$, $\alpha_1 = 60^{\circ}$ and $0.25 \le \lambda \le 0.85$ for six different values of N

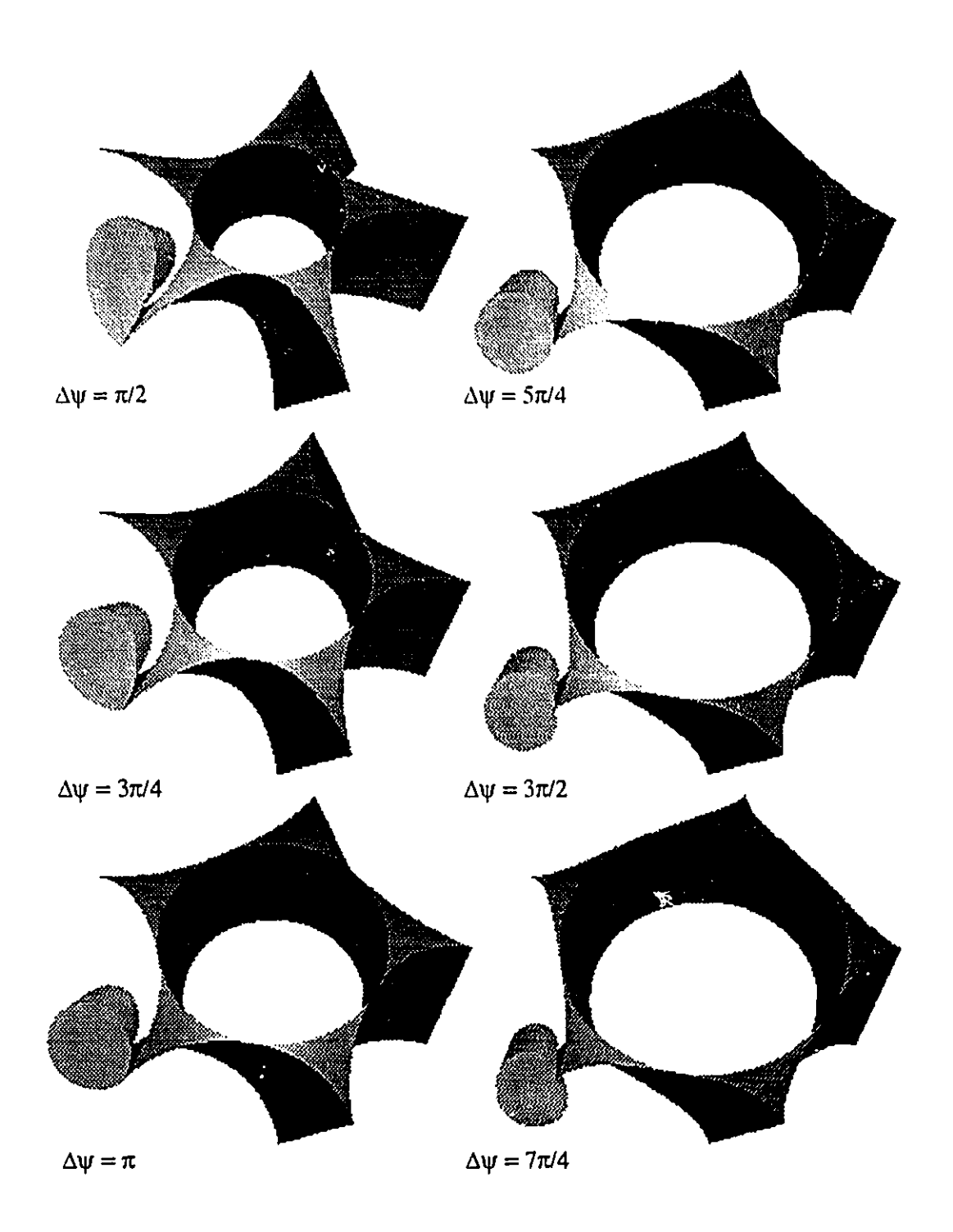


Figure 4.3 Spatial RHR-ICM with $N=5,\,a_1=0.8,\,\alpha_1=45^\circ$ and $0.4\leq\lambda\leq1.0$ for six different values of $\Delta\psi$

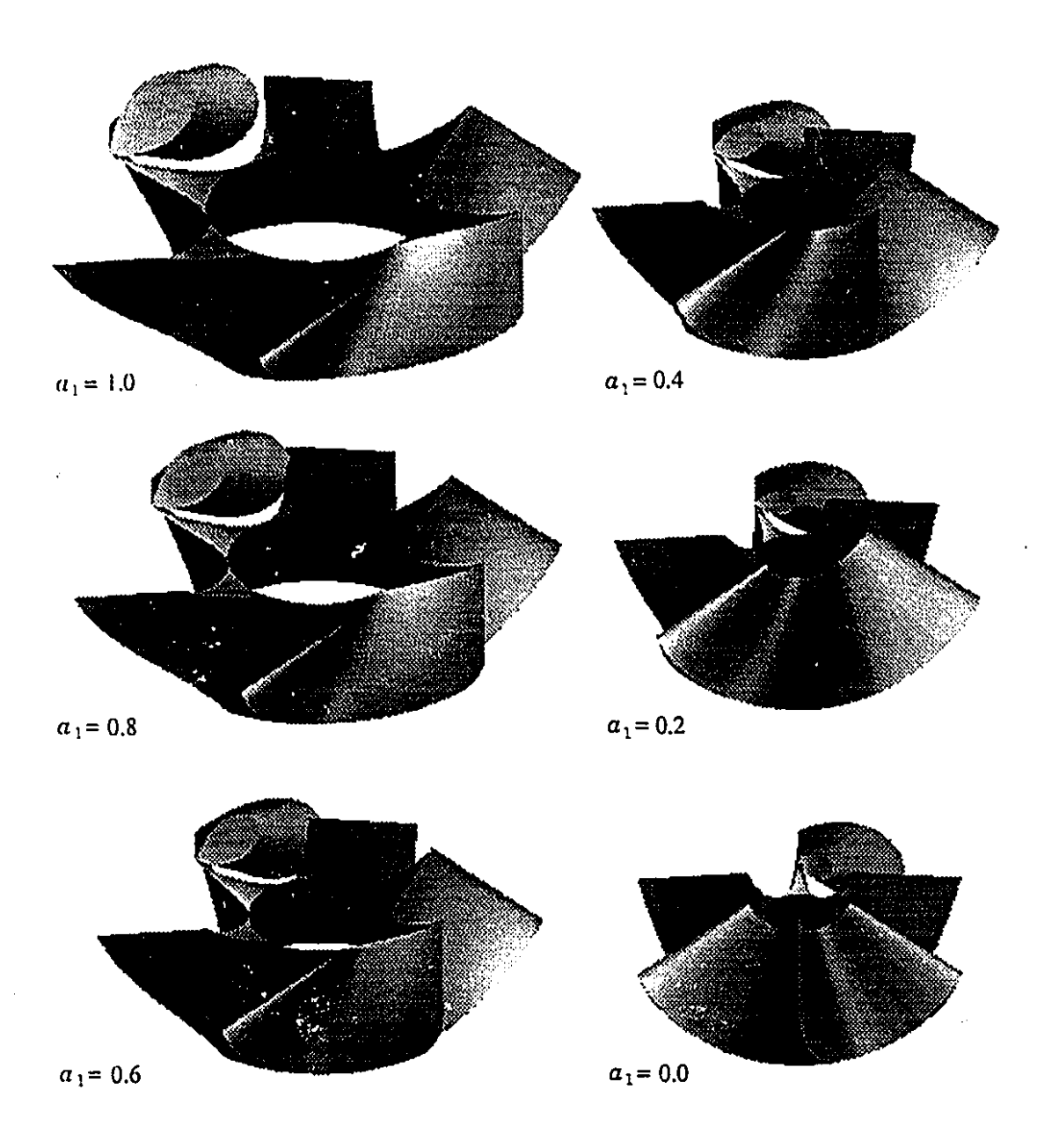


Figure 4.4 Transition from spatial to spherical RHR-ICM with N=6, $\Delta\psi=120^{\circ}$, $\alpha_1=70^{\circ}$ and $0.3\leq\lambda\leq0.95$

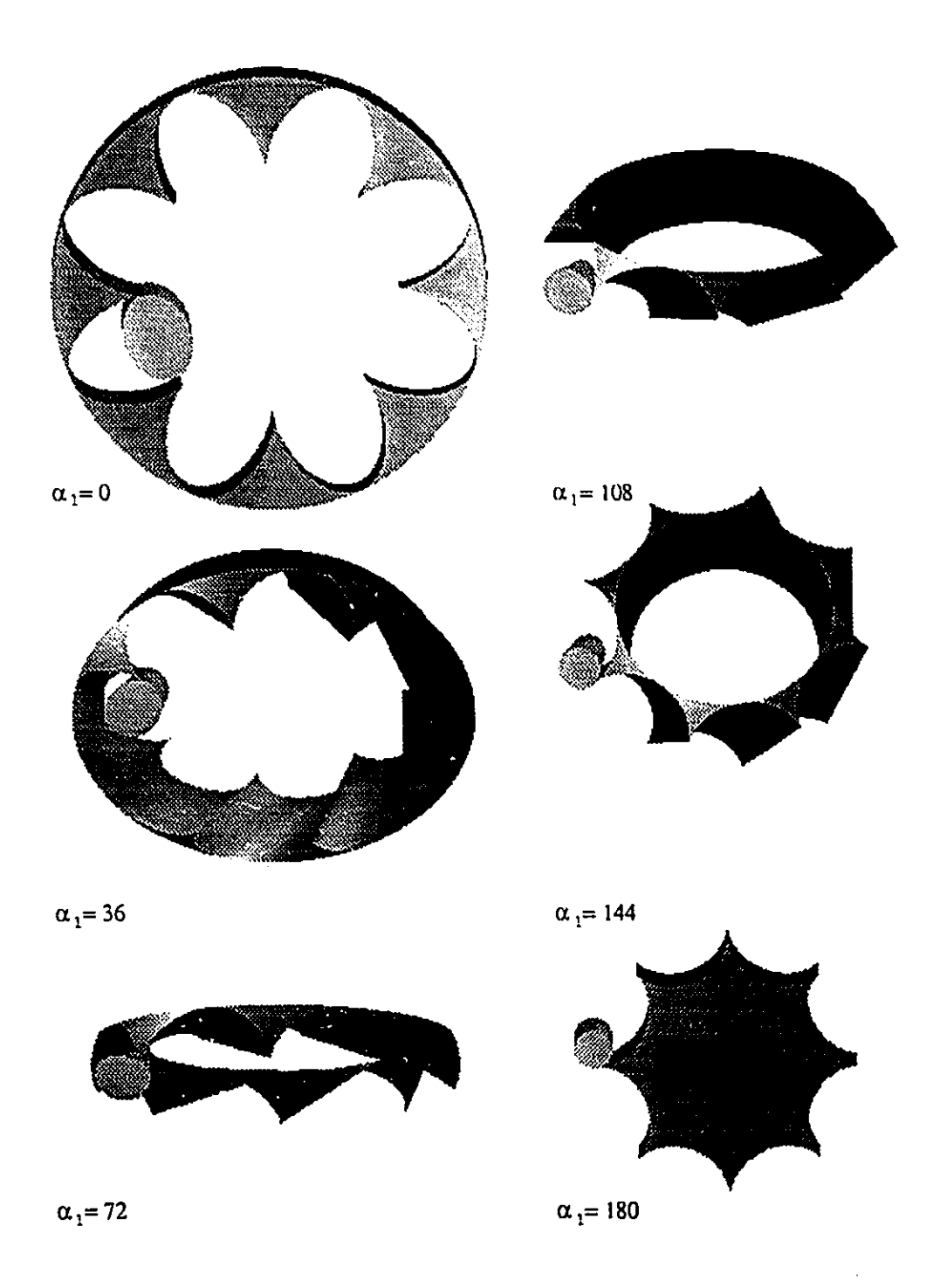


Figure 4.5 Transition from internal to external RHR-ICM with $N=8, \, \Delta\psi=220^{\circ}, \, a_1=1$ and $0.4\leq\lambda\leq1.0$

4.4 ICM of RHCR Type

The theory for the synthesis of RHCR mechanisms was already introduced in Section 3.2.1. Thus, what defines an ICM is the input-output function, which is given as

$$\phi = \phi_m + \frac{2\pi}{N}\tau \left(\frac{\psi}{\Delta\psi}\right) \tag{4.4}$$

where ϕ_m is the value of ϕ upon engagement of the roller with the cam as illustrated in Fig. 4.6. For the applications presented in Chapter 5, ϕ_m is defined as

$$\phi_m = \pi \left(1 - \frac{1}{N} \right) \tag{4.5}$$

In Fig. 4.6a ϕ_m is shown for an internal ICM, whereas in Fig. 4.6b ϕ_m is shown for an external ICM.

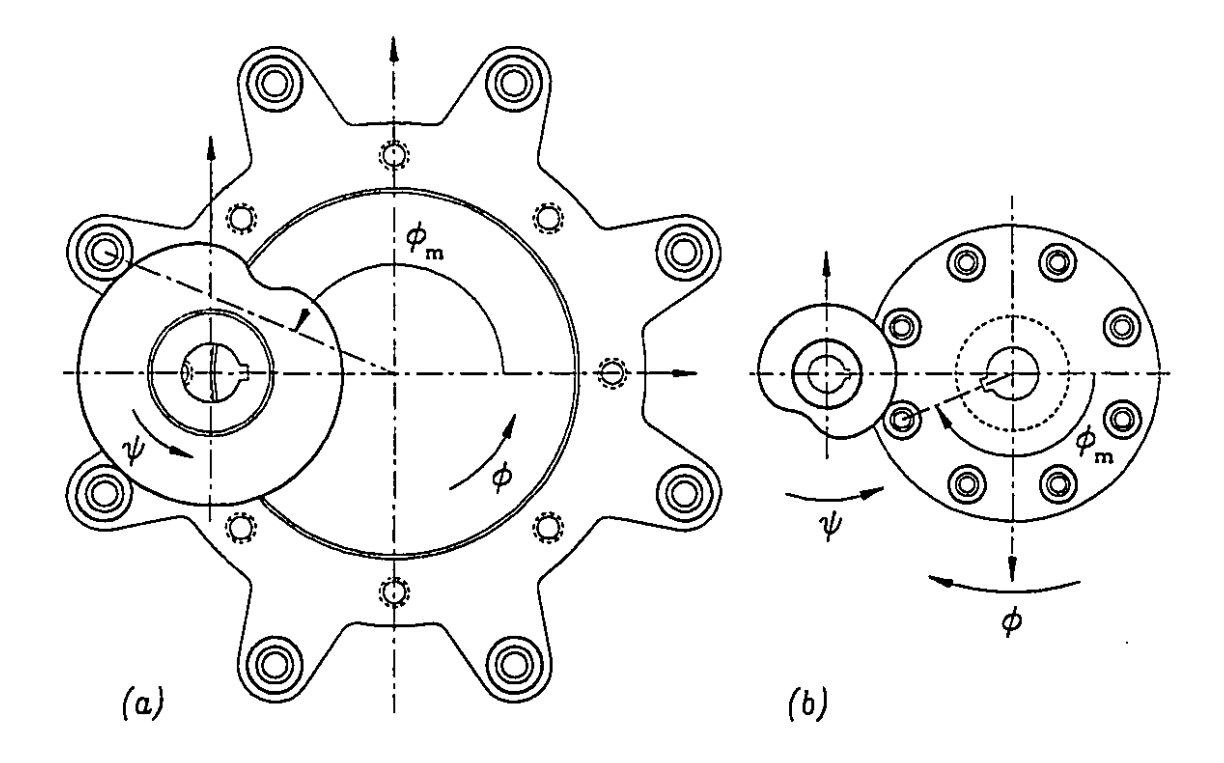


Figure 4.6 Definition of ϕ_m for RHCR-ICM: a) internal; b) external

There are two approaches to determine the geometry of an RHCR-ICM. The first one consists of the application of eqs.(3.27), and the second, of the application of eqs.(3.98 & 3.99). The latter was found more reliable from the computational point of view; it was therefore, applied in *USYCAMS*¹, the software written for the unified synthesis of RHCR-ICM.

Equation (3.98) is rewritten here for quick reference, namely,

$$\mathbf{s}_{c} \equiv \mathbf{e}_{42} + \epsilon \mathbf{m}_{42} = \hat{\mathbf{S}}^{T}(\psi) \hat{\mathbf{Q}}(\hat{\alpha}_{1}) \hat{\mathbf{S}}(\phi) \hat{\mathbf{Q}}(\hat{\alpha}_{3}) \hat{\mathbf{S}}(\hat{\nu}) \hat{\mathbf{Q}}(\hat{\alpha}_{4})$$

where $\hat{\nu}$ defined in eq.(3.23) as

$$\tan \hat{\nu} \equiv \tan \nu + \epsilon z_{43} (1 + \tan^2 \nu) = \frac{-\sin \hat{\beta} \sin \hat{\phi}}{\cos \hat{\beta} \sin \hat{\alpha}_3 + \cos \hat{\alpha}_3 \cos \hat{\phi} \sin \hat{\beta}}$$

which can be readily expanded in its primal and dual parts, namely,

$$\tan \nu = \frac{-\sin \beta \sin \phi}{\cos \beta \sin \alpha_3 + \cos \alpha_3 \sin \beta \cos \phi} \tag{4.6a}$$

$$z_{43} = \frac{a_3 \sin \beta (\cos \beta \cos \alpha_3 - \sin \alpha_3 \sin \beta \cos \phi) - d \sin \alpha_3}{(\cos \beta \sin \alpha_3 + \cos \alpha_3 \sin \beta \cos \phi)^2 + \sin^2 \beta \sin^2 \phi} \sin \phi$$
 (4.6b)

where $\beta = \alpha_1 - \theta_2$ and $d = a_1 - b_2$.

Thus, given N, $\Delta \psi$, $\phi(\psi)$ and the dual angles $\hat{\alpha}_1$, $\hat{\alpha}_3$ and $\hat{\alpha}_4$, which are described in Table 3.1, the cam profile of an RHCR-ICM can be obtained with the aid of USYCAMS. However, the dual angle $\hat{\alpha}_3$ cannot be chosen arbitrarily as discussed in Chapter 5, where we show how to specify it. A solid model of this type of ICM was implemented using USYCAMS. The transition from internal to external RHCR-ICM is shown in Fig. 4.7 with N=8 and $\Delta \psi=240^\circ$, while, in Fig. 4.8, the transition from spatial to spherical RHCR-ICM is shown.

¹Pronounced you see cams, for Unified Synthesis of Cam Mechanisms

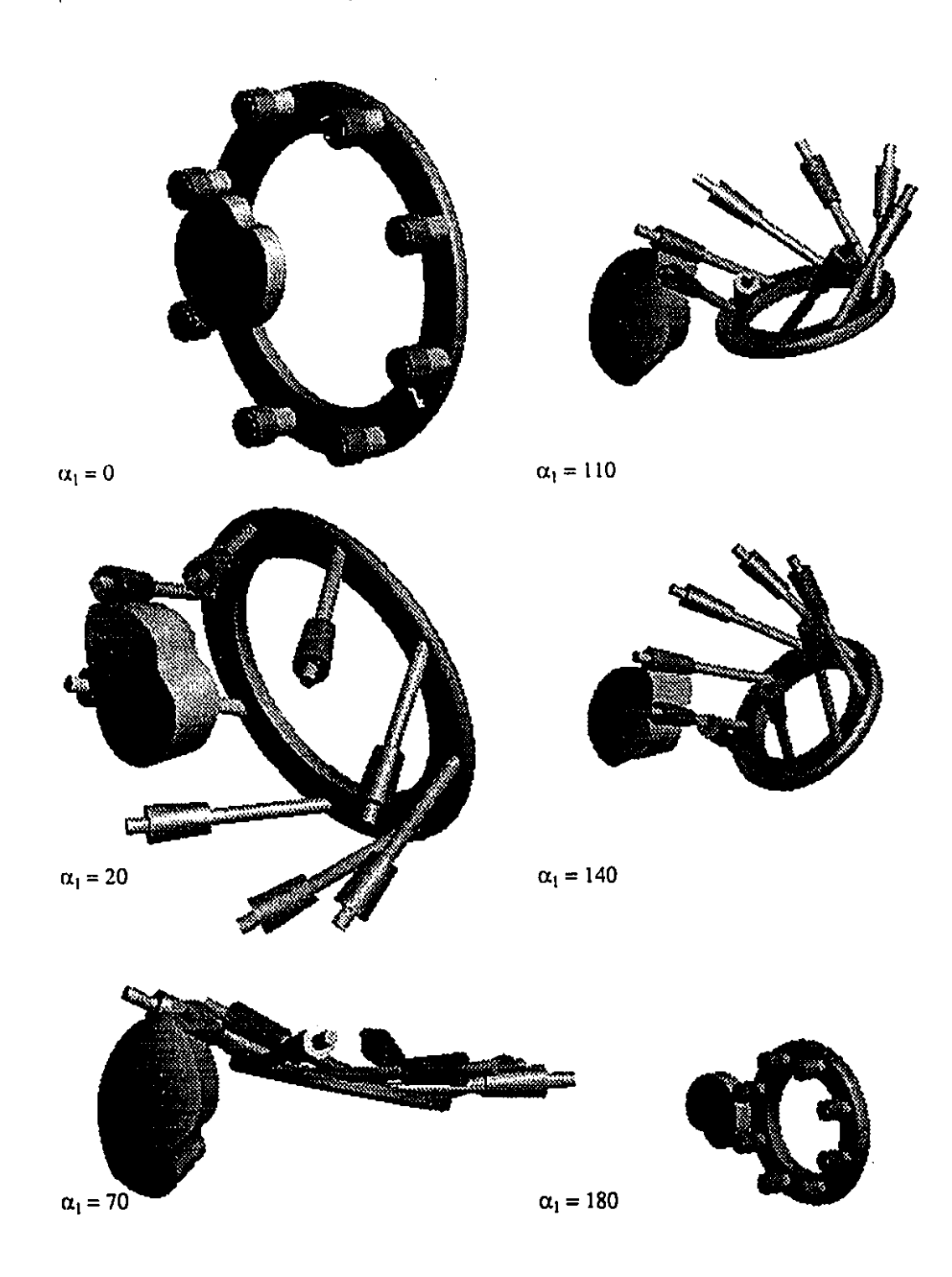


Figure 4.7 Transition from internal to external RHCR-ICM with $N=8,\,\Delta\psi=240^\circ$

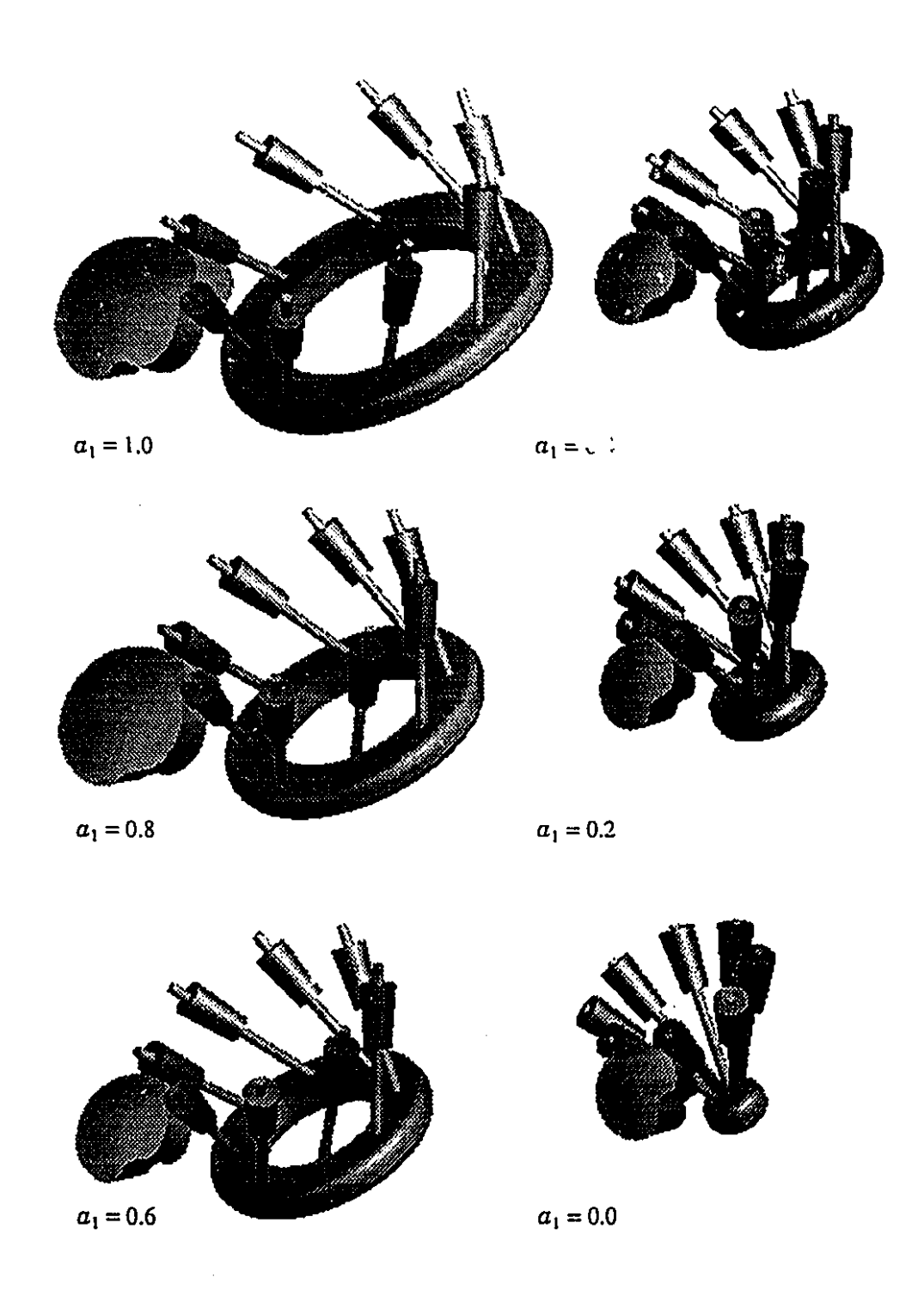


Figure 4.8 Transition from spatial to spherical RIICR-ICM with $N=8, \, \Delta\psi=240^{\circ}, \, \alpha_1=135^{\circ}$ and $0.3\leq\lambda\leq0.95$

Chapter 5

Pure-Rolling Motion with ICM

5.1 Introduction

Indexing cam mechanisms ICM with helical springs to maintain contact have been designed in the past (Johnson, 1958). However, the use of springs in cam mechanisms leads to dynamic problems of vibration. Consequently, the design of planar cam mechanisms with positive motion, i.e., without springs, has been proposed as an alternative (Jackowski and Dubil, 1967; Wunderlich, 1971; Hunt, 1973). This concept has been applied to the design of planar ICM (Makino, 1979; Jones and Tsang, 1987; Gouxun, Zhengyang and Huimin, 1988). In the latter reference, pure-rolling motion has been achieved. However, the mechanisms thus designed have the disadvantage that the pressure angle is large, especially at and near the dwell positions. Indexing mechanisms such as the Geneva mechanism have been studied, e.g., (Fenton, 1965, 1975a, 1975b; Oledzki and Szydlowski, 1975), but these mechanisms have jerk discontinuities and wear problems. The elimination of jerk discontinuities in this context was reported by Sadek, Lloyd, and Smith (1990).

ICM with direct contact for spatial, spherical and planar motions were introduced

in González-Palacios and Angeles (1990). A unified approach of ICM with roller followers is presented in (González-Palacios and Angeles, 1992). Both approaches being discussed in Chapter 4. These formulations are combined in this Chapter to obtain a new type of mechanism that is termed here PRICAM (Pure Rolling Indexing Cam Mechanism) with positive motion, pure rolling and improved pressure-angle distribution. The pressure angle vanishes at the beginning and at the middle of the rise, which makes PRICAM a unique design. The condition applied on the design of PRICAM being the elimination of wear, and hence, two versions are proposed here, namely, planar and spherical mechanisms.

5.2 Primary and Secondary Mechanisms

Here we distinguish two mechanisms, namely, the primary mechanism (PM), which is an RHR ICM, and the secondary mechanism (SM), which is constituted by an RHRR ICM.

The generation of the higher-pair contact surface of both PM and SM is based on the minimization of the magnitude of the relative velocity at the contact points, namely, cam-follower pair for the PM and cam-roller pair for the SM. It was discussed in Section 2.2.1 that, for planar and spherical RHR mechanisms, the relative velocity v_{32} is zero. Similarly, for planar and spherical RHRR mechanisms, it was shown in Section 3.2.1 that the velocity v_{42} between cam and roller is zero as well. Thus, as discussed in Chapters 2 and 3, those surfaces are generated as ruled surfaces and represented in the parametric form

$$\mathbf{r}(\psi,\lambda) = \mathbf{p}(\psi) + \lambda \mathbf{e}(\psi) \tag{5.1}$$

where $r(\psi, \lambda)$ is the position vector of a point of the surface, ψ is the angle of rotation of the cam, λ is a real number, p is the position vector of the directrix, and e is a unit vector parallel to the generatrix.

5.2.1Primary Mechanism

We regard here, as in Chapter 3, planar mechanisms as special cases of spherical mechanisms. Accordingly, we study the latter first, then the former.

Spherical PM

From the definition of the geometry of spherical RHR mechanisms with $a_1 = 0$, the geometry of the spherical PM is given as,

$$\mathbf{r}_{2} = \lambda \begin{bmatrix} -\sin \psi \sin \theta_{2} \\ -\cos \psi \sin \theta_{2} \\ \cos \theta_{2} \end{bmatrix}$$
 (5.2a)

$$\mathbf{r}_{2} = \lambda \begin{bmatrix} -\sin \psi \sin \theta_{2} \\ -\cos \psi \sin \theta_{2} \\ \cos \theta_{2} \end{bmatrix}$$

$$\mathbf{r}_{3} = \lambda \begin{bmatrix} -\sin \psi \sin(\theta_{2} - \alpha_{1}) \\ -\cos \psi \sin(\theta_{2} - \alpha_{1}) \\ \cos(\theta_{2} - \alpha_{1}) \end{bmatrix}$$

$$(5.2a)$$

$$(5.2b)$$

with θ_2 defined as in eq(2.16c), i.e.,

$$\tan \theta_2 = \frac{\phi' \sin \alpha_1}{\phi' \cos \alpha_1 - 1} \tag{5.3}$$

Moreover, the pressure angle can be computed from eq.(2.55) as,

$$\tan \mu = \frac{\phi' \sqrt{\phi'^2 - 2\phi' \cos \alpha_1 + 1}}{\phi''}$$
 (5.4)

Planar PM

The geometry of the planar PM is defined by the geometry of planar RHR mechanisms with $\alpha_1 = 0, \pi$. Thus, the position vectors of both cam and follower are derived from eqs.(2.18a & 2.18b), namely,

$$\mathbf{r}_{2} = \frac{\phi' a_{1}}{\phi' \pm 1} \begin{bmatrix} \cos \psi \\ -\sin \psi \\ 0 \end{bmatrix} + \lambda \begin{bmatrix} 0 \\ 0 \\ 1 \end{bmatrix}$$

$$\mathbf{r}_{3} = \frac{a_{1}}{\phi' \pm 1} \begin{bmatrix} \cos \phi \\ -\sin \phi \\ 0 \end{bmatrix} + \lambda \begin{bmatrix} 0 \\ 0 \\ 1 \end{bmatrix}$$

$$(5.5a)$$

$$\mathbf{r}_{3} = \frac{a_{1}}{\phi' \pm 1} \begin{bmatrix} \cos \phi \\ -\sin \phi \\ 0 \end{bmatrix} + \lambda \begin{bmatrix} 0 \\ 0 \\ 1 \end{bmatrix}$$
 (5.5b)

The pressure angle is as defined in eq.(2.61), namely,

$$\tan \mu = \frac{\phi'(\phi' \pm 1)}{\phi''} \tag{5.6}$$

the plus and minus signs corresponding to external and internal PM, respectively.

5.2.2 Secondary Mechanism

Spherical SM

The pitch and the cam surfaces for the spherical mechanism are defined as in eqs. (3.28) & 3.29), namely,

$$\mathbf{r}_{P} \equiv \lambda \mathbf{e}_{P} = \lambda \begin{bmatrix} s\alpha_{3}s\phi c\psi - (s\alpha_{1}c\alpha_{3} + c\alpha_{1}s\alpha_{3}c\phi)s\psi \\ -s\alpha_{3}s\phi s\psi - (s\alpha_{1}c\alpha_{3} + c\alpha_{1}s\alpha_{3}c\phi)c\psi \\ c\alpha_{1}c\alpha_{3} - s\alpha_{1}s\alpha_{3}c\phi \end{bmatrix}$$

$$\mathbf{r}_{C} \equiv \lambda \mathbf{e}_{C} = \lambda \begin{bmatrix} s(\theta_{3} - \alpha_{4})s\delta c\psi - [s\theta_{2}c(\theta_{3} - \alpha_{4}) + c\theta_{2}s(\theta_{3} - \alpha_{4})c\delta]s\psi \\ -s(\theta_{3} - \alpha_{4})s\delta s\psi - [s\theta_{2}c(\theta_{3} - \alpha_{4}) + c\theta_{2}s(\theta_{3} - \alpha_{4})c\delta]c\psi \end{bmatrix}$$

$$c\theta_{2}c(\theta_{3} - \alpha_{4}) - s\theta_{2}s(\theta_{3} - \alpha_{4})c\delta$$

$$(5.7)$$

$$\mathbf{r}_{C} \equiv \lambda \mathbf{e}_{C} = \lambda \begin{bmatrix} s(\theta_{3} - \alpha_{4})s\delta c\psi - [s\theta_{2}c(\theta_{3} - \alpha_{4}) + c\theta_{2}s(\theta_{3} - \alpha_{4})c\delta]s\psi \\ -s(\theta_{3} - \alpha_{4})s\delta s\psi - [s\theta_{2}c(\theta_{3} - \alpha_{4}) + c\theta_{2}s(\theta_{3} - \alpha_{4})c\delta]c\psi \end{bmatrix} (5.8)$$

$$c\theta_{2}c(\theta_{3} - \alpha_{4}) - s\theta_{2}s(\theta_{3} - \alpha_{4})c\delta$$

where θ_2 , θ_3 and δ , are given as,

$$\tan \theta_2 = \frac{\phi' \sin \alpha_1}{\phi' \cos \alpha_1 - 1} \tag{5.9a}$$

$$\tan \theta_3 = \frac{\sqrt{[c(\alpha_1 - \theta_2)c\phi s\alpha_3 + c\alpha_3 s(\alpha_1 - \theta_2)]^2 + s^2\alpha_3 s^2\phi}}{c\alpha_3 c(\alpha_1 - \theta_2) - c\phi s\alpha_3 s(\alpha_1 - \theta_2)}$$
(5.9b)

$$\tan \delta = \frac{s\alpha_3 s\phi}{s\alpha_3 c(\alpha_1 - \theta_2) c\phi + c\alpha_3 s(\alpha_1 - \theta_2)}$$
 (5.9c)

Furthermore, the pressure angle is as defined in eq.(3.81), i.e.,

$$\tan \mu = \frac{(\phi' - \cos \alpha_1) \sin \alpha_3 - \sin \alpha_1 \cos \alpha_3 \cos \phi}{\sin \alpha_1 \sin \phi}$$
 (5.10)

In the design of spherical RHRR ICM, $N, \Delta \psi$ and α_1 are given as design specifications. However, α_3 cannot be assigned arbitrarily for, beyond a certain bound, undercutting will occur. The maximum allowable value of α_3 , defined as $\bar{\alpha}_3$, can be derived by analyzing the spherical radius of curvature of the pitch curve Γ .

In order to generalize the solution, we write the radius of curvature as $\rho = \rho(\psi, \alpha_3, \alpha_1, N, \Delta \psi)$. Thus, in terms of \mathbf{e}_P , defined in eq.(5.7), and its first and second derivatives with respect to ψ , ρ is expressed as (Guggenheimer, 1977)

$$\rho = \arctan\left(\frac{(\mathbf{e}_P' \cdot \mathbf{e}_P')^{3/2}}{\mathbf{e}_P \times \mathbf{e}_P' \cdot \mathbf{e}_P'}\right)$$
 (5.11)

Now, we are interested on those points of Γ where cusps occur, i.e., where $\rho = 0$. First we search for the values ψ_0 where ρ attains a minimum value, i.e., we make $d\rho/d\psi = 0$, which readily leads to

$$f(\psi_0, \alpha_3, \alpha_1, N, \Delta \psi) \equiv e_P \times e_P' \cdot [3(e_P' \cdot e_P')e_P'' - (e_P' \cdot e_P')e_P''] = 0$$
 (5.12)

The analysis of the motion covers one indexing step and hence, it starts at $\phi(-\Delta\psi/2) = -\pi/N$ and finishes at $\phi(\Delta\psi/2) = \pi/N$. For a cycloidal motion, ϕ and ϕ' are readily derived, namely,

$$\phi = \Delta \phi(x + \frac{1}{2\pi} \sin 2\pi x), \quad x \equiv \frac{\psi}{\Delta \psi}, \quad \Delta \phi \equiv \frac{2\pi}{N}$$
 (5.13)

$$\phi' = \frac{\Delta \phi}{\Delta \psi} (1 + \cos 2\pi x), \qquad -\frac{1}{2} \le x \le \frac{1}{2}$$
 (5.14)

With the aid of symbolic algebra, we found that $\psi_0 = 0$ always satisfies eq.(5.12), i.e., $f(0, \alpha_3, \alpha_1, N, \Delta \psi) \equiv 0$. Moreover, we found graphically that f can have one or three roots; however, the minimum absolute value of ρ is found at $\psi_0 = 0$.

Now, $\bar{\alpha}_3$ is obtained as a solution of $\rho(0, \bar{\alpha}_3, \alpha_1, N, \Delta \psi) = 0$. In view of eq.(5.11), ρ is zero if

$$\mathbf{e}_{P}' \cdot \mathbf{e}_{P}' = 0 \tag{5.15}$$

Furthermore, from eq.(5.7), e'_P at $\psi = 0$ is readily obtained as

$$\mathbf{e}_{P}'(0) = [-\sin\alpha_{1}\cos\bar{\alpha}_{3} + (\phi_{0}' - \cos\alpha_{1})\sin\bar{\alpha}_{3}, \quad 0, \quad 0]^{T}$$
 (5.16)

where $\phi_0' = 4\pi/N\Delta\psi$ is computed from eq.(5.14) at $\psi = 0$.

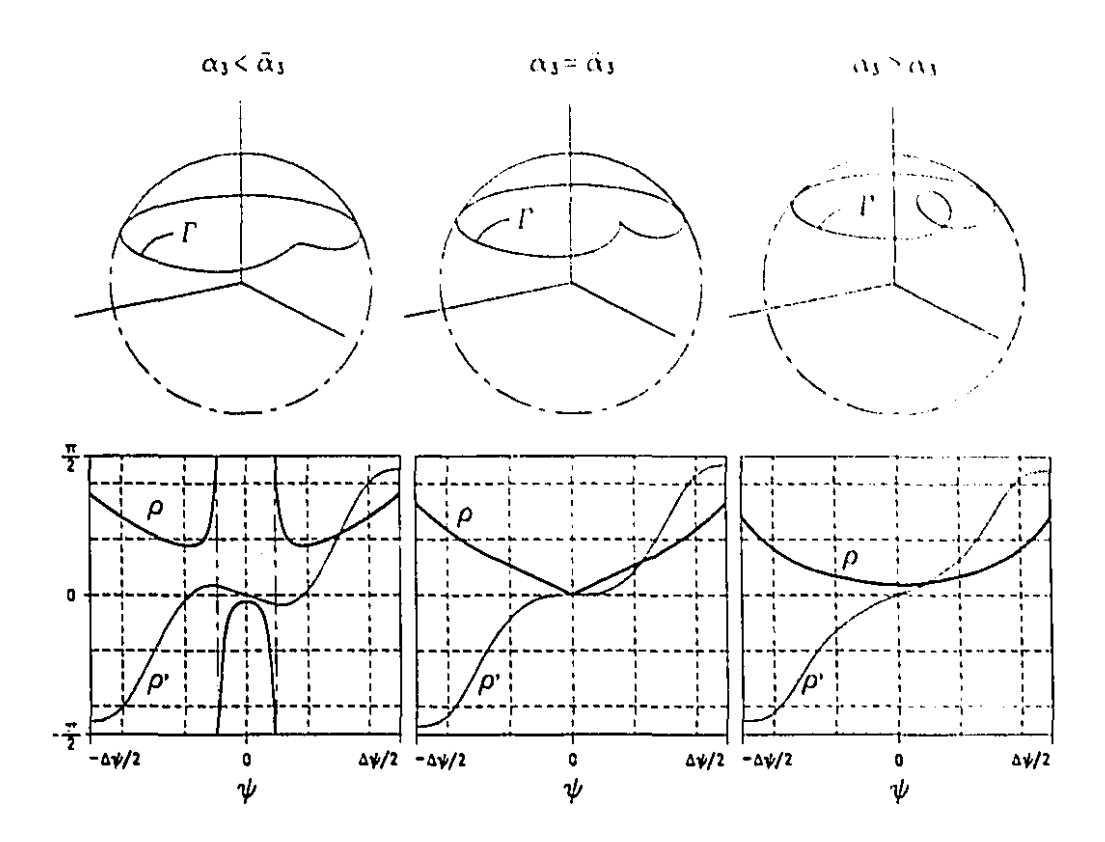


Figure 5.1 The pitch curve and the corresponding plots of ρ and ρ' for three values of α_3 .

Substituting eq.(5.16) into eq.(5.15), the limiting value of α_3 is readily derived, namely,

$$\tan \bar{\alpha}_3 = \frac{\sin \alpha_1}{4\pi/N\Delta\psi - \cos \alpha_1} \tag{5.17}$$

Figure 5.1 illustrates the pitch curve for three different values of α_3 , with the corresponding plots of ρ and ρ' . Notice that, for $\alpha_3 < \bar{\alpha}_3$, ρ' has three roots but ρ attains its minimum at $\psi = 0$.

These results are now summarized below:

Theorem 5.1: Given α_1 , N, $\Delta \psi$ and the input-output function defined as in eq.(4.1), the pitch curve of a spherical RHRR ICM reaches a cusp at $\psi = 0$ if $\alpha_3 = \bar{\theta}_2 - \alpha_1$, $\bar{\theta}_2$ being the value of θ_2 at $\psi = 0$.

We prove this theorem showing that $\hat{\theta}_2 - \alpha_1 \equiv \bar{\alpha}_3$, with $\bar{\alpha}_3$ defined above as the maximum value attained by α_3 . First, we expand $\tan(\theta_2 - \alpha_1)$, namely,

$$\tan(\bar{\theta}_2 - \alpha_1) = \frac{\tan\bar{\theta}_2 - \tan\alpha_1}{1 + \tan\bar{\theta}_2 \tan\alpha_1}$$
 (5.18)

Now, substituting eq.(5.9a) into eq.(5.18), we obtain

$$\tan(\bar{\theta}_2 - \alpha_1) = \frac{\sin \alpha_1}{\phi_0' - \cos \alpha_1} \equiv \tan \bar{\alpha}_3 \tag{5.19}$$

thereby proving the theorem.

Planar SM

The geometry of planar SM is defined by the geometry of planar RHRR mechanisms with $\alpha_1 = \pi$ for external and $\alpha_1 = 0$ for internal SM. Thus, the pitch and the cam surfaces are defined according to eqs.(3.35-3.37) as

$$\mathbf{r}_{P} = \begin{bmatrix} c\psi a_{1} + c(\psi \pm \phi)a_{3} \\ -s\psi a_{1} - s(\psi \pm \phi)a_{3} \\ 0 \end{bmatrix} + \lambda \begin{bmatrix} 0 \\ 0 \\ 1 \end{bmatrix}$$

$$\mathbf{r}_{C} = \begin{bmatrix} c\psi b_{2} + c(\psi - \delta)(b_{3} - a_{4}) \\ -s\psi b_{2} - s(\psi - \delta)(b_{3} - a_{4}) \\ 0 \end{bmatrix} + \lambda \begin{bmatrix} 0 \\ 0 \\ 1 \end{bmatrix}$$
(5.20)

$$\mathbf{r}_{C} = \begin{bmatrix} c\psi b_{2} + c(\psi - \delta)(b_{3} - a_{4}) \\ -s\psi b_{2} - s(\psi - \delta)(b_{3} - a_{4}) \\ 0 \end{bmatrix} + \lambda \begin{bmatrix} 0 \\ 0 \\ 1 \end{bmatrix}$$
 (5.21)

with

$$b_2 = \frac{\phi'}{\phi' \pm 1} a_1 \tag{5.22a}$$

$$b_3 = \sqrt{(a_3c\phi + a_1 - b_2)^2 + a_3^2s^2\phi}$$
 (5.22b)

$$\tan \delta = \frac{a_3 s \phi}{a_3 c \phi + a_1 - b_2} \tag{5.22c}$$

(5.22d)

The pressure angle is defined as in eq. (3.86), namely,

$$\tan \mu = \frac{a_3(\phi' \pm 1) \pm a_1 \cos \phi}{a_1 \sin \phi}$$

The plus sign of the double signed terms, refer to external SM, whereas the minus, to internal SM.

As a counterpart of the spherical SM, the pitch curve of planar SM can be analyzed to determine the allowable value of a_3 , defined as \bar{a}_3 , so that undercutting can be avoided. Thus, the following theorem is established:

Theorem 5.2: Given a_1 , N, $\Delta \psi$ and the input-output function defined as in eq.(4.1), the pitch curve of a planar RHRR ICM reaches a cusp at $\psi = 0$ if $a_3 = \bar{b}_2 - a_1$, \bar{b}_2 being the value of b_2 at $\psi = 0$.

5.3 Positive Action and Positive Motion

In the design of cam mechanisms we distinguish two kinds of actuating forces at the contact between the cam and the follower, namely, the force that transmits the motion to the follower, and the force that tries to stop the motion of the follower. The action of each of these forces is termed here positive action (PA) and negative action (NA), respectively. Moreover, we call positive motion that in which both PA and NA are present in the transmission, and hence, there are at least two contact points or lines in a cam follower—system of this type, i.e., two or more cams attached to the input shaft interacting with two or more followers attached to the output shaft. Notice that cases like constant-breadth cam mechanisms use the same cam and follower interacting in two different points.

In order to identify the type of action that takes place on the follower, we resort to the value of the pressure angle. We assume in the pressure-angle analysis that friction forces are negligible, and hence, the direction of the contact force is parallel to the common normal. Furthermore, μ varies from 0° to 180° and PA and NA arise according to the rule given below:

If
$$0^{\circ} \le \mu < 90^{\circ}$$
, then PA
If $90^{\circ} < \mu \le 180^{\circ}$, then NA

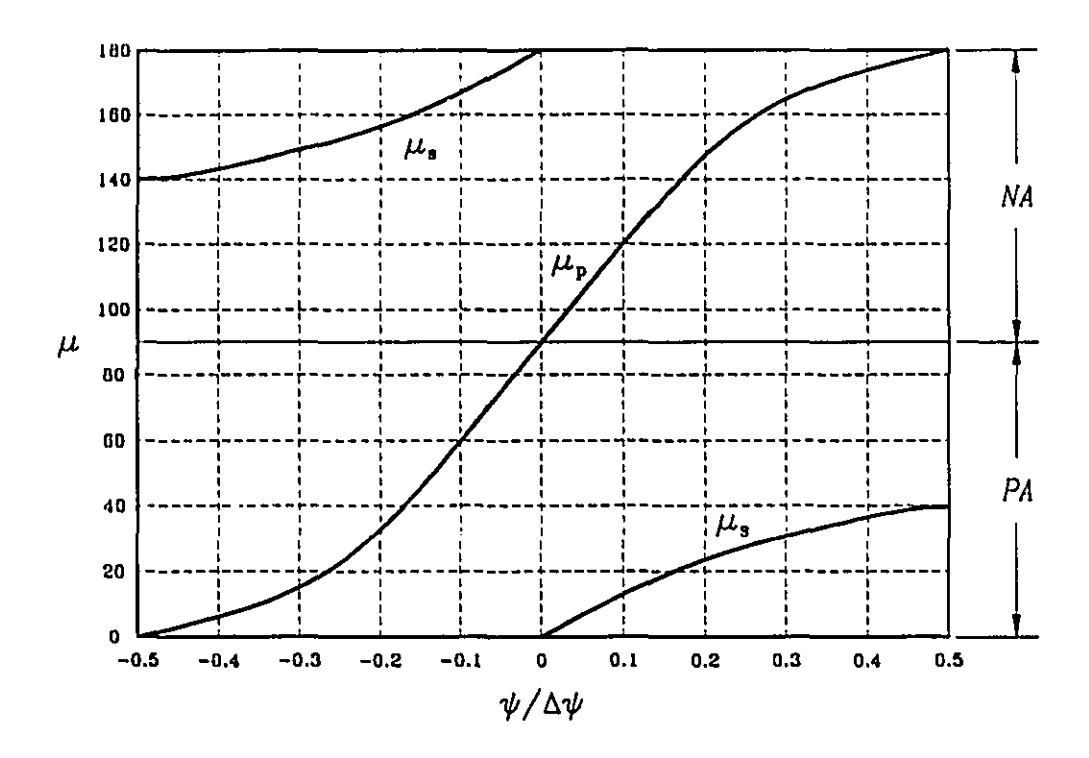


Figure 5.2 Pressure angle distribution of PRICAM

In Fig. 5.2 we present the distribution of the pressure angle of both mechanisms for N=4, $\Delta\psi=120^\circ$ and $\alpha_1=90^\circ$, for an input-output function of the cycloidal type. Similar curves arise for other input-output functions. It is clear that the combination of the two mechanisms satisfy the condition of positive motion. On the first half of the rise, the primary mechanism is under PA and starts with a zero pressure angle, while the secondary mechanism is under NA. In the second half, PA is present in the secondary mechanism, starting with a zero pressure angle. Shown in Fig. 5.3, is the pressure-angle distribution for three rotations of the cam. The encircled numbers indicate which roller is interacting with the cam. During the dwell phase, two rollers interact with the cam and lock the shaft of the follower.

Two prototypes, one planar and one spherical, were designed with the following characteristics:

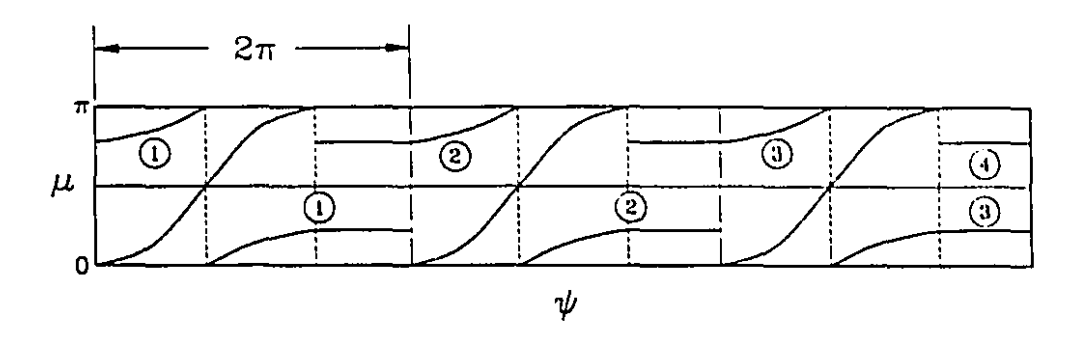


Figure 5.3 Three cycles of the cam motion

- Four indexing steps, i.e., for a full rotation of the cam, the follower rotates 90° from one dwell to another.
- The dwell from one index to another is 2/3 of the rotation of the cam.

A set of CAD drawings for both planar and spherical indexing cam mechanisms is presented in Figs. 5.4-5.7, with dimensions in mm.

Prior to the manufacturing of the prototypes, solid models of both designs were created on a Silicon Graphics Power Series Workstation (IRIS 4D/420VGX) to animate the motion of PRICAM in its two versions. Three dimensional renderings of these designs are shown in Figs. 5.8 and 5.9, while photographs of the prototypes are shown in Figs. 5.10-5.13.

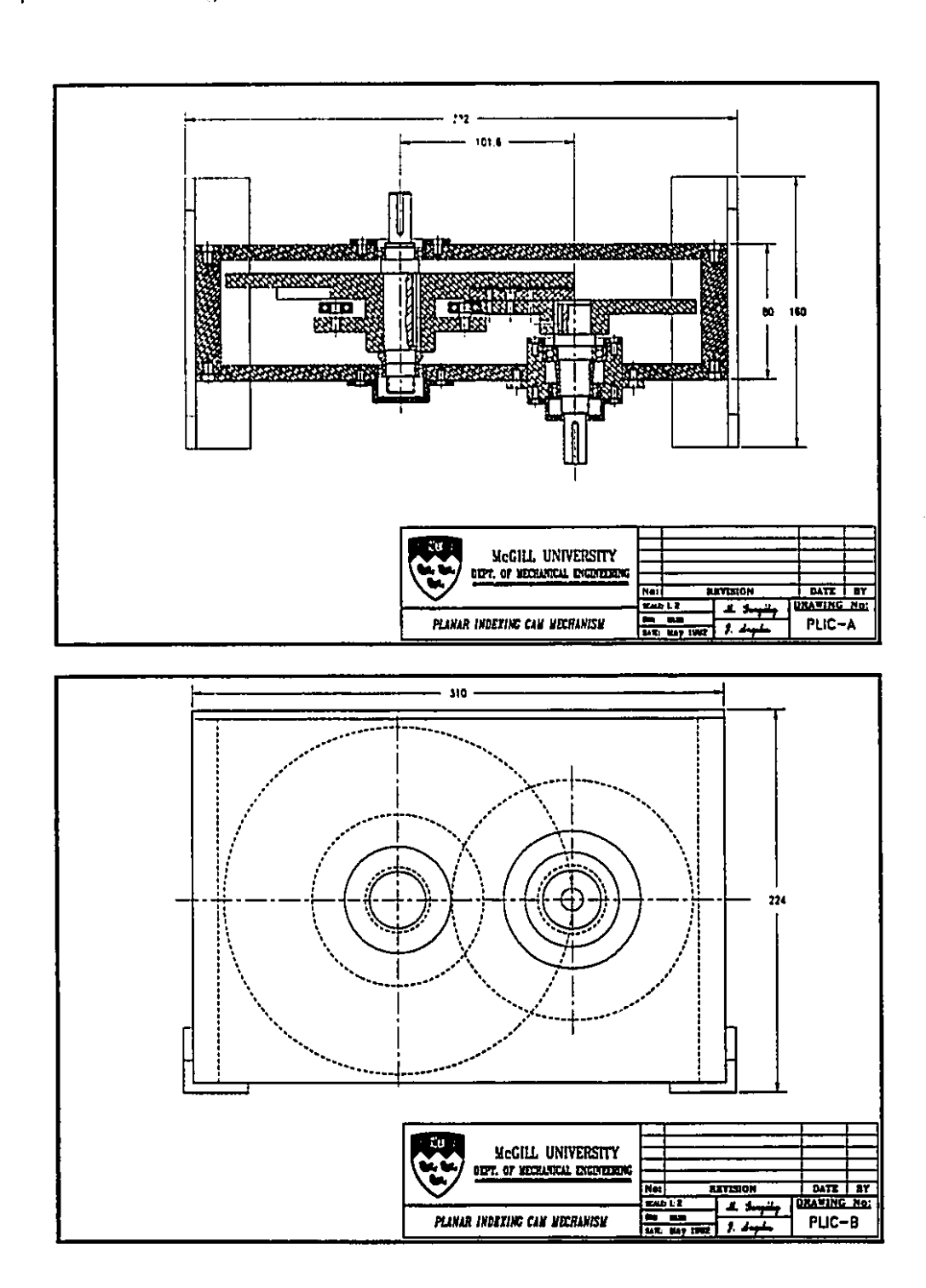
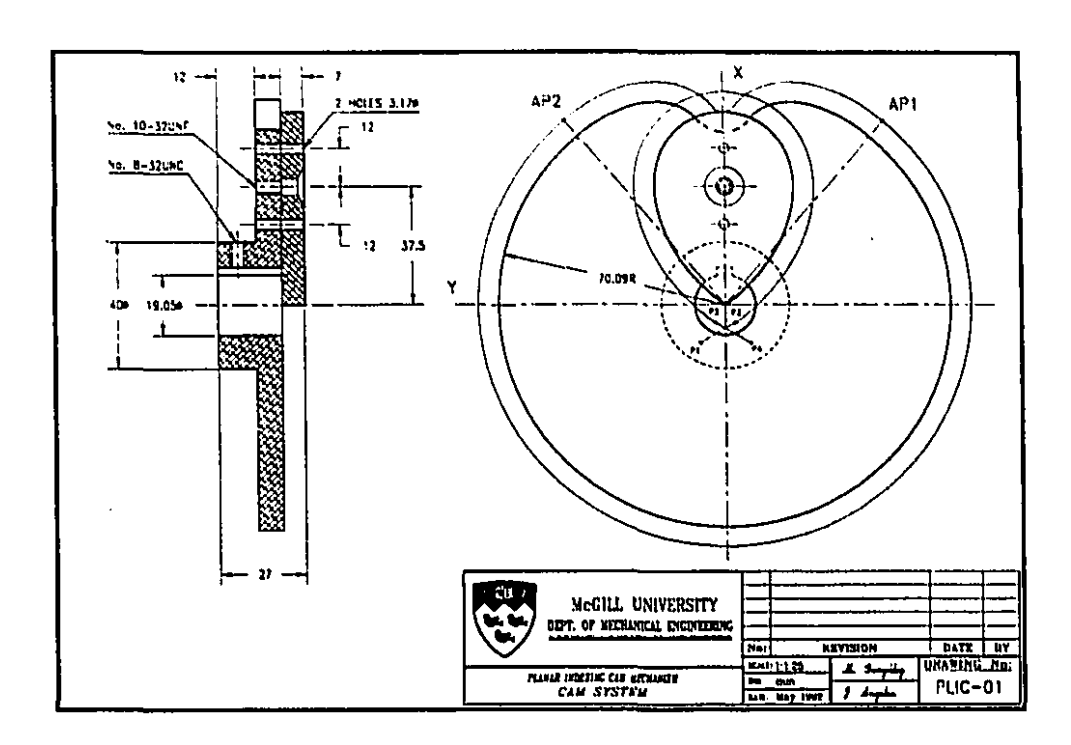


Figure 5.4 Top and front views of planar PRICAM



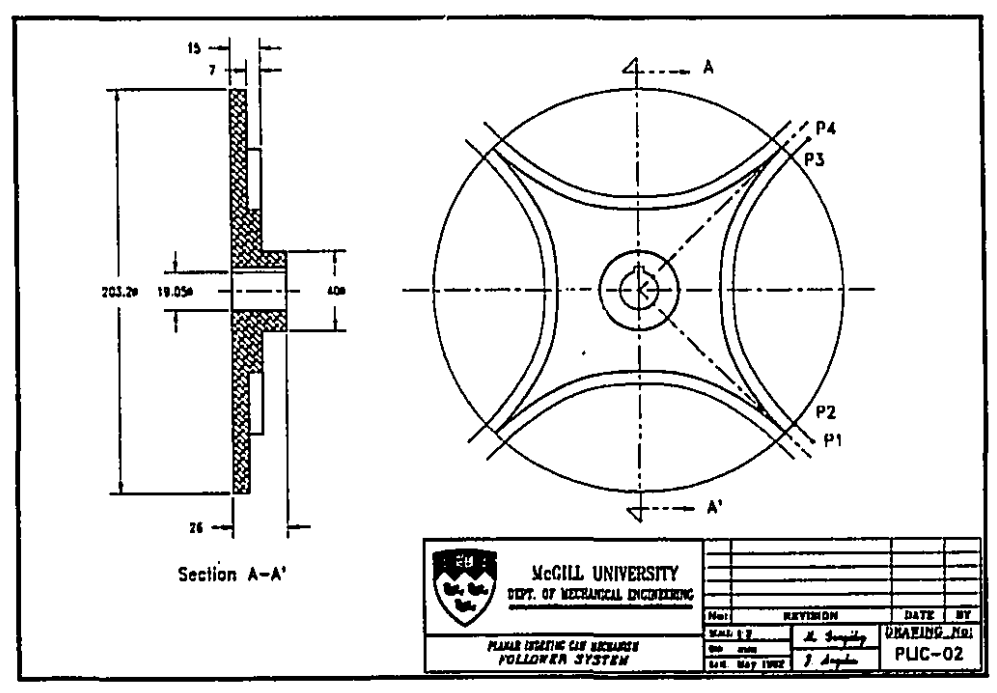


Figure 5.5 Cam and follower of planar PRICAM

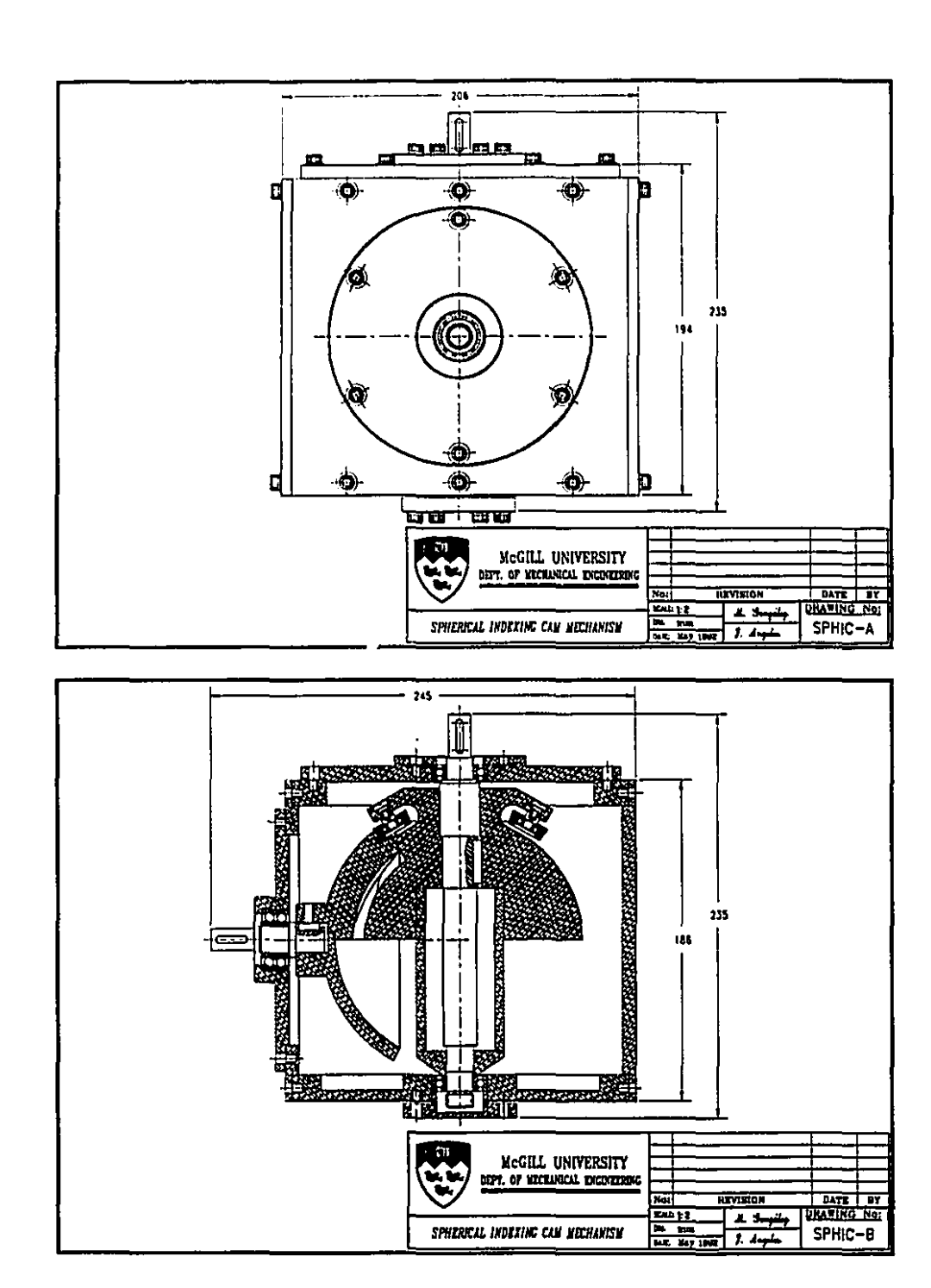
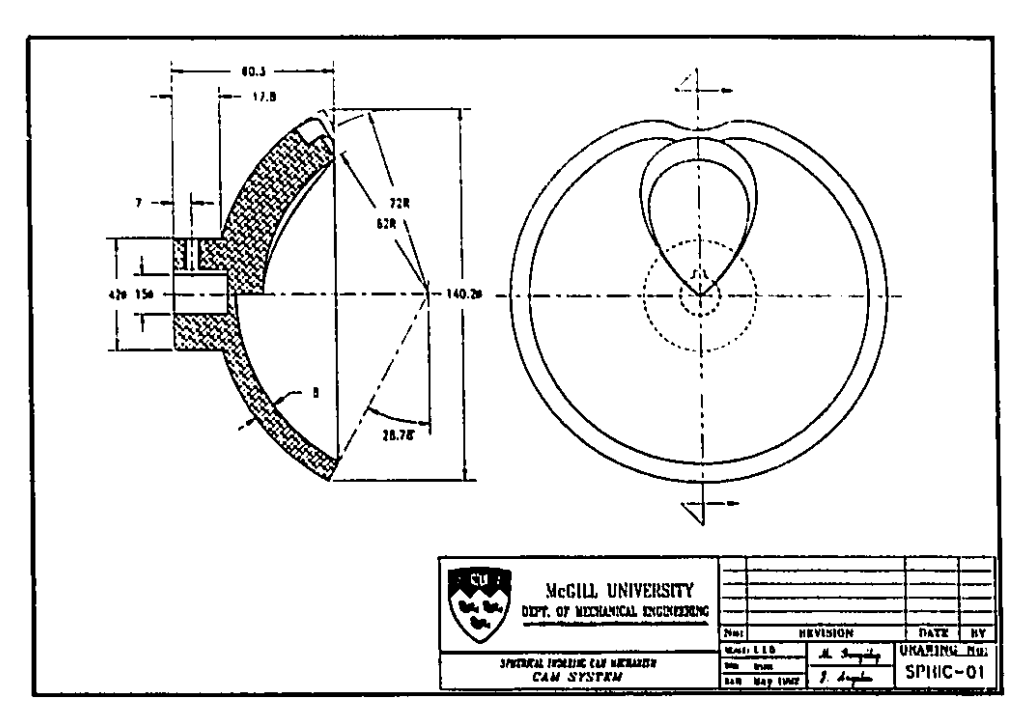


Figure 5.6 Front and lateral views of spherical PRICAM



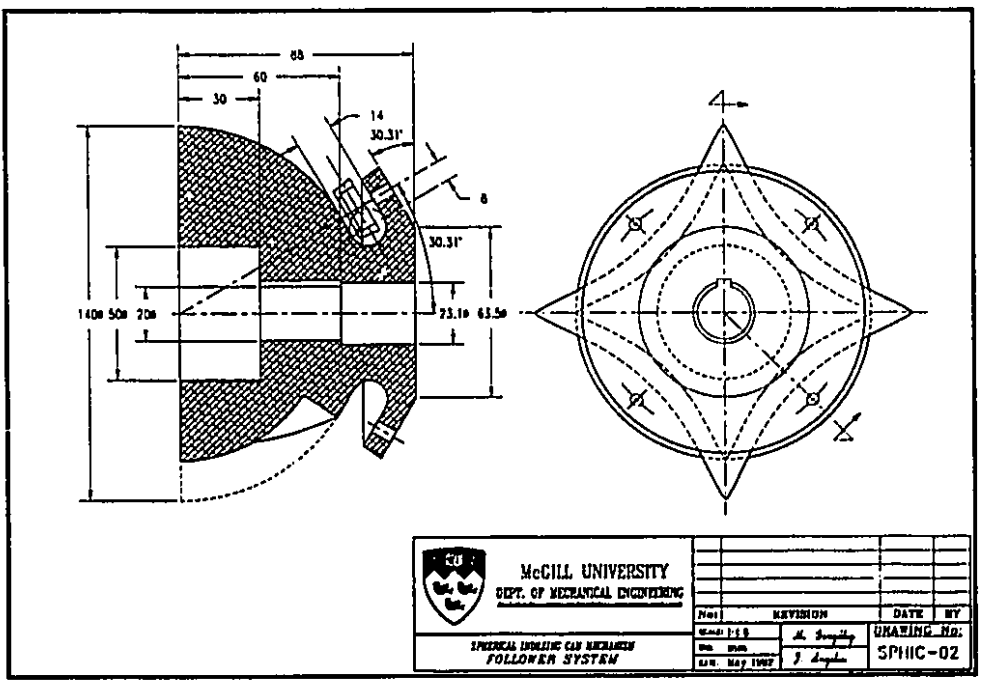


Figure 5.7 Cam and follower of spherical PRICAM

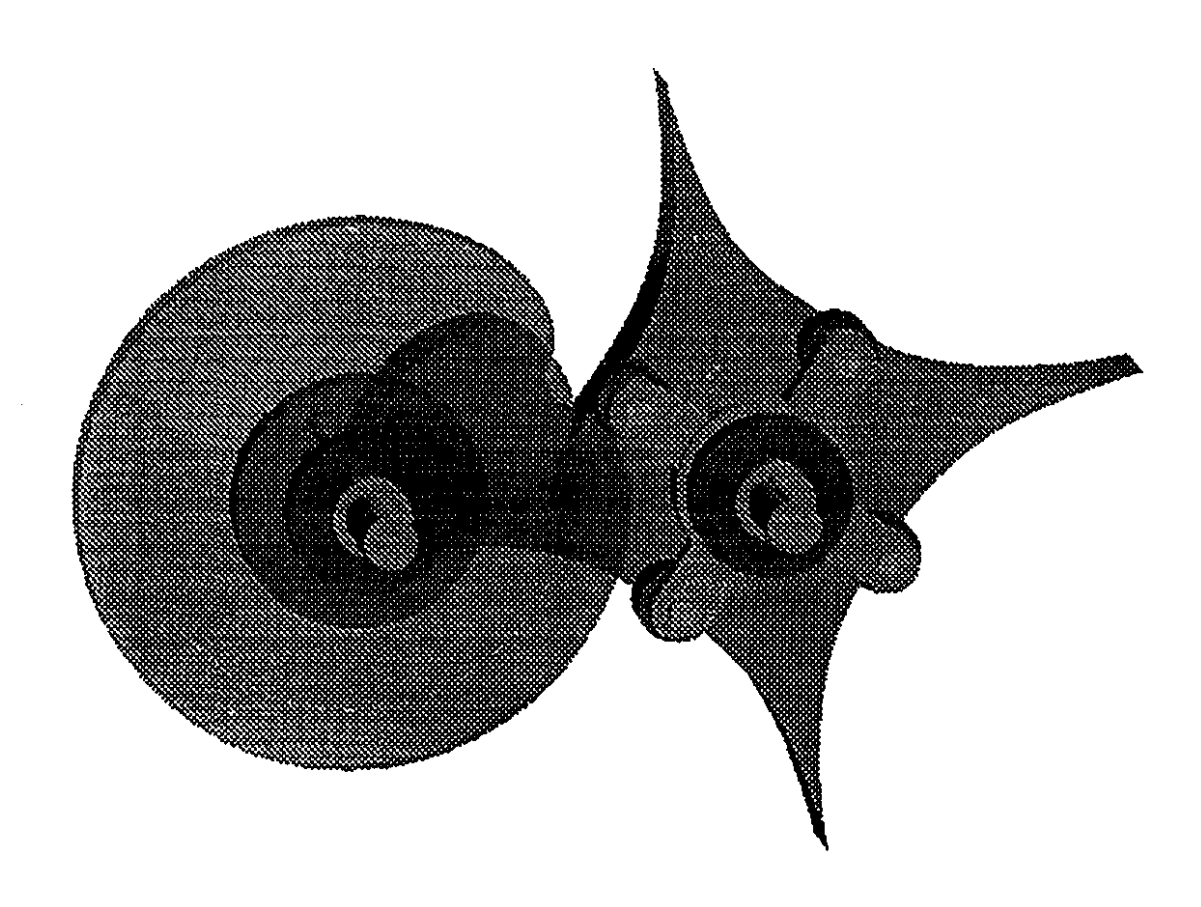


Figure 5.8 Solid model of a planar PRICAM.

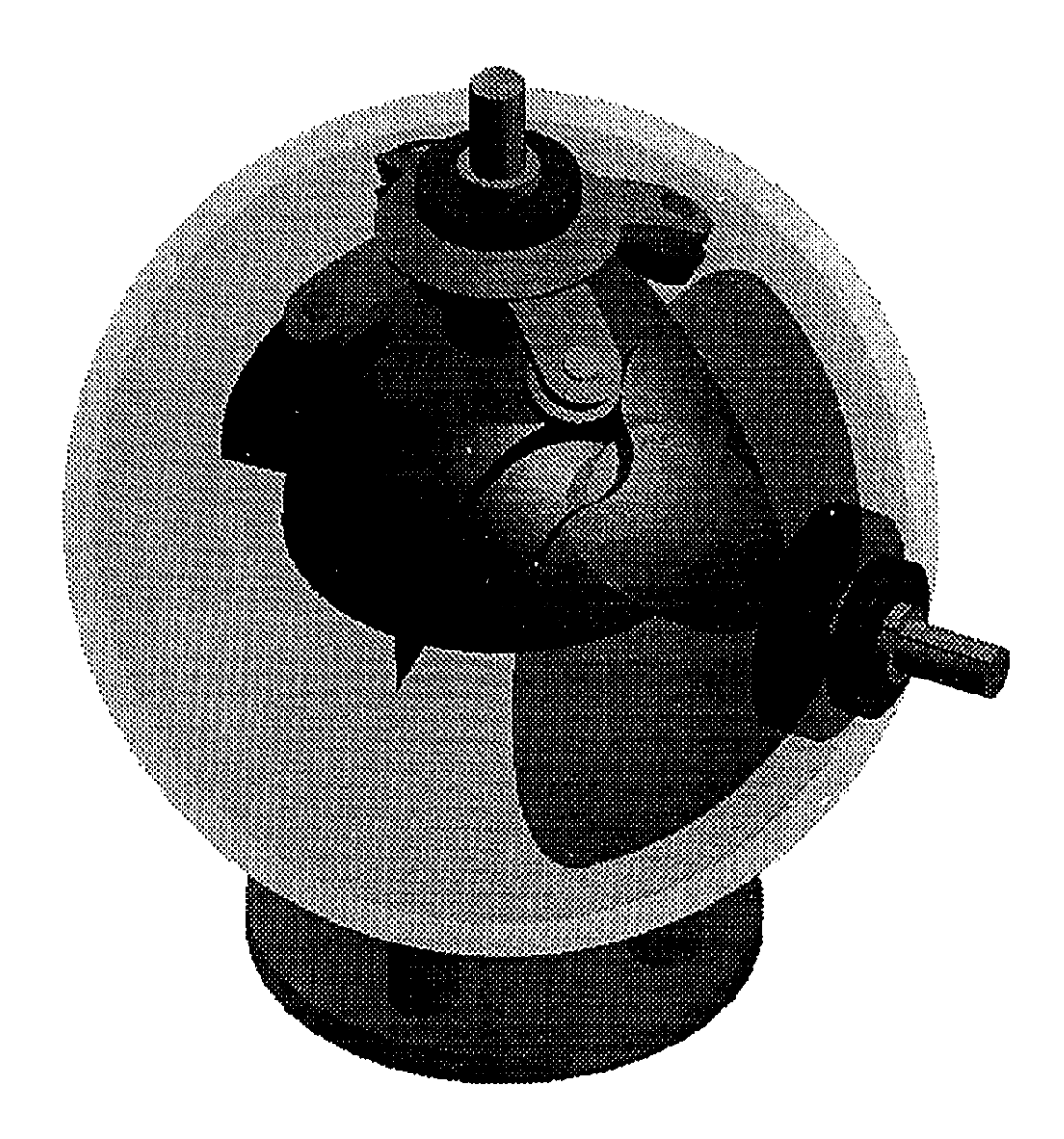


Figure 5.9 Solid model of a spherical PRICAM.

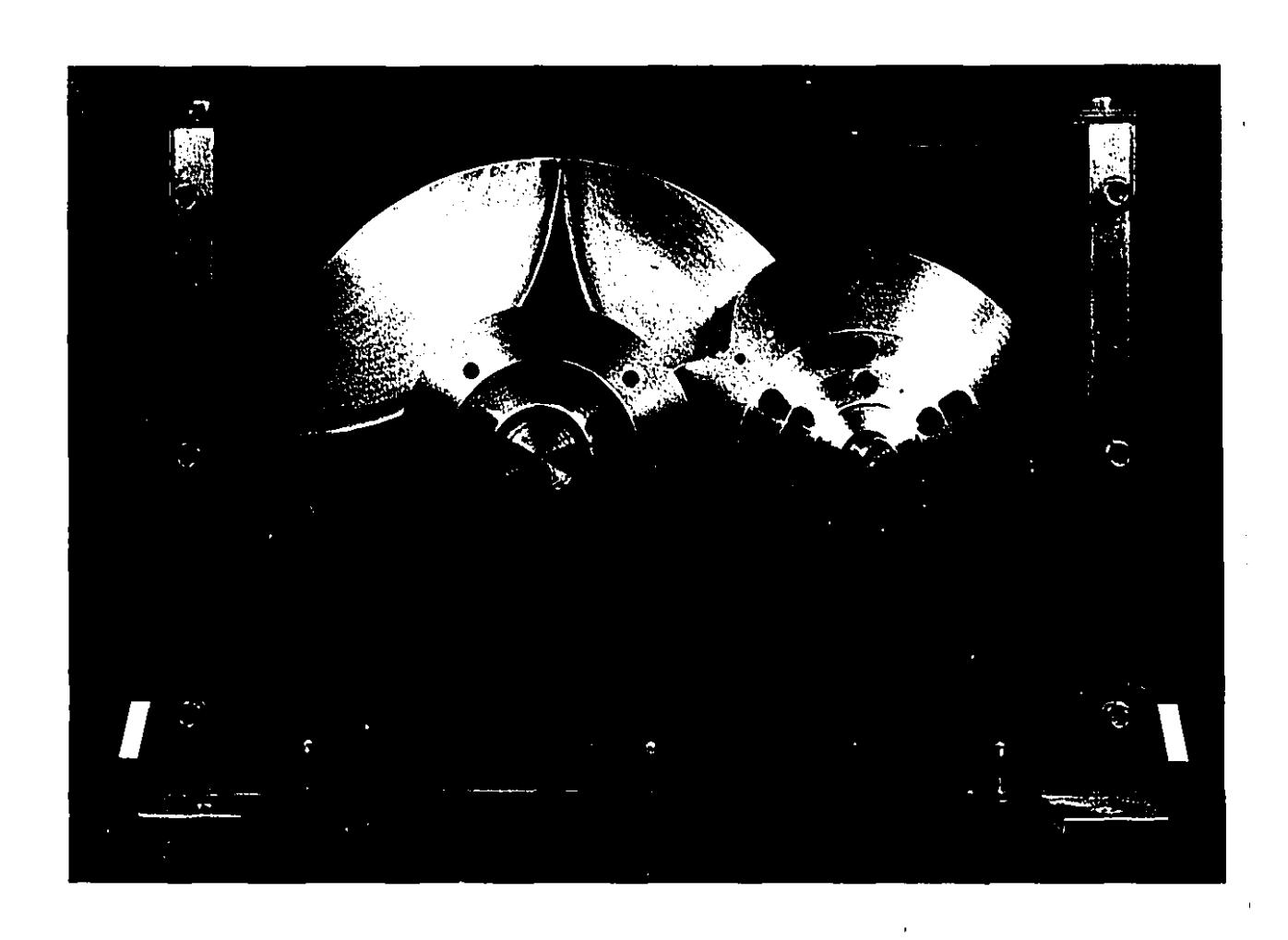


Figure 5.10 Front view of the planar PRICAM prototype

Ü

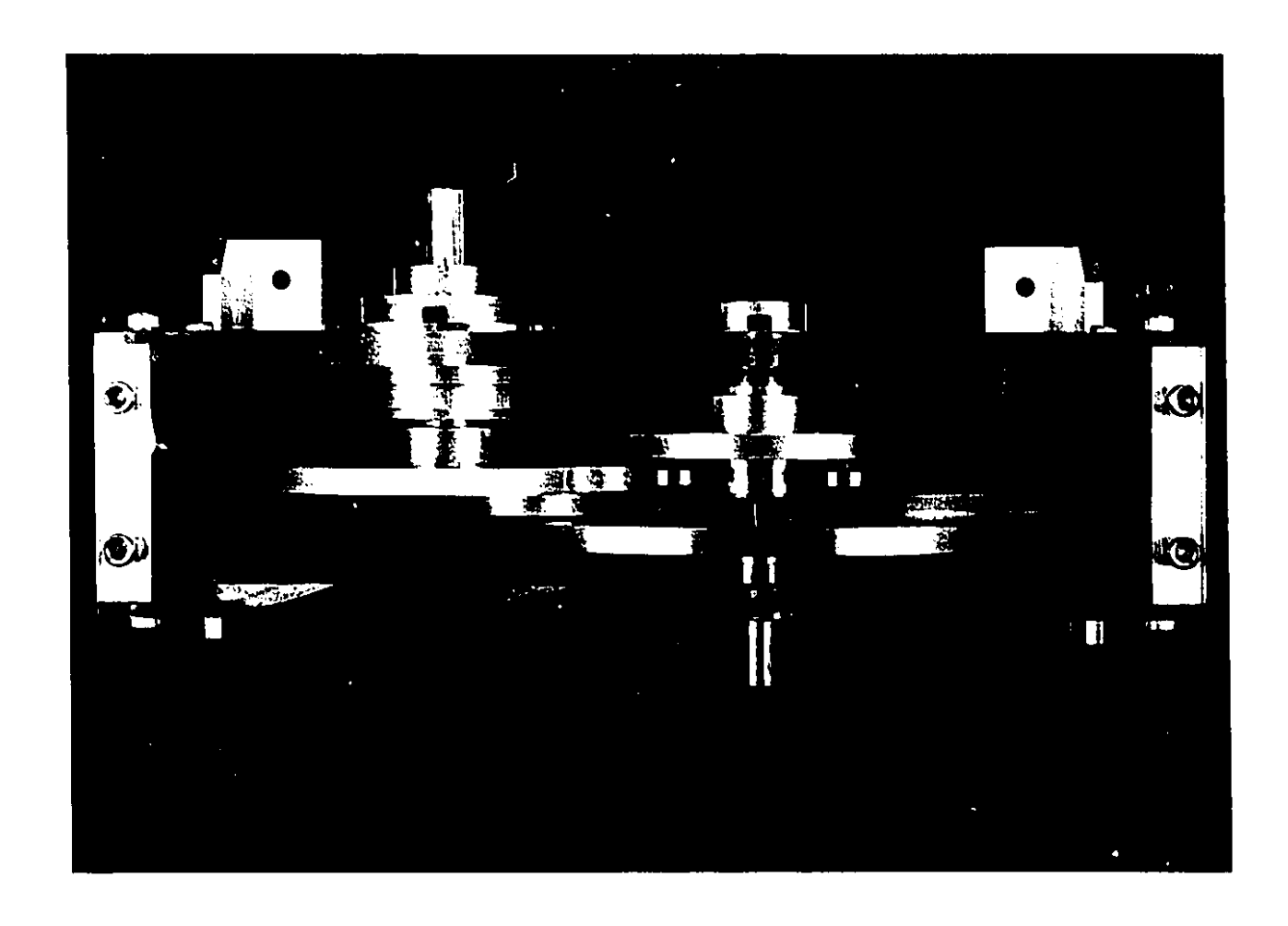


Figure 5.11 Top view of the planar PRICAM prototype

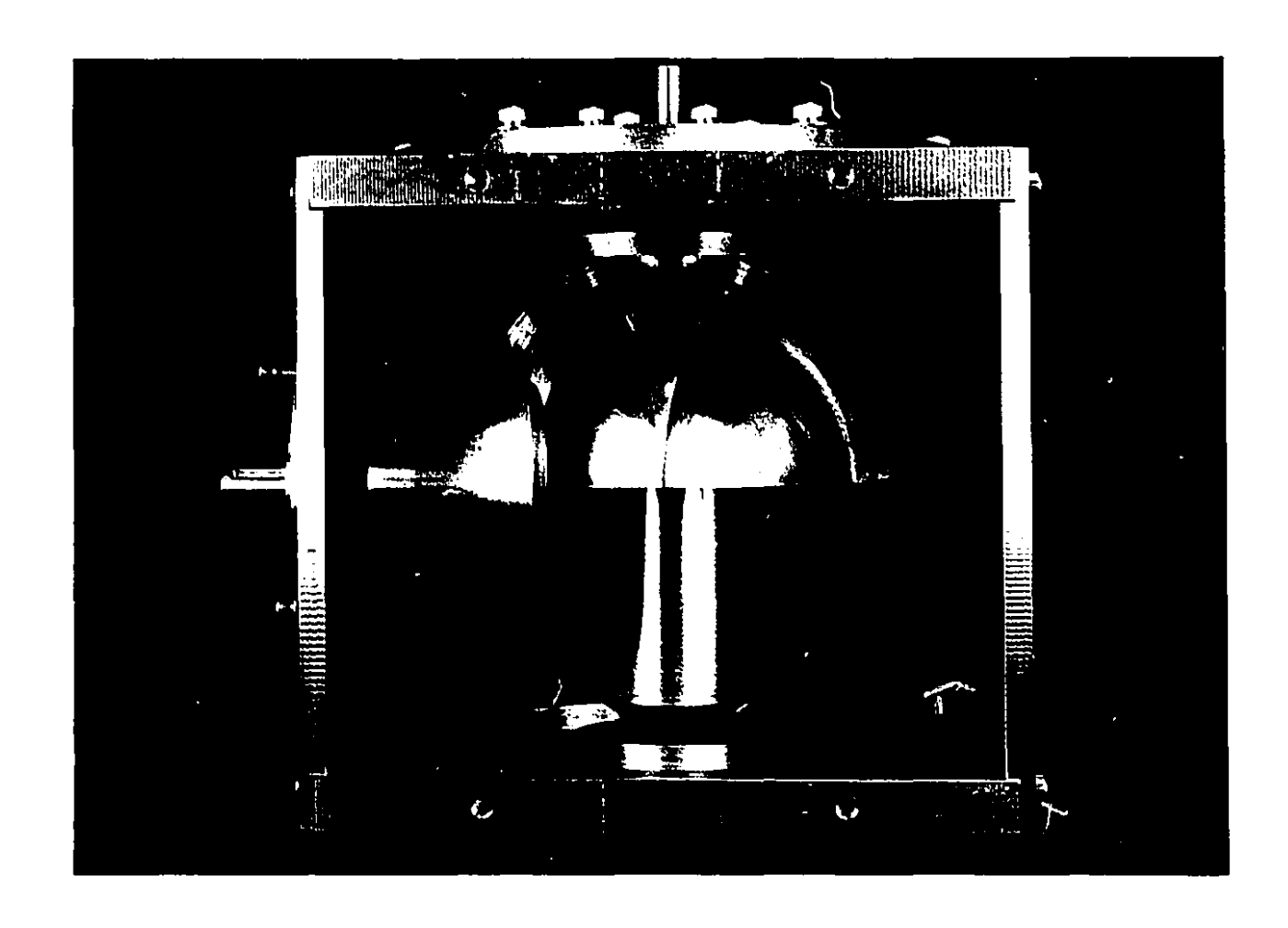


Figure 5.12 Front view of the spherical PRICAM prototype



Figure 5.13 Lateral view of the spherical PRICAM prototype

Chapter 6

Concluding Remarks

6.1 Conclusions

The classification of cam mechanisms according to the relative layout of their kinematic pairs was used to simplify the unified synthesis of this type of mechanisms. For each of the two kinds of mechanisms treated here, namely, three- and four-link mechanisms, when either the input or the output pairs are of the prismatic type, two basic theorems were stated.

With the criterion of minimum sliding velocity in the higher pair of a cam mechanism, an important result for four-link mechanisms was derived: In general, the roller-follower coupling is a *cylindrical* kinematic pair and the shape of the roller is a *hyperboloid* of revolution.

Novel cam mechanisms were found within the unified framework proposed here. Moreover, it is believed that the mathematical tool of dual numbers is applied to the theory of cam mechanisms for the first time, which has proven to ease the synthesis in this context.

Although the mechanisms discussed in Chapters 2 and 3 have only prismatic or revolute pairs at their input and output axes, the formulation presented is more general, i.e., it allows for screw pairs as well.

4

The concept of minimum sliding between cam-follower or cam-roller was applied to the synthesis of indexing cam mechanisms (ICM). Interesting results were obtained when three- and four-link ICM were combined in planar and spherical layouts, that lead to pure rolling, positive motion and zero pressure angle at the ends and at the midpoint of the follower stroke. A novel mechanism, called *PRICAM*, was designed with these features in the two aforementioned versions, planar and spherical.

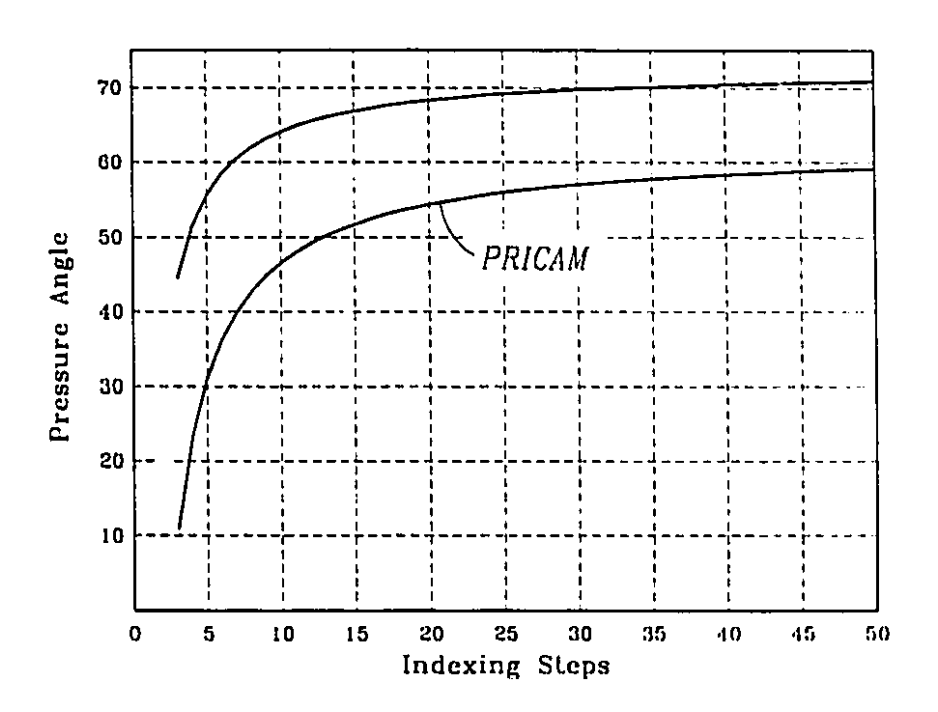


Figure 6.1 Maximum pressure angle between planar PRICAM and mirror-image conjugate cam mechanisms

The preliminary design of *PRICAM* was based on a three-link cam mechanism which, nevertheless, was found to entail some disadvantages. In fact, the mechanism had to be spring-loaded at all times in order to maintain the contact between cam and follower, which introduces dynamic problems, namely, undesirably low natural frequencies. Another disadvantage was that, during the dwell phase, the output shaft was not locked. These problems were solved in the final design of *PRICAM* with

the introduction of an additional four-link cam mechanism. Thus, with this combination of three- and four-link mechanisms, called primary and secondary systems, respectively, positive motion was achieved without springs and positive action was defined based on the value of the pressure angle. Moreover, the *PRICAM* prototype is self-locking during the dwell phase.

One of the parameters to measure the quality of the transmission of a cam mechanism is the pressure angle. Optimum transmission is reached when this angle is zero and no transmission is possible when this angle is 90°. In this context, the planar *PRICAM* was compared with an existing indexing cam mechanism, called the mirror-image conjugate cam mechanism. The overall maximum pressure angle of the former was found to be 35% smaller than the maximum pressure angle of the latter. The plots of the pressure angle of the two mechanisms are shown in Fig. 6.1.

Bounds on the angle between the output axis and the axis of the roller in the secondary system of the spherical *PRICAM* were established in order to avoid undercutting, the maximum value depending on the design parameters. This result was stated in Theorem 5.1. Similarly, Theorem 5.2 was stated for the secondary system of the planar *PRICAM*.

The software package *USYCAMS*, an invaluable tool in this research, implements the synthesis methodology reported here on a *Silicon Graphics IRIS 4D/420VGX* workstation.

All the cam profiles shown in the figures of Chapter 3 were generated with the application of the results presented in Chapters 2 and 3.

6.2 Considerations for Future Work

A few items that we recommend for future research are listed below:

• The stochastic analysis of the effect of overall error on the output motion of a cam mechanism, due to manufacturing and assembly errors, as well as to intentional clearances in the joints, warrants research on its own.

- With advanced CAD systems it is possible to compute the inertia properties of solid shapes. However, cams are generated as ruled surfaces, and hence, show some special features that could be exploited to develop suitable algorithms to determine the inertia properties of cams more accurately than with commercial software;
- Dynamic unbalance is an unavoidable problem when spatial cam mechanisms are used, mostly due to the unusual shapes involved. The dynamic balancing of cams calls for further research;
- The requirements of a certain application can be satisfied by different types of cam mechanisms. To find the optimum type from the point of view of efficiency and minimum cost is a challenging problem to be considered as a continuation of this research work.

Agrawal, O., P., 1987, "Hamilton Operators and Dual-Number-Quaternions in Spatial Kinematics," *Mechanism and Machine Theory*, Vol. 22, pp. 569-575.

Amarnath, C., and Gupta, B. K., 1975, "On a Cam Mechanism with Multiple Dwell Capability," Proc. 4th World Congress on Theory of Machines and Mechanisms, Newcastle upon Tyne, Vol. 4, pp. 773-776.

Amarnath, C., and Gupta, B., K., 1978, "Novel Cam-Linkage Mechanisms for Multiple Dwell Generation," Cams and Cam Mechanisms, The Institution of Mechanical Engineers, pp. 123-127.

Angeles, J., 1982, Spatial Kinematic Chains, Springer-Verlag, Berlin, pp 149-157.

Angeles, J., 1986a, "Automatic Computation of the Screw Parameters of Rigid-Body Motions. Part I: Finitely-Separated Positions," J. Dynamic Systems, Measurement, and Control Trans. ASME, Vol.108, pp. 32-38.

Angeles, J., 1986b, "Automatic Computation of the Screw Parameters of Rigid-Body Motions. Part II: Infinitesimally-Separated Positions," J. Dynamic Systems, Measurement, and Control Trans. ASME, Vol.108, pp. 39-43.

Angeles, J. and López-Cajún, C., 1991, Optimization of Cam Mechanisms, Kluwer Academic Publishers, Dordrecht.

Angeles, J., López-Cajún, C. and Saha, S. K., 1991, "The Design of Cam Mechanisms with Translating Flat-Face Followers Under Curvature Constraints", to appear in ASME Journal of Mechanisms, Transmissions, and Automation in Design.

Angeles, J., López-Cajún, C., Saha, S. K. and González-Palacios. M. A., 1991, "The Design Optimization of Cam Mechanisms with Oscillating Flat-Face Followers Under Curvature Constraints", to appear in ASME Journal of Mechanisms, Transmissions, and Automation in Design.

Aronhold, S. H., 1872, "Outline of Kinematic Geometry", Verh. Ver. Gew Fleiss., Berl. 51, pp 129-155.

Backhouse, C. J. and Jones J. R., 1990, "Envelope Theory Applied to Globoidal Cam Surface Geometry", Proc. Institution of Mechanical Engineers, Vol. 204, pp. 409-416.

Ball, R., S., 1875, "The Theory of Screws. A Geometrical Study of the Kinematics, Equilibrium, and Small Oscillations of a Rigid Body," Trans. R. Irish Acad., Vol. 25, pp. 157-217.

Ball, R., S., 1900, A Treatise on the Theory of Screws, Cambridge University Press.

Beggs, J. S., 1959, Ein Beitrag zur Analyse Räumlicher Mechanismen, Doctoral Thesis, Technische Hochschule Hannover, Hanover.

Beggs, J., S., 1960, "Mirror-Image Kinematics," Journal of the Optical Society of America, Vol. 50, pp. 388-393.

Benedetto A., D., 1975, "Some Methods of Kinematic Synthesis of Cam Profiles for Prescribed Jerk Pattern," Proc. 4th World Congress on Theory of Machines and Mechanisms, Newcastle upon Tyne, Vol. 4, pp. 963-968.

Berzak, N., and Freudenstein, F., 1979, "Optimization Criteria in Polydine Cam Design," Proc. 5th World Congress on Theory of Machines and Mechanisms, Vol. 2, pp. 1303-1306.

Bialkowicz, B., Klimowicz, T., and Swietlik, M., 1979, "Chages of the Dynamic Properties of the Real Cam Profile During its Wear," Proc. 5th World Congress on Theory of Machines and Mechanisms, Vol. 2, pp. 984-987.

Bickford J. H., 1965, "Mechanisms for Intermittent Rotary Motion", Machine Design, December, 23, 1965, pp. 119-131.

Bickford J. H., 1972, Mechanisms for Intermittent Motion, Industrial Press Inc., New York.

Bottema, O. and Roth, B., 1979, Theoretical Kinematics, North-Holland Publishing Co., Amsterdam.

Chakraborty, J. and Dhande, S. G., 1977, Kinematics and Geometry of Planar and Spatial Cam Mechanisms, John Wiley and Sons, Inc., New York.

Chen, F., Y., 1977, "A Survey of the State of the Art of Cam System Dynamics," Mechanism and Machine Theory, Vol. 12, pp. 201-224.

Chen, F. Y., 1982, Mechanics and Design of Cam Mechanisms, Pergamon Press, New York.

Chen, P., and Roth, B., 1969a, "A Unified Theory for the Finitely and Infinitesimally Separated Position Problems of Kinematic Synthesis," J. Engng. Ind., Trans. ASME, Vol. 91, pp. 208-203.

Chen, P., and Roth, B., 1969b, "Design Equations for the Finitely and Infinitesimally Separated Position Synthesis of Binary Links and Combined Link Chains," J. Engng. Ind., Trans. ASME, Vol. 91, pp. 209-219.

De Sa, S., and Roth, B., 1981a, "Kinematic Mappings. Part 1: Classification of Algebraic Motions in the Plane," J. Mech. Design Trans. ASME, Vol. 103, pp. 585-591.

De Sa, S., and Roth, B., 1981b, "Kinematic Mappings. Part 2: Rational Algebraic Motions in the Plane," J. Mech. Design Trans. ASME, Vol. 103, pp. 712-717.

Dhande, S. G., Bhadoria, B., S., and Chakraborty, J., 1975, "A Unified Approach to the Analytical Design of Three-Dimensional Cam Mechanisms," *Trans. ASME*, Vol. 97, pp. 327-333.

Dhande, S., G., and Chakraborty, J., 1975, "Mechanical Error Analysis of Cam-Follower Systems. A Stochastic Approach," Proc. 4th World Congress on Theory of Machines and Mechanisms, Newcastle upon Tyne, Vol. 4, pp. 957-962.

Dittrich, G., 1966, "Konstruktion und Herstellung sphärischer Kurvengetriebe", Konstruktion, Vol. 10, pp. 421–426.

Dittrich, G., and Zakel, H., 1979, "Classification and Design of Three-Dimensional Cam Mechanisms," (German) Proc. 5th World Congress on Theory of Machines and Mechanisms, Vol. 2, pp. 1086-1089.

Dizioglu, B., 1989, "Kinematische Geometrie der Axoiden Und die Bahnfläche Einer Geraden," Mechanism and Machine Theory, Vol. 24, pp. 431-438.

DoCarmo, M., P., 1976, Differential Geometry of Curves and Surfaces, Prentice-Hall, Englewood Cliffs.

Dudiță, Fl., Gogu, Gr., Diaconescu, D., and Starețu, I., 1989, Curs de Mecanisme. Fascicula 2. Angrenaje. Mecanisme cu Cama. Cinematica, University of Brașov, Brașov.

Dudley, W. M., 1948, "New Methods in Valve Cam Design", SAE Quarterly Transactions, 2(7), 19-33.

Dudley, D. W., 1962, Gear Handbook, MacMillan, New York.

Fenton, R., G., 1965, "Dynamic Analysis of Geneva Mechanisms," Machine Design, Vol. 37, No. 2, pp. 177-182.

Fenton, R., G., 1966a, "Determining Minimum Cam Size," Machine Design, Vol. 38, No. 2, pp. 155-158.

Fenton, R., G., 1966b, "Reducing Noise in Cams," Machine Design, Vol. 38, No. 8, pp. 187-190.

Fenton, R., G., 1975a, "Geneva Mechanisms Connected in Series," Trans. ASME, Vol. 97, pp. 603-608.

Fenton, R., G., 1975b, "Dynamic Analysis of Geneva Mechanisms Connected in Series," *Proc. 4th Wld Congr. Theory of Machines and Mechanisms*, Newcastle-upon-Tyne, 8-12 September, Vol. 4, pp. 885-888.

Fenton, R., G., 1975c, "Optimum Design of Disc Cams," Proc. 4th World Congress on Theory of Machines and Mechanisms, Newcastle upon Tyne, Vol. 4, pp. 781-784.

Freudenstein, F., 1965, "Higher Path-Curvature Analysis in Plane Kinematics", Journal of Engineering for Industry. Trans ASME, Series B, Vol. 27, pp. 184-190.

Gibson, C., G., and Hunt, K., H., 1990a, "Geometry of Screw Systems-1. Screws: Genesis and Geometry," Mechanism and Machine Theory, Vol. 25, No. 1 pp. 1-10.

Gibson, C., G., and Hunt, K., H., 1990b, "Geometry of Screw Systems-2. Classification of Screw Systems," *Mechanism and Machine Theory*, Vol. 25, No. 1 pp. 11-27.

González-Palacios, M. A. and Angeles, J., 1990, "The Generation of Contact Surfaces of Indexing Cam Mechanisms. A Unified Approach," *Proc.* 1990 ASME Design Automation Conference, Advances in Design Automation, Vol. 2, pp. 359-364.

González-Palacios, M. A. and Angeles, J., 1991, "Synthesis of Contact Surfaces of Spherical Cam-Oscillating Roller-Follower Mechanisms. A General Approach", Proc.

1991 ASME Design Automation Conference, Advances in Design Automation, Vol. 2, pp. 255-260.

González-Palacios, M. A. and Angeles, J., 1992a, "The Synthesis of Cam-Oscillating Roller-Follower Mechanisms. A Unified Approach", to be presented at the 1992 ASME Mechanisms Conference, Phoenix.

González-Palacios, M. A. and Angeles, J., 1992b, "On the Design of Planar and Spherical Pure-Rolling Indexing Cam Mechanisms", to be presented at the 1992 ASME Mechanisms Conference, Phoenix.

Gouxun, P., Zhengyang, X. and Huimin, T., 1988, "Unified Optimal Design of External and Internal Parallel Indexing Cam Mechanisms," *Mechanism and Machine Theory*, Vol. 23, pp. 313-318.

Grewal, P., S., and Newcombe, W., R., 1988, "Dynamic Performance of High-Speed Semi-Rigid Follower Cam Systems-Effects of Cam Profile Errors," Mechanism and Machine Theory, Vol. 23, pp. 121-133.

Gürsoy, O., 1990, "The Dual Angle of Pitch of a Closed Ruled Surface," Mechanism and Machine Theory, Vol. 25, No. 2 pp. 131-140.

Hain, K., 1970, "Challenge: To Design Better Cams," J. Mechanisms, Vol. 5, pp. 283-286.

Hain, K., 1971, "Optimization of a Cam Mechanism-to give good transmissibility, maximal output angle of swing and minimal acceleration," J. Mechanisms, Vol. 6, pp. 419-434.

Hain, K., 1978, "Optimization of an Intermittent Motion-Mechanism with Fixed Cam," Cams and Cam Mechanisms, The Institution of Mechanical Engineers, pp. 111-115.

Hon-Cheung, Y., 1987, "Four Co-reciprocal Screws and Their Kinematic Significance," Mechanism and Machine Theory, Vol. 22, pp. 190-203.

Hunt, K., H., 1967a, "Prismatic Pairs in Spatial Linkages," J. Mechanisms, Vol. 2, pp. 213-230.

Hunt, K., H., 1967b, "Screw Axes and Mobility in Spatial Mechanisms Via the Linear Complex," J. Mechanisms, Vol. 3, pp. 307-327.

Hunt, K. H., 1973, "Profiled-Follower Mechanisms," Mechanism and Machine Theory, Vol. 8, pp. 371-395.

IFToMM Commission A, 1991, "Terminology for the Theory of Machines and Mechanisms", Mechanism and Machine Theory, Vol. 26, No. 5, pp. 435-539.

Jackowski, C. S., and Dubil, J. F., 1967, "Single-Disk Cams with Positively Controlled Oscillating Followers," J. Mechanisms, Vol. 2, pp. 157-184.

Jacobs, R. J., 1949, "Indexing with Concave Barrel Cams", Machine Design, Vol. 21, No. 3, February, pp. 93-96.

Jensen, P. W., 1965, Cam Design and Manufacture, Industrial Press, New York.

Johnson, R., C., 1955, "Cam Design," Machine Design, Vol. 27, No. 11, November, pp. 195-204.

Johnson, R., C., 1956a, "Cam Mechanisms," Machine Design, Vol. 28, No. 2, January, pp. 105-108.

Johnson, R., C., 1956b, "Minimizing Cam Vibrations," Machine Design, Vol. 28, No. 16, August, pp. 103-104.

Johnson, R., C., 1956c, "Cam Profiles," Machine Design, Vol. 28, No. 25, December, pp. 129-132.

Johnson, R. C., 1958, "Development of a High-Speed Indexing Mechanism," Machine Design, Vol. 30, Sept., pp. 134-138.

Johnson, R., C., 1957, "Cam Dynamics," Machine Design, Vol. 29, No. 3, February, pp. 105-108.

Jones, J., R., 1978a, "Mechanisms. Cam Cutting Co-ordinates," Engineering, Vol. 218, March, pp. 220-224.

Jones, J., R., 1978b, "Mechanisms. Pressure Angles and Forces in Cams," Engineering, Vol. 218, July, pp. 703-706.

Jones, J., R., 1978c, "Mechanisms. Cam Curvature and Interference," Engineering, Vol. 218, May, pp. 460-463.

Jones, J. R., and Tsang, K. S., 1987, "Optimal configurations for Parallel Shaft Indexing Mechanisms," Proc. 7th World Congress on Theory of Machines and Mechanisms, Sevilla, 17-22 September, Vol. 3, pp. 1687-1690.

Kass, R., C., and Chace, M. A., 1975, "An Approach to the Simulation of Two-Dimensional Higher Pair Contacts," *Proc. 4th World Congress on Theory of Machines and Mechanisms*, Newcastle upon Tyne, Vol. 4, pp. 1057-1063.

Kennedy, A. B. W., 1886, Mechanics of Machinery, 1st Ed., Macmillan, London.

Kerr, D. R., and Sanger, D., J., 1989, "The Inner Product in the Evaluation of Reciprocal Screws," Mechanism and Machine Theory, Vol. 24, pp. 87-92.

Kohli, D., and Soni, A. H., 1975, "Synthesis of Spatial Mechanisms Via Successive Screw Displacements and Pair Geometry Constraints," Proc. 4th Wld Congr. Theory of Machines and Mechanisms, Newcastle upon Tyne, Vol. 4, pp. 711-716.

Koloc, V., and Václavíc, M., 1988, Vačkové Mechanismy, SNTL-Nakladatelství Techniké Literatury, Prague.

Köse, Ö., 1982a, "On The Dual Spherical Motions-I," Mechanism and Machine Theory, Vol. 17, pp. 185-190.

Köse, Ö., 1982b, "On The Dual Spherical Motions-II," Mechanism and Machine Theory, Vol. 17, pp. 185-190.

Koster, M., P., 1975, "Digital Simulation of the Dynamics of Cam Followers and Camshafts," *Proc. 4th World Congress on Theory of Machines and Mechanisms*, Newcastle upon Tyne, Vol. 4, pp. 969-974.

Loeff, L., and Soni, H., 1975, "Optimum Sizing of Planar Cams," Proc. 4th World Congress on Theory of Machines and Mechanisms, Newcastle upon Tyne, Vol. 4, pp. 777-780.

Makino, H., 1979, "Basic Analysis and Optimal Design of In-line Transfer Indexing Cam," Proc. 5th World Congress on Theory of Machines and Mechanisms, Montreal, 8-13 July, Vol. 2, pp. 875-878.

McCarthy, J., M., and Roth, B., 1981, "The Curvature Theory of Line Trajectories in Spatial Kinematics," J. Mech. Design Trans. ASME, Vol. 103, pp. 718-724.

McCarthy, J., M., 1987a, "The Differential Geometry of Curves in an Image Space of Spherical Kinematics," Mechanism and Machine Theory, Vol. 22, pp. 205-211.

McCarthy, J. M., 1987b, "On The Scalar and Dual Formulation of the Curvature Theory of Line Trajectories", ASME J. Mechanisms, Transmissions, and Automation Design, Vol. 109, pp. 101–106.

Müller, J., 1987, "The history of Cams and Cam Mechanisms", Proc. 7th World Congress on Theory of Machines and Mechanisms, Seville, pp. 1649-1652.

Müller, J. and Mauersberger, K., 1988, "Zur Entwicklungsgeschichte der Kurvengetriebe", Wissenschaftliche Zeiturg der Wilhelm-Pieck Universität Rostock, W.-P. Universität Rostock, Rostock, Vol. 37, No. 7, pp. 66-88.

Neklutin, C. N., 1959, "Tring-Type Cam Profiles", Machinery Design, Oct. 15, pp. 175-187.

Norton, R., L., 1988, "Effect of Manufacturing Method on Dynamic Performance of Cams-An Experimental Study. Part I-Eccentric Cams," Mechanism and Machine Theory, Vol. 23, pp. 191-199.

Norton, R., L., Levasseur, D., Pettit, A., and Alamsyah, C., 1988, "Analysis of the Effect of Manufacturing Methods and Heat Treatment on the Performance of Double Dwell Cams," *Mechanism and Machine Theory*, Vol. 23, pp. 461-473.

Ohwovoriole, M., S., and Roth, B., 1981, "An Extension of Screw Theory," J. Mech. Engng. Trans. ASME, Vol 103, pp. 725-735.

Oledzki, A., and Szydlowski, W., 1975, "Modelling of the Geneva Mechanisms," *Proc.* 4th World Congress on Theory of Machines and Mechanisms, Newcastle-upon-Tyne, 8-12 September, Vol. 4, pp. 889-893.

Osman, M., O., M., Bahgat, B., M., and Osman Mohsen, 1987, "Dynamic Analysis of a Cam Mechanism with Bearing Clearances," *Mechanism and Machine Theory*, Vol. 22, pp. 303-314.

Pandrea, N., and Voiculescu, D., 1975, "Analysis of Screw Displacements of the Right Line and the Plane by Means of the Screw Theory and of the Dual Matrices," *Proc.* 4th Wld Congr. Theory of Machines and Mechanisms, Newcastle upon Tyne, Vol. 4, pp. 285-288.

Parkin, J., A., 1990, "Co-ordinate Transformations of Screws with Applications to Screw Systems and Finite Twists," *Mechanism and Machine Theory*, Vol. 25, No. 6 pp. 689-699.

Phillips, J. R., and Hunt, K., H., 1964, "On The Theorem of Three Axes in the Spatial Motion of Three Bodies," Aust. J. Appl. Sci., Vol. 15, pp. 267-287.

Rao, J., S., and Raghavacharyulu, E., 1975, "Experimental Determination of Jump Characteristics in Cam-Follower Systems," *Proc. 4th World Congress on Theory of Machines and Mechanisms*, Newcastle upon Tyne, Vol. 4, pp. 951-956.

Raven, F., H., 1959, "Analytical Design of Cams and Three-Dimensional Cams by Independent Position Equations," J. Appl. Mech. Trans. ASME, pp. 18-24.

Rooney, J., 1975a, "On Obtaining the Velocity Motor of Any link in a General N-Link Spatial Manipulator," *Proc. 4th Wld Congr. Theory of Machines and Mechanisms*, Newcastle upon Tyne, Vol. 4, pp. 1083-1087.

Rooney, J., 1975b, "On the Principle of Transference," Proc. 4th Wld Congr. Theory of Machines and Mechanisms, Newcastle upon Tyne, Vol. 4, pp. 1089-1094.

Rosenberg J., and Křen, K., 1987, "Kinematic Analysis of Mechanism Links Connected by a Higher Kinematic Pair and Its Application," *Mechanism and Machine Theory*, Vol. 22, pp. 393-398.

Roth, B., 1967, "On the Screw Axes and Other Special Lines Associated With Spatial Displacements of Rigid Body," J. Engng. Ind., Trans. ASME, Vol 89, pp. 102-110.

Rothbart, H. A., 1956, Cams. Design, Dynamics, and Accuracy, John Wiley, New York.

Sadler, J., P., and Yang, Z., 1990, "Optimal Design of Cam-Linkage Mechanisms for Dynamic-Force Characteristics," *Mechanism and Machine Theory*, Vol. 25, pp. 41-57.

Shadek, K., S., H., Lloyd, J., L., and Smith, M., R., 1990, "A New Design of Geneva Drive to Reduce Shock Loading," *Mechanism and Machine Theory*, Vol. 25, pp. 589-595

Sodh, R., and Shoup, T. E., 1982, "Axodes for the Four-Revolute Spherical Mechanism," *Mechanism and Machine Theory*, Vol. 17, pp. 173-178.

Sticher, F., 1989, "On the Finite Screw Axis Cylindroid," Mechanism and Machine Theory, Vol. 24, pp. 143-155.

Stoddart, D. S., 1953, "Polydyne Cam Design," Machine Design, Vol. 25, January, pp. 121-135.

Stoddart, D. S., 1953, "Polydyne Cam Design-II," Machine Design, Vol. 25, February, pp. 146-154.

Struik, D. J., 1961, Lectures on Classical Differential Geometry, Addison-Wesley Company, Inc.

Sugimoto, K., and Duffy, J., 1982, "Application of Linear Algebra to Screw Systems," Mechanism and Machine Theory, Vol. 17, pp. 73-83.

Sun, W., H., and Waldron, K., 1982, "The Order Problem of Spatial Motion Generation Synthesis," Mechanism and Machine Theory, Vol. 17, pp. 289-294.

Takano, M., and Toyama, S., 1979, "Dynamics of Indexing Cam Mechanism and Speed-Up of Its Motion," Proc. 5th World Congress on Theory of Machines and Mechanisms, Vol. 2, pp. 1408-1411.

Tesar, D. and Matthew, G. K., 1976, The Dynamic Synthesis, Analysis, and Design of Modeled Cam Systems, Lexington Books, Lexington (Massachusetts).

Vadasz, A., F., and Soni, A., H., 1979, "Analytical Determination of the Space Burmester lines for Cylindric-Cylindric Cranks," Proc. 5th Wld Congr. Theory of Machines and Mechanisms, Vol. 2, pp. 1036-1039.

Veldkamp, G., R., 1967a, "Canonical Systems and Instantaneous Invariants in Spatial Kinematics," J. Mechanisms, Vol. 3, pp. 329-388.

Veldkamp, G., R., 1967b, "Some Remarks on Higher Curvature Theory," J. Engng. Ind., Trans. ASME, Vol 89, pp. 84-86.

Veldkamp, G. R., 1976, "On the Use of Dual Numbers, Vectors and Matrices in Instantaneous, Spatial Kinematics," *Mechanism and Machine Theory*, Vol. 11, pp. 141-156.

Waldron, K. J., 1972, "A Method of Studying Joint Geometry," Mechanism and Machine Theory, Vol. 7, pp. 347-353.

Wiederrich, J., L., and Roth, B., 1975, "Dynamic Synthesis of Cams Using Finite Trigonometric Series," Trans. ASME, Vol. 97, pp. 287-293.

Wilson, C. E., Sadler, J. P. and Michels, W., J., 1983, Kinematics and Dynamics of Machinery, Harper & Row, Publishers, New York.

Wunderlich, W., 1971, "Contributions to the Geometry of Cam Mechanisms with Oscillating Followers", J. Mechanisms, Vol. 6, pp. 1-20.

Xiao, D. Z.,, and Yang, A. T., 1989, "Kinematics of Three Dimensional Gearing," Mechanism and Machine Theory, Vol. 24, No. 4 pp. 245-255.

Yang, A., T., 1963, Application of Quaternion Algebra and Dual Numbers to the Analysis of Spatial Mechanisms, Doctoral Dissertation, Columbia University, New York City, No. 64-2803 (University Microfilm, Ann Arbor, Michigan).

Yang, A. T., Freudenstein, F., 1964, "Application of Dual-Number Quaternion Algebra to the Analysis of Spatial Mechanisms", J. Appl. Mech. Trans. ASME, 31, pp. 300-308.

Yang, A., T., 1974, "Calculus of Screws," Basic Questions of Design Theory, in W. R. Spillers (editor), American Elsevier Publishing Co., Inc., N. Y., pp. 265-281.

Yang, A., T., Kirson, Y., and Roth, B., 1975, "On a Kinematic Curvature Theory for Ruled Surfaces," *Proc. 4th Wld Congr. Theory of Machines and Mechanisms*, Newcastle upon Tyne, Vol. 4, pp. 737–742.

Zhong-tang, R., Jing-ping, H., 1989, "Synthesis of Planar Cam Mechanisms Based on Theory of Conjugate Surfaces," International Federation for the Theory of Machines and Mechanisms, Berlin, pp. 73-83.

Zigo, M., 1967, "A General Numerical Procedure for the Calculation of Cam Profiles from Arbitrarily Specified Acceleration Curves," J. Mechanisms, Vol. 2, pp. 407-414.

Appendix A

Dual Numbers

A brief account of dual numbers is presented here as a quick reference for the reader. Those readers unfamiliar with this tool are referred to (Yang, 1963, 1974; Yang and Freudenstein, 1964; Veldkamp, 1976; Bottema and Roth, 1979) for a comprehensive account of this topic.

A dual scalar, vector or matrix quantity is represented as the sum of a primal part and a dual part, the latter beginning with the dual unity ϵ , which has the property that $\epsilon^2 = 0$.

Let $\hat{a} = a + \epsilon a^*$ and $\hat{b} = b + \epsilon b^*$ be two dual scalars, with a, b, a^* and b^* being all real numbers. Equality, addition, multiplication and division are defined, respectively, as

$$\hat{a} = \hat{b} \Leftrightarrow a = b, \ a^* = b^* \tag{A.1a}$$

$$\hat{a} + \hat{b} = (a+b) + \epsilon(a^* + b^*) \tag{A.1b}$$

$$\hat{a}\hat{b} = ab + \epsilon(ab^{\bullet} + a^{\bullet}b) \tag{A.1c}$$

$$\frac{\hat{a}}{\hat{b}} = \frac{a}{b} - \epsilon \left(\frac{ab^* - a^*b}{b^2} \right), \ (b \neq 0) \tag{A.1d}$$

Furthermore, a line \mathcal{L} can be defined via the dual vector

$$\hat{\mathbf{e}} = \mathbf{e} + \epsilon \mathbf{m} \tag{A.2}$$

where $\mathbf{e}^T \mathbf{e} = 1$ and $\mathbf{e}^T \mathbf{m} = 0$. Here, \mathbf{e} defines the direction of \mathcal{L} , while \mathbf{m} the moment of \mathcal{L} with respect to a self-understood point O, namely,

$$\mathbf{m} = \mathbf{p} \times \mathbf{e} \tag{A.3}$$

p being the vector directed from O to an arbitrary point P of \mathcal{L} . Moreover, \mathbf{e} and \mathbf{m} are called the primal and dual parts of $\hat{\mathbf{e}}$, respectively. Thus, the components of $\hat{\mathbf{e}}$ are defined as the *line coordinates* of \mathcal{L} (Yang et al., 1975). Furthermore, the six components of the two vectors \mathbf{e} and \mathbf{m} in eq. (A.2) constitute the *Plücker coordinates* of \mathcal{L} . An alternative representation of \mathcal{L} is given as

$$\mathbf{r} = \mathbf{p} + \lambda \mathbf{e} \tag{A.4}$$

where λ is a real number. The components of r are defined as the *point coordinates* of \mathcal{L} . The transformation relation between line coordinates and point coordinates is derived from eq. (A.3), upon cross-multiplying its two sides by vector \mathbf{e} , namely,

$$e \times m = e \times (p \times e) \tag{A.5}$$

Expanding the right-hand side of eq.(A.5), one obtains

$$e \times m = p - e^{T}pe \tag{A.6}$$

If P is chosen as that lying closest to the origin, henceforth denoted by P_O , of position vector \mathbf{p}_O , then, from eq.(A.6),

$$p_O = e \times m \tag{A.7}$$

and vector r of eq.(A.4) is given by

$$\mathbf{r} = \mathbf{e} \times \mathbf{m} + \lambda \mathbf{e} \tag{A.8}$$

Now, let \mathcal{L}_1 and \mathcal{L}_2 be, in general, two skew lines. Their dual angle is defined as

$$\hat{\nu} = \nu + \epsilon h \tag{A.9}$$

where ν is the angle between \mathbf{e}_1 and \mathbf{e}_2 and h is the distance between \mathcal{L}_1 and \mathcal{L}_2 . The trigonometric functions of $\hat{\nu}$ can be expressed as (Yang, 1974; Veldkamp, 1976)

$$\sin \hat{\nu} = \sin \nu + \epsilon h \cos \nu \tag{A.10a}$$

$$\cos \hat{\nu} = \cos \nu - \epsilon h \sin \nu \tag{A.10b}$$

$$\tan \hat{\nu} = \tan \nu + \epsilon h (1 + \tan^2 \nu) \tag{A.10c}$$

$$\cot \hat{\nu} = \cot \nu - \epsilon \frac{h}{\sin^2 \nu}, (\sin \nu \neq 0) \tag{A.10d}$$

Furthermore, let \mathcal{F}_1 and \mathcal{F}_2 be two initially coincident coordinate frames. Assume that \mathcal{F}_2 is rotated through an angle ν about its X-axis and translated a distance h along the same axis. Thus, the transformation from \mathcal{F}_2 - to \mathcal{F}_1 -coordinates is given by the dual screw matrix shown below:

$$\hat{\mathbf{Q}}(\hat{\nu}) = \begin{bmatrix} 1 & 0 & 0 \\ 0 & \cos \hat{\nu} & -\sin \hat{\nu} \\ 0 & \sin \hat{\nu} & \cos \hat{\nu} \end{bmatrix}$$
(A.11a)

In other words, $\hat{\mathbf{Q}}(\hat{\nu})$ represents a dual rotation through $\hat{\nu}$ about the X-axis. Similarly, the dual rotations through $\hat{\nu}$ about the Y- and Z-axes are given by

$$\hat{\mathbf{R}}(\hat{\nu}) = \begin{bmatrix} \cos \hat{\nu} & 0 & \sin \hat{\nu} \\ 0 & 1 & 0 \\ -\sin \hat{\nu} & 0 & \cos \hat{\nu} \end{bmatrix}$$
 (A.11b)

and

$$\hat{\mathbf{S}}(\hat{\nu}) = \begin{bmatrix} \cos \hat{\nu} & -\sin \hat{\nu} & 0 \\ \sin \hat{\nu} & \cos \hat{\nu} & 0 \\ 0 & 0 & 1 \end{bmatrix}$$
 (A.11c)

respectively.

Dual vector operations, like multiplication by a (dual) scalar, inner product, cross-product, etc., have the same rules as those for operations of real vectors. However, the norm of a dual vector $\hat{\mathbf{x}} = \mathbf{x} + \epsilon \mathbf{x}^*$, according to Veldkamp (1976), is defined as

$$\parallel \hat{\mathbf{x}} \parallel = \parallel \mathbf{x} \parallel + \epsilon \frac{\mathbf{x} \cdot \mathbf{x}^*}{\parallel \mathbf{x} \parallel}, \qquad (\mathbf{x} \neq \mathbf{0})$$
 (A.12)

where $\|\cdot\|$ denotes Euclidean norm of its vector argument. Moreover, $\hat{\mathbf{x}}$ is called a unit dual vector if $\|\hat{\mathbf{x}}\| = 1$. Any dual vector can be expressed as

$$\hat{\mathbf{x}} = \parallel \hat{\mathbf{x}} \parallel \hat{\mathbf{e}} \tag{A.13}$$

where ê is a unit dual vector, and is computed as

$$\hat{\mathbf{e}} = \frac{\mathbf{x}}{\parallel \mathbf{x} \parallel} + \epsilon \frac{(\mathbf{x} \times \mathbf{x}^{\bullet}) \times \mathbf{x}}{\parallel \mathbf{x} \parallel^{3}} \tag{A.14}$$

Moreover, let \hat{a} and \hat{b} be two unit dual vectors, and \hat{n} be the unit dual vector with the same direction as the resultant dual vector of the cross product $\hat{a} \times \hat{b}$. Thus, the dual angle between \hat{a} and \hat{b} is defined as

$$\sin \hat{\nu} = \hat{\mathbf{a}} \times \hat{\mathbf{b}} \cdot \hat{\mathbf{n}} \tag{A.15}$$

$$\cos \hat{\nu} = \hat{\mathbf{a}} \cdot \hat{\mathbf{b}} \tag{A.16}$$

We present below a complement to the cross product of two unit dual vectors for the particular case when they represent two parallel lines. It is believed that this analysis is not given in the literature.

Let the point coordinates of two parallel lines be defined as

$$\mathcal{L}_i: \mathbf{r}_i = \mathbf{q}_i + \lambda \mathbf{e}, \qquad i = 1, 2$$
 (A.17)

Now, their line-coordinate representations are given as

$$\hat{\mathbf{e}}_i = \mathbf{e} + \epsilon \mathbf{m}_i \tag{A.18}$$

with $m_i = q_i \times e$. We now have

Theorem A.1: Let two lines \mathcal{L}_1 and \mathcal{L}_2 passing through points Q_1 and Q_2 , be parallel to the unit vector \mathbf{e} . Moreover, let P_1 and P_2 be the points of \mathcal{L}_1 and \mathcal{L}_2 closest to the origin. Then, the line passing through P_1 and P_2 is perpendicular to \mathbf{e} , and hence, to \mathcal{L}_1 and \mathcal{L}_2 .

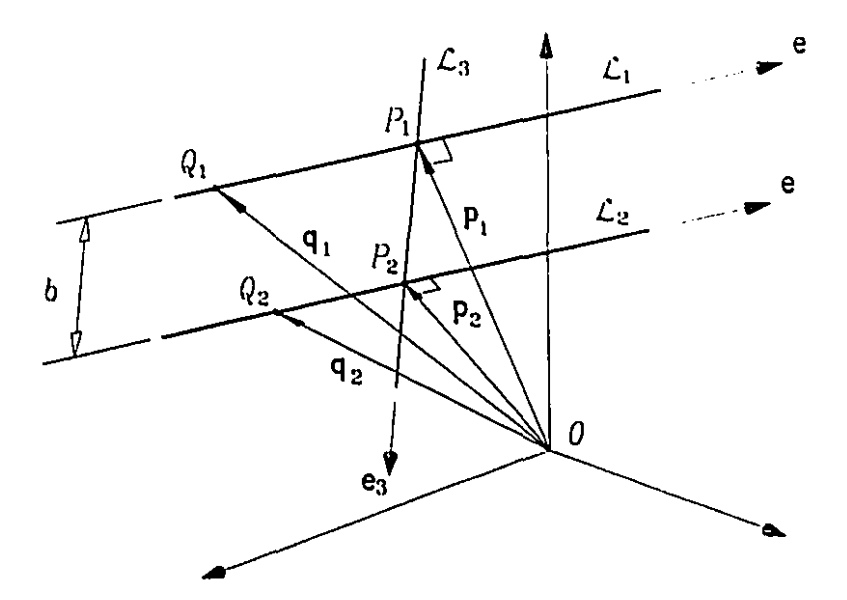


Figure A.1 The common perpendicular to two parallel lines

Proof: Let p_i be the position vector of P_i . Then, from eq.(Λ .7),

$$p_i = e \times m_i$$

Hence

$$\mathbf{p}_2 - \mathbf{p}_1 = \mathbf{e} \times (\mathbf{m}_2 - \mathbf{m}_1)$$

which is obviously perpendicular to e and the theorem follows.

Now, considering Theorem A.1, the line \mathcal{L}_3 perpendicular to both \mathcal{L}_1 and \mathcal{L}_2 passing through points P_1 and P_2 of \mathcal{L}_1 and \mathcal{L}_2 , respectively, as shown in Fig. A.1, is defined by its vector of point coordinates as

$$\mathbf{r}_3 = \mathbf{p}_1 + \lambda \mathbf{e}_3 \tag{A.19}$$

where

$$e_3 = \frac{p_2 - p_1}{b} \tag{A.20a}$$

and

$$\mathbf{p}_i = \mathbf{e} \times \mathbf{m}_i \tag{A.20b}$$

Appendix A. Dual Numbers

and $b = \parallel \mathbf{p}_2 - \mathbf{p}_1 \parallel$.

Now, the line coordinates of \mathcal{L}_3 are given as

$$\hat{\mathbf{e}}_3 = \mathbf{e}_3 + \epsilon \mathbf{p}_1 \times \mathbf{e}_3 \tag{A.21}$$

Substituting eq.(A.20a) into eq.(A.21), one can readily obtain the dual representation of \mathcal{L}_3 as

$$\hat{\mathbf{e}}_3 = \frac{\mathbf{p}_2 - \mathbf{p}_1}{b} + \epsilon \frac{\mathbf{p}_1 \times \mathbf{p}_2}{b} \tag{A.22}$$

Notice that this result cannot be obtained directly from the cross product $\hat{\mathbf{e}}_1 \times \hat{\mathbf{e}}_2$.

Appendix B

The Aronhold-Kennedy Theorem

For quick reference, we include here the discussion of the Aronhold-Kennedy Theorem in three dimensions, first stated by Beggs (1959), as proposed by Veldkamp (1976).

The relative screw motion of two rigid bodies becomes relative spherical motion in dual space. Thus, one can imagine these bodies in dual space as two concentric dual unit spheres S_1 and S_2 . Under the assumption that S_2 moves with respect to S_1 , the dual angular velocity is given as

$$\hat{\omega}_{21} = \hat{\omega}_{21} \hat{\mathbf{e}}_{21} \equiv (\omega_{21} + \epsilon v_{21}) \hat{\mathbf{e}}_{21} \tag{B.1}$$

where $\hat{\mathbf{e}}_{21}$ is a unit dual vector defining point \hat{P}_{21} , and the two components of the dual scalar $\hat{\omega}_{21}$, ω_{21} and υ_{21} , represent, in real space, the signed magnitudes of the angular velocity and the velocity of the points lying on the screw axis. The velocity of any point \hat{P} of \mathcal{S}_2 defined by the unit dual vector $\hat{\mathbf{p}}$ is given by

$$\hat{\mathbf{v}}_{21} = \hat{\omega}_{21} \times \hat{\mathbf{p}} \tag{B.2}$$

It is clear that $\hat{\mathbf{v}}_{21} = \mathbf{0}$ if \hat{P} coincides with \hat{P}_{21} , which is known as the pole of the motion.

Now, the three dual angular velocities of the unit dual spheres S_1 , S_2 and S_3 in relative motion are related as

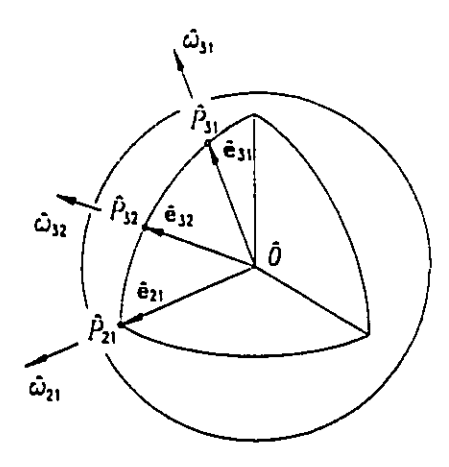


Figure B.1 The Aronhold-Kennedy Theorem

$$\hat{\omega}_{31} = \hat{\omega}_{32} + \hat{\omega}_{21} \tag{B.3}$$

Similarly, the dual velocities of a point are expressed as

$$\hat{\mathbf{v}}_{31} = \hat{\mathbf{v}}_{32} + \hat{\mathbf{v}}_{21} \tag{B.4}$$

Equation (B.3) can also be expressed in the form

$$\hat{\omega}_{31}\hat{\mathbf{e}}_{31} = \hat{\omega}_{32}\hat{\mathbf{e}}_{32} + \hat{\omega}_{21}\hat{\mathbf{e}}_{21} \tag{B.5}$$

where $\hat{\mathbf{e}}_{ij}$ indicates the three poles \hat{P}_{ij} , and $\hat{\omega}_{ij}$ are the signed norms of the dual vectors $\hat{\omega}_{ij}$, defined as

$$\hat{\omega}_{ij} = \omega_{ij} + \epsilon v_{ij} \tag{B.6}$$

As a result of eq.(B.5), the Aronhold-Kennedy Theorem is expressed as (Veldcamp, 1976)

Theorem B.1 (Aronhold-Kennedy) The poles \hat{P}_{21} , \hat{P}_{31} and \hat{P}_{32} of three unit dual spheres in relative motion lie on the same great circle.

Thus, the Aronhold-Kennedy Theorem defined in the dual space involves pure rotations, pure translations and general screw motions. Theorem B.1 is illustrated in Fig. B.1.

Appendix C

Ruled-Surface Geometry

A surface \mathcal{R} generated by the motion of a line \mathcal{L} , defined as in eq.(A.4), is called a ruled surface, \mathcal{L} being its generatrix (Struik, 1961). Thus, the position vector of \mathcal{R} is given by

$$\mathbf{r}(\psi, \lambda) = \mathbf{p}(\psi) + \lambda \mathbf{e}(\psi)$$
 (C.1)

where ψ and λ are the parameters of \mathcal{R} . The curve defined by the points $p(\psi)$ is called the *directrix* of \mathcal{R} , and the vectors $e(\psi)$ with origin at the centre of a unit sphere describe the *spherical indicatrix* of \mathcal{L} . Moreover, if $p(\psi)$ is a constant, \mathcal{R} is a cone, whereas \mathcal{R} is a cylinder if e is a constant.

The striction curve, as discussed in Section 2.3, is given by the position vector

$$g(\psi) = p - \frac{e' \cdot p'}{e' \cdot e'} e$$
 (C.2)

the prime denoting differentiation with respect to ψ .

Now, the unit normal of R can be derived from eq. (C.1) as

$$n(\psi, \lambda) = \frac{\mathbf{u}}{\parallel \mathbf{u} \parallel} \tag{C.3}$$

where

$$\mathbf{u} = \frac{\partial \mathbf{r}}{\partial \psi} \times \frac{\partial \mathbf{r}}{\partial \lambda} \tag{C.4}$$

In terms of eq. (C.1), $n(\psi, \lambda)$ becomes

$$n = \frac{(p' + \lambda e') \times e}{\parallel u \parallel}$$
 (C.5)

At every point of the striction curve, a trihedron of the unit vectors a, c and e is defined and called the *natural trihedron*. Moreover, a and c, called *asymptotic normal* and *central normal* vectors, respectively, can be expressed in terms of e as (McCarthy 1987b)

$$a = \lim_{\lambda \to -\infty} n(\psi, \lambda) = \frac{-e' \times e}{\parallel e \parallel}$$
 (C.6)

$$c = \frac{e'}{\parallel e \parallel} \tag{C.7}$$

Moreover, the geodesic Frenet equations of the {a, c, e} triad are given by

$$d\mathbf{e}/ds = \mathbf{c} \tag{C.8}$$

$$d\mathbf{c}/ds = \gamma \mathbf{a} - \mathbf{e} \tag{C.9}$$

$$d\mathbf{a}/ds = -\gamma \mathbf{c} \tag{C.10}$$

where s represents the arc length of the spherical indicatrix of e, while γ is the geodesic curvature. The latter is expressed in terms of e and its derivatives with respect to ψ as

$$\gamma = \frac{\mathbf{e} \times \mathbf{e}' \cdot \mathbf{e}''}{\|\mathbf{e}'\|^3} \tag{C.11}$$

The positional variation of the trihedron defined by a, c and e is given by

$$d\mathbf{g}/ds = \Delta \mathbf{a} + \Gamma \mathbf{e} \tag{C.12}$$

where

$$\Delta \equiv \frac{\mathbf{p'} \cdot \mathbf{e} \times \mathbf{e'}}{\parallel \mathbf{e'} \parallel^2} \tag{C.13}$$

and

$$\Gamma \equiv \frac{\mathbf{p'} \cdot \mathbf{e}}{\parallel \mathbf{e'} \parallel} - \frac{1}{\parallel \mathbf{e'} \parallel} \frac{d}{dt} \left(\frac{\mathbf{p'} \cdot \mathbf{e}}{\parallel \mathbf{e'} \parallel^2} \right) \tag{C.14}$$

Now, the dual spherical radius of curvature of $\mathcal{R},\,\hat{\rho}=\rho+\epsilon r,$ is given by (McCarthy, 1987b)

$$\tan \hat{\rho} = \frac{1/\hat{\kappa}}{\hat{\gamma}/\hat{\kappa}} \tag{C.15}$$

where

$$\hat{\kappa} = \kappa + \epsilon (K - \kappa \Delta) \tag{C.16}$$

$$\hat{\gamma} = \gamma + \epsilon (\Gamma - \gamma \Delta) \tag{C.17}$$

and the definitions below:

$$\kappa \equiv \sqrt{1 + \gamma^2} \tag{C.18}$$

$$\kappa \equiv \sqrt{1 + \gamma^2}$$

$$K \equiv \frac{\gamma \Gamma + \Delta}{\kappa}$$
(C.18)
(C.19)

Appendix D

Displacement Program Functions

The functions describing the rise or return in the displacement program of the synthesis of cam mechanisms have been studied extensively in the literature (Rothbart, 1956; Jensen, 1965; Tesar and Matthew, 1976; Chen, 1982; Angeles and López-Cajún, 1991). Because of the scope of this thesis, only some of the functions of those types having the property of zero velocity and acceleration at the ends of the rise (or return) phase are presented here. Moreover, these functions are defined as

$$\tau = \tau(x), \qquad 0 \le \tau \le 1, \quad 0 \le x \le 1$$
 (D.1)

D.1 Generalized Input-Output Function

In the theory presented in Chapters 2 and 3, the dimensions and symbols of the variables of the input-output functions change according to the type of kinematic pair of the mechanism to be considered. Two kinds of pairs have been considered either for the input or the output motions, namely, revolute or prismatic. A total of four combinations is achieved, namely, R-R, R-P, P-R and P-P, and are applicable to both three- and four-link cam mechanisms. However, all of them can be regarded as

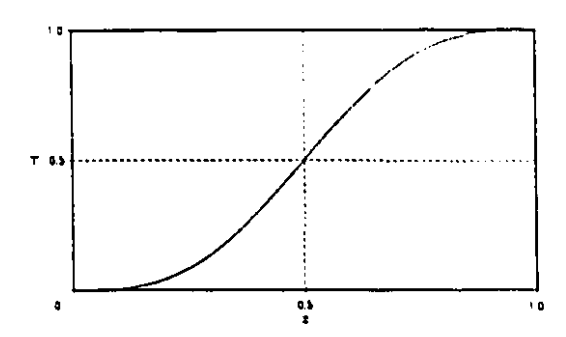


Figure D.1 Normalized input-output function

Generalized Input-Output Function

Type	₽≣	$h \equiv$	$x \equiv$	$x' \equiv$
R-R	$\phi(\psi)$	$\Delta \phi$	$\psi/\Delta\psi$	$dx/d\psi = 1/\Delta\psi$
R-P	$z_3(\psi)$	Δz_3	$\psi/\Delta\psi$	$dx/d\psi = 1/\Delta\psi$
P-R	$\phi(z_2)$	$\Delta \phi$	$z_2/\Delta z_2$	$dx/dz_2 = 1/\Delta z_2$
P-P	$z_3(z_2)$	Δz_3	$z_2/\Delta z_2$	$dx/dz_2 = 1/\Delta z_2$

one generalized input-output function, namely,

$$\varphi(x) = h\tau(x) \tag{D.2a}$$

h being the rise of the follower and τ the normalized function as defined in eq.(D.1) and shown in Fig. D.1. Definitions of φ , h, and x for each of the four types of the mechanisms mentioned above are shown in Table D.1. The derivatives of $\varphi(x)$ are taken with respect to ψ or z_2 , depending on the type of the input motion. Thus, the chain rule is applied to φ to obtain its first and second derivatives with respect to the input variable, and denoted φ' and φ'' , thereby obtaining

$$\varphi' = hx'\frac{d\tau}{dx} \tag{D.2b}$$

$$\varphi' = hx'\frac{d\tau}{dx}$$
 (D.2b)
$$\varphi'' = hx'^2\frac{d^2\tau}{dx^2}$$
 (D.2c)

where x' is defined as in the Table D.1

D.2 Cycloidal Function

The cycloidal function satisfies the condition of zero velocity and zero acceleration at the ends. This function and its first and second derivatives are defined below:

$$\tau = x - \frac{1}{2\pi} \sin 2\pi x \tag{D.3a}$$

$$\frac{d\tau}{dx} = (1 - \cos 2\pi x) \qquad 0 \le x \le 1 \tag{D.3b}$$

$$\frac{d^2\tau}{dx^2} = 2\pi \sin 2\pi x \tag{D.3c}$$

D.3 Polynomial Functions

If the rise is represented by a polynomial, then its coefficients are determined from the conditions to be satisfied. The methodology to determine the polynomial coefficients can be found in (Dudley, 1948; Angeles and López-Cajún, 1991). Some of the solutions are presented below:

D.3.1 3-4-5 Polynomial

$$\tau = 10x^2 - 15x^4 + 6x^5 \tag{D.4a}$$

$$\frac{d\tau}{dx} = 30x^2 - 60x^3 + 30x^4 \qquad 0 \le x \le 1$$
 (D.4b)

$$\frac{d^2\tau}{dx^2} = 60x - 180x^2 + 120x^3 \tag{D.4c}$$

D.3.2 4-5-6-7 Polynomial

$$\tau = 35x^4 - 84x^5 + 70x^6 - 20x^7 \tag{D.5a}$$

$$\frac{d\tau}{dx} = 140x^3 - 420x^4 + 420x^5 - 140x^6 \qquad 0 \le x \le 1$$
 (D.5b)

$$\frac{d^2\tau}{dx^2} = 420x^2 - 1680x^3 + 2100x^4 - 840x^5$$
 (D.5c)

D.4 Combined Functions

In order to improve the performance of the basic curves as defined above, designers have tried combinations of them. The aim has been to produce a follower motion with bounded jerk. One of these combinations is the called the trapezoid function, which is a combination of cubic and parabolic curves. This type, from the point of view of the maximum value of $d^2\tau/dx^2$, is slightly better than the cycloidal curve (Chen, 1982). From the same point of view, an even better function was proposed, the modified trapezoidal function (Neklutin, 1959), which replaces the cubic curves by cycloidal curves. This function is presented below, a detailed derivation of this curve being found in (Tesar and Matthew, 1976; Chen, 1982).

D.4.1 Modified Trapcroidal Acceleration

$$\tau = 0.09724612(4x - \frac{1}{\pi}\sin 4\pi x) \tag{D.6a}$$

$$\frac{d\tau}{dx} = 0.3889845(1 - \cos 4\pi x) \qquad 0 \le x < \frac{1}{8}$$
 (D.6b)

$$\frac{d^2\tau}{dx^2} = 4.888124\sin 4\pi x \tag{D.6c}$$

$$\tau = 2.444406184x^2 - 0.22203097x + 0.00723407$$
 (D.6d)

$$\frac{d\tau}{dx} = 4.888124x - 0.22203097 \qquad \qquad \frac{1}{8} \le x < \frac{3}{8} \qquad (D.6e)$$

$$\frac{d^2\tau}{dx^2} = 4.888124\tag{D.6f}$$

$$\tau = 1.6110154x - 0.0309544 \sin(4\pi x - \pi) - 0.3055077$$
 (D.6g)

$$\frac{d\tau}{dx} = 1.6110154 - 0.3889845\cos(4\pi x - \pi) \qquad \frac{3}{8} \le x < \frac{1}{2}$$
 (D.6h)

$$\frac{d^2\tau}{dx^2} = 4.888124\sin(4\pi x - \pi) \tag{D.6i}$$

$$\tau = 1.6110154x + 0.03009544\sin(4\pi x - 2\pi) - 0.3055077 \tag{D.6j}$$

$$\frac{d\tau}{dx} = 1.6110154 + 0.3889845\cos(4\pi x - 2\pi) \qquad \frac{1}{2} \le x < \frac{5}{8} \quad (D.6k)$$

$$\frac{d^2\tau}{dx^2} = -4.888124\sin(4\pi x - 2\pi) \tag{D.6l}$$

$$\tau = 4.6660917x - 2.44406184x^2 - 1.2292648 \tag{D.6m}$$

$$\frac{d\tau}{dx} = 4.6660917 - 4.888124x \qquad \qquad \frac{5}{8} \le x < \frac{7}{8} \qquad (D.6n)$$

$$\frac{d^2\tau}{dx^2} = -4.888124\tag{D.60}$$

$$\tau = 0.6110154 + 0.3889845x + 0.0309544\sin(4\pi x - 3\pi)$$
 (D.6p)

$$\frac{d\tau}{dx} = 0.3889845[1 + \cos(4\pi x - 3\pi)] \qquad \frac{7}{8} \le x \le 1 \quad (D.6q)$$

$$\frac{d^2\tau}{dx^2} = -4.888124\sin(4\pi x - 3\pi) \tag{D.6r}$$

Appendix E

CAD-Based Methods. Planar Applications

E.1 Introduction

Graphical methods for the synthesis of cam mechanisms could be considered obsolete with present-day computer technology. However, the ever increasing availability of CAD systems makes graphical methods of cam synthesis worth revisiting, if in light of current technology.

In this chapter we revisit graphical methods of cam synthesis and propose a novel CAD-based method. In the realm of traditional graphical methods (Rothbart, 1956; Jensen, 1965; Chen 1982) the cam profile is obtained as the tangent curve to a sequence of placements of the geometric entity—circle, line or arbitrary curve—representing the follower. Hence, the accuracy of the profile thus obtained is totally dependent upon draftsman's skill. In the realm of CAD systems, the skill-dependence feature is eliminated, but then a problem remains, namely, the digital approximation of the tangent curve, that is numerically cumbersome. This problem was overcome in the early days of CAD/CAM technology with the introduction of envelopes (Struik,

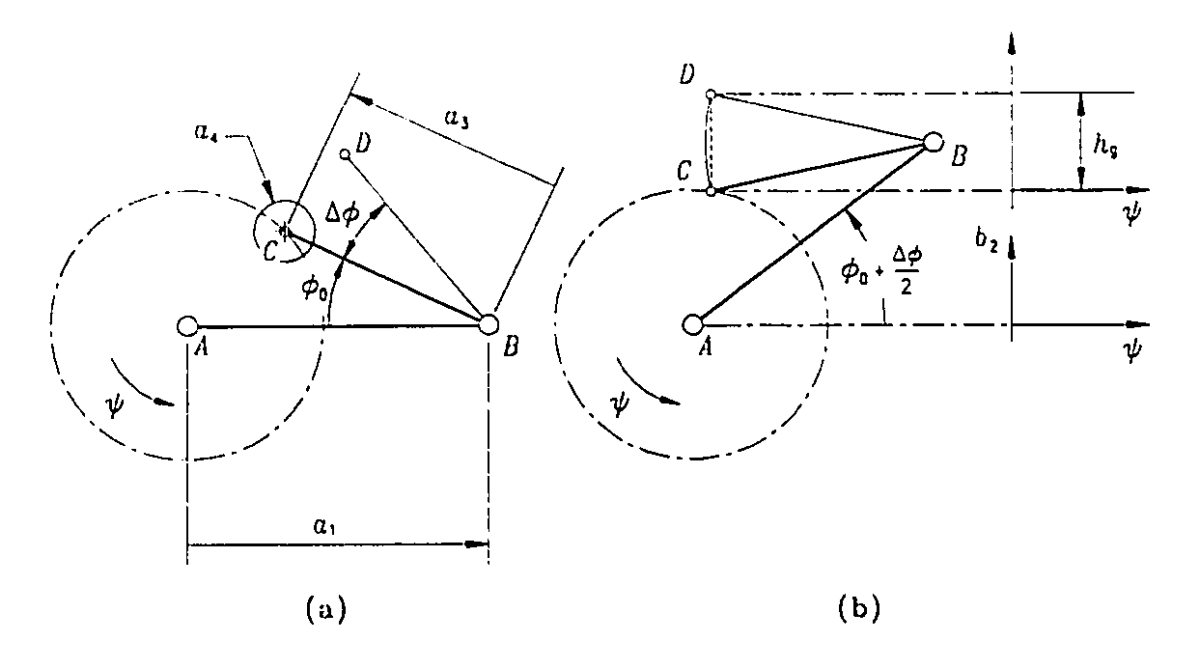


Figure E.1 RHRR mechanism layout

1961; Wilson, Sadler and Michels, 1983; Backhouse and Jones, 1990) that yield the cam profile coordinates directly and hence, eliminates the inaccuracies of tangent-curve tracing. While the envelope method is very reliable and has found extensive acceptance, it is still essentially a numerical method that does not exploit the interactive capabilities of CAD systems. This state of affairs prompted us to propose an innovation in the rendering of the profile. This innovation consists of finding the contact points between cam and follower, in a totally graphical and interactive fashion that exploits features available in commercial CAD systems.

The theory presented in Chapters 2 and 3 is the basis of the method presented here. The profile of a three-link mechanism is used as a reference for the construction of a four-link mechanism; in other words, RHR and RHP mechanisms are the two basic groups of the four types of mechanisms discussed here. These four types pertain to two families, namely, the {RHRR, RHHR} family based on RHR mechanisms and the {RHRP, RHHP} family based on RHP mechanisms. Although not presented here, the synthesis of those groups pertaining to PHR and PPP mechanisms can follow the

same methodology. We assume henceforth that all geometric parameters of the cam have been either prescribed by an experienced cam designer or determined using an optimization procedure, as described in detail in (Angeles and López-Cajún, 1991).

Moreover, all procedures discussed below can be readily automated with the aid of a CAD system. We have implemented them in AutoCADTM.

E.2 RHRR Mechanisms

An illustration of the cam mechanism presented in this section is shown in Fig. 3.6. The parameters given to start the design with are shown in Fig. E.1a, where a_1 is the distance between the centres of the fixed revolutes, a_3 the distance between the fixed and moving revolute centres of the follower, a_4 the radius of the roller, ϕ_0 the angle of the follower corresponding to the lowest position of the follower and $\Delta \phi$ is the rise of the follower.

Once the parameters mentioned above are fixed, the method starts by rotating the segment AB through an angle $\phi_0 + \Delta \phi/2$ so that the segment CD is parallel to the ordinate axis of the displacement coordinate frame, as shown in Fig. E.1b. Thus, the displacement program is based on the length of segment CD, namely, the chord of the arc with radius a_3 subtending angle DBC. Then, as the follower rotates, the projections of the successive positions of centre of the roller onto segment CD are represented by h, i.e.,

$$h = h_g \tau \tag{E.1}$$

where h_g is the length of the aforementioned chord, to be determined either graphically or numerically, and is evaluated as

$$h_g = 2a_3 \sin \frac{\Delta \phi}{2} \tag{E.2}$$

while τ is the normalized function defined as in eq.(D.1).

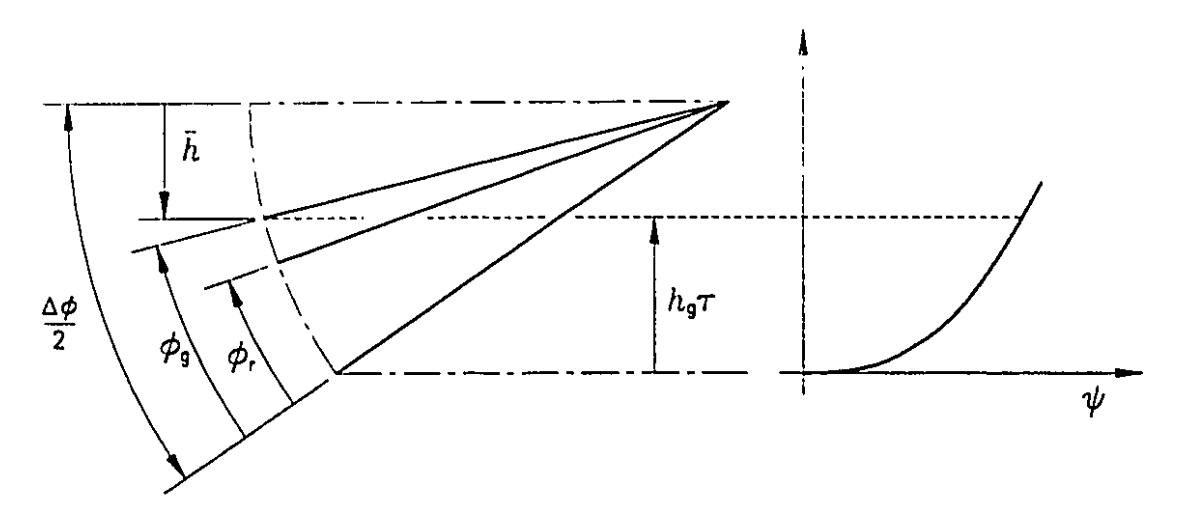


Figure E.2 Difference between ϕ_g and ϕ_r

It is pointed out that, with the application of eq.(E.2), the actual angle of displacement of the follower, ϕ_r , and the angle of displacement obtained graphically ϕ_g , are identical only at the ends of the follower motion and at the middle point of this motion. In any other position there is a difference, which, when normalized with respect to $\Delta \phi$, is denoted by ξ , and measures the relative error involved, i.e.,

$$\xi = \frac{\phi_g - \phi_r}{\Delta \phi} \tag{E.3}$$

Moreover,

$$\phi_{\tau} = \Delta \phi \tau \tag{E.4a}$$

$$\phi_g = \frac{\Delta \phi}{2} - \sin^{-1} \frac{\bar{h}}{a_3} \tag{E.4b}$$

where \bar{h} , as shown in Fig. E.2, is given as

$$\bar{h} = a_3 \sin \frac{\Delta \phi}{2} - h_g \tau \tag{E.5}$$

Now, combining eqs.(E.2, E.4 & E.5) with eq.(E.3), the latter readily leads to

$$\xi(\tau) = \frac{1}{2} - \tau - \frac{1}{\Delta\phi} \sin^{-1} \left[(1 - 2\tau) \sin \frac{\Delta\phi}{2} \right]$$
 (E.6)

1

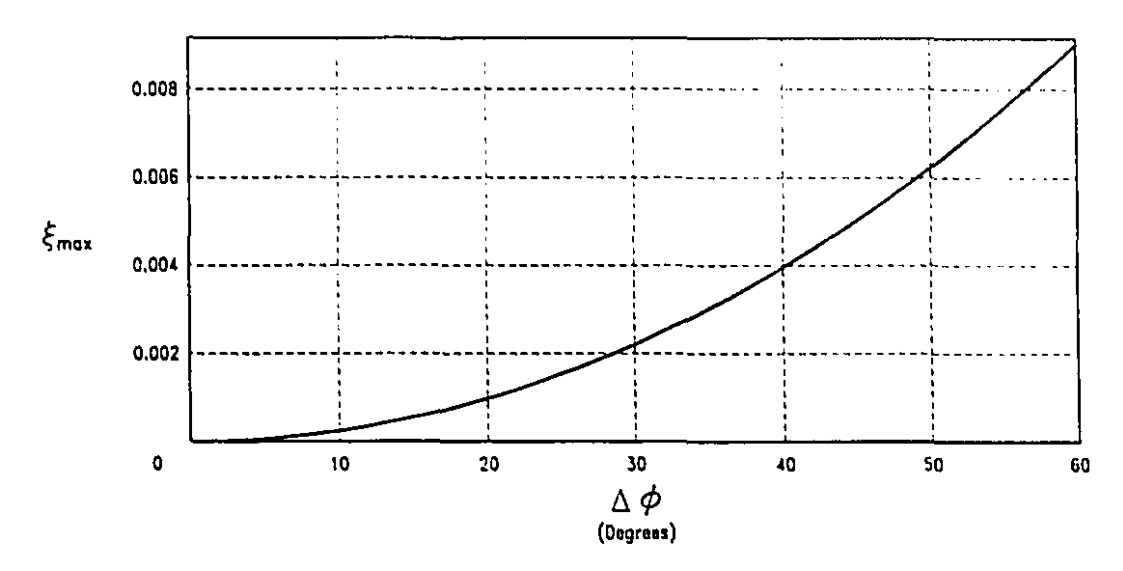


Figure E.3 Plot of ξ_{max} vs. $\Delta \phi$

The maximum value of ξ , for a given value of $\Delta \phi$, can be computed as $\xi_M = \xi(\tau_M)$, where τ_M is obtained from the equation $d\xi/d\tau = 0$. For example, for a cycloidal input-output motion, τ_M is given as

$$\tau_M = \frac{1}{2} \pm \frac{1}{2\Delta\phi} \sqrt{\frac{\Delta^2\phi}{\sin^2\frac{\Delta\phi}{2}} - 4}$$
 (E.7)

Thus, with $\Delta \phi = 30^{\circ}$ for example, $\xi_M = 0.00221$. Moreover, a plot of ξ_M vs. $\Delta \phi$ is shown in Fig. E.3. The magnitude of ξ_M is apparently negligible for the purposes of this chapter, and hence, eq.(E.2) can be considered as an acceptable approximation.

Now, the coordinate axes b_2 and ψ are located as shown in Fig. E.1b, where b_2 is defined in Chapter 3 as the distance from the axis of rotation of the cam to the contact line between cam and follower of the RHR cam mechanism, and is recalled below for quick reference:

$$b_2 = \frac{\phi'}{\phi' - 1} a_1 \tag{3.44}$$

1

Next, the cam is considered fixed and the frame of the mechanism is rotated in the opposite direction of the assumeed rotation of the cam. Thus, for $\psi = \psi_b$, the points corresponding to h and b_2 are projected onto the arc \mathcal{A} and the line \mathcal{L} , respectively,

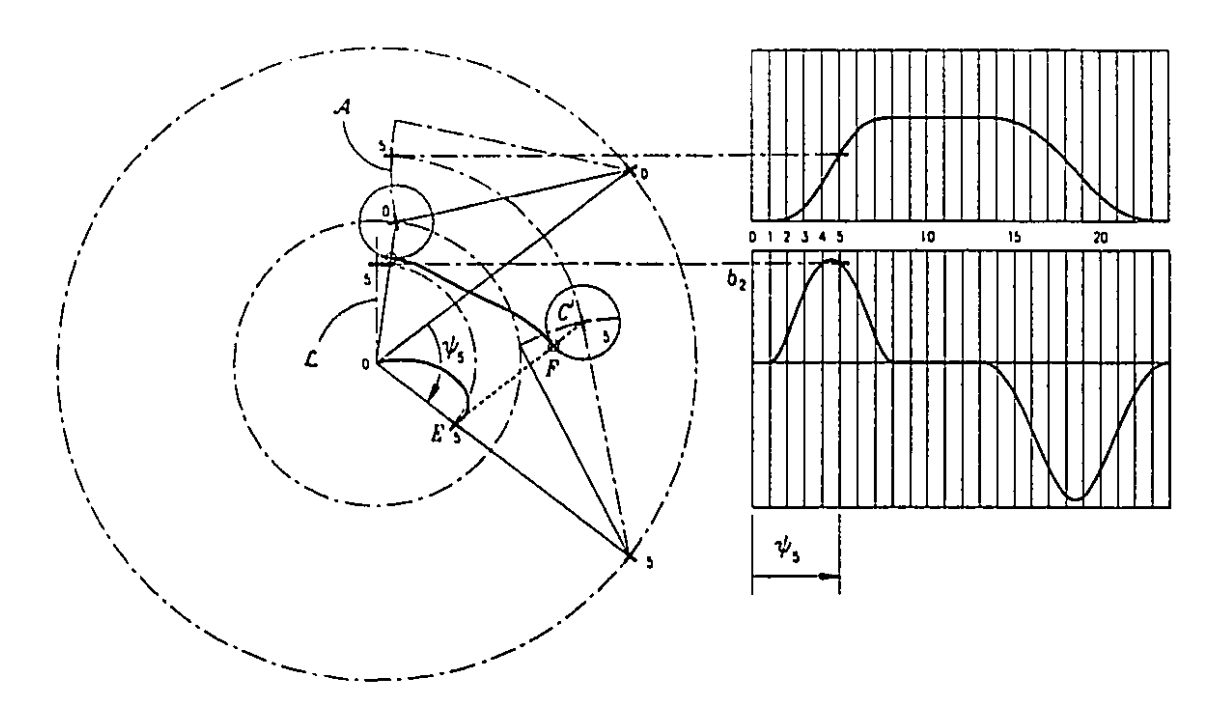


Figure E.4 Contact point for $\psi=\psi_5$ of the RHRR mechanism

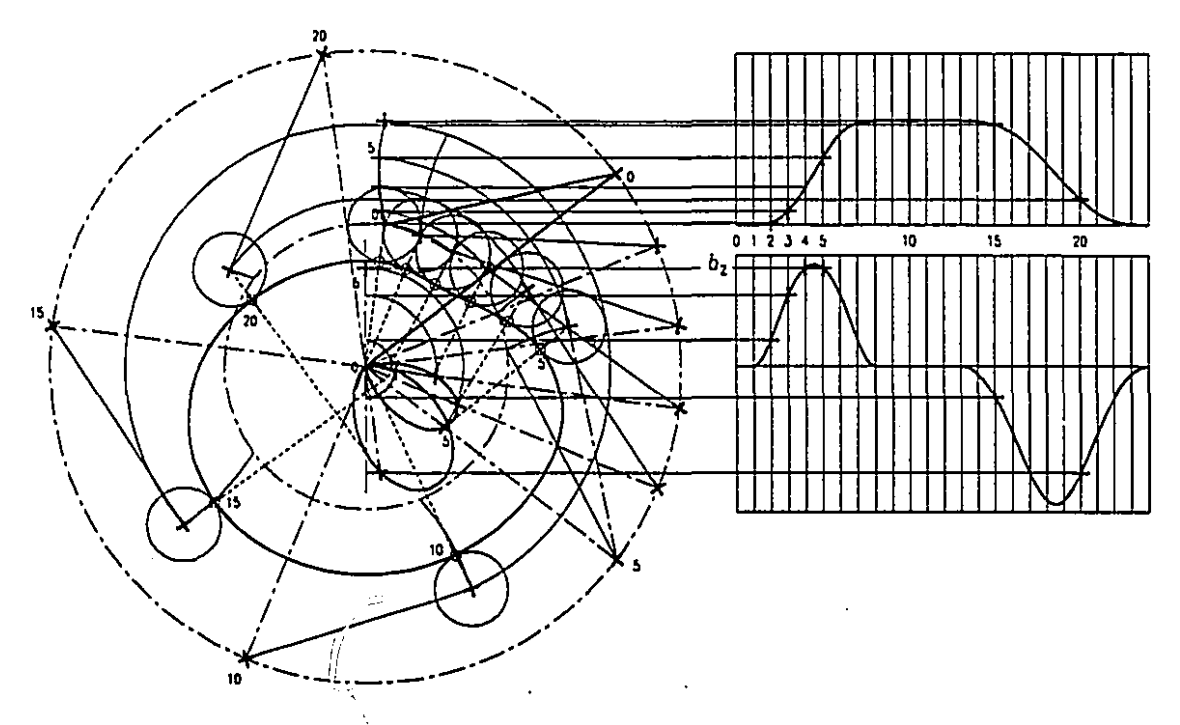


Figure E.5 Cam profile of the RHRR mechanism

4

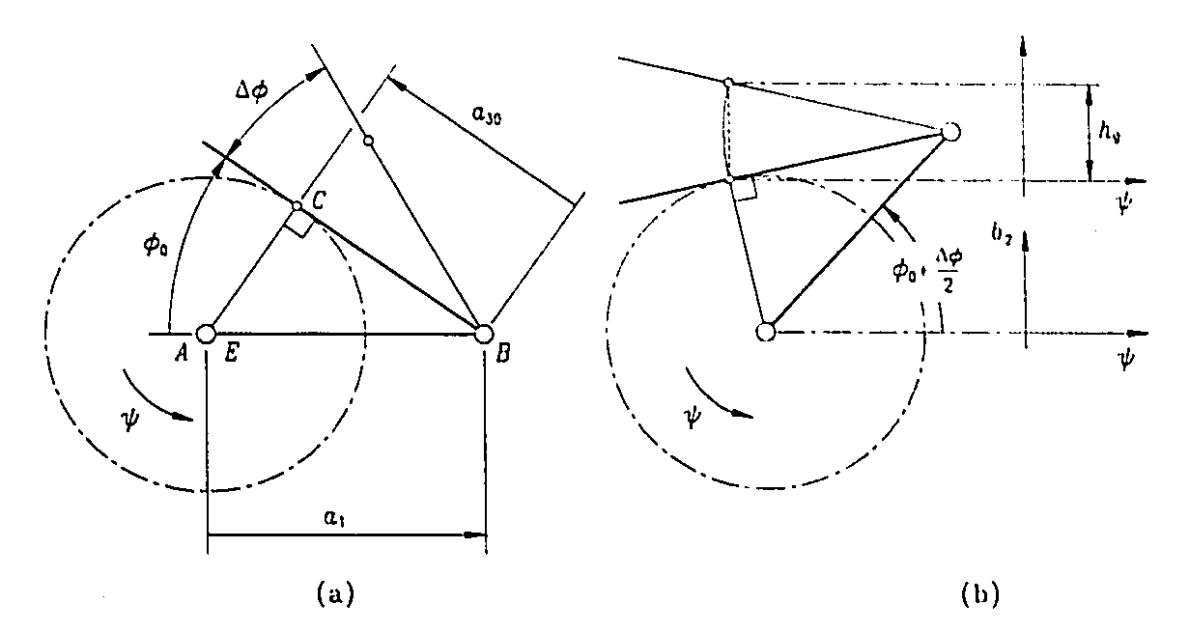


Figure E.6 RHHR mechanism layout

as shown in Fig. E.4. Then, the location of C' and E for ψ_5 are readily obtained, where C' and E are points of I_{43} and I_{32} , respectively.

Further, we determine F, the contact between cam and roller, as the intersection of the circle with centre C' and radius a_4 with segment EC', as indicated in Fig. E.4. This procedure is repeated for each value ψ_i , where $i=0,1,\cdots,n$, and n is the number of subdivisions of the full rotation of the cam. The profile thus resulting is the locus of point F, as shown in Fig. E.5.

E.3 RHHR Mechanisms

The type of mechanism presented here is shown in Fig. 3.12. As stated in Chapter 3, the synthesis of RHRR mechanisms is similar to the synthesis of RHRR mechanisms, with only two important differences: a) the distance a_3 is variable and b) the pressure angle is identically zero, i.e., segment EC, is always perpendicular to segment BC, as shown in Fig. E.6a.

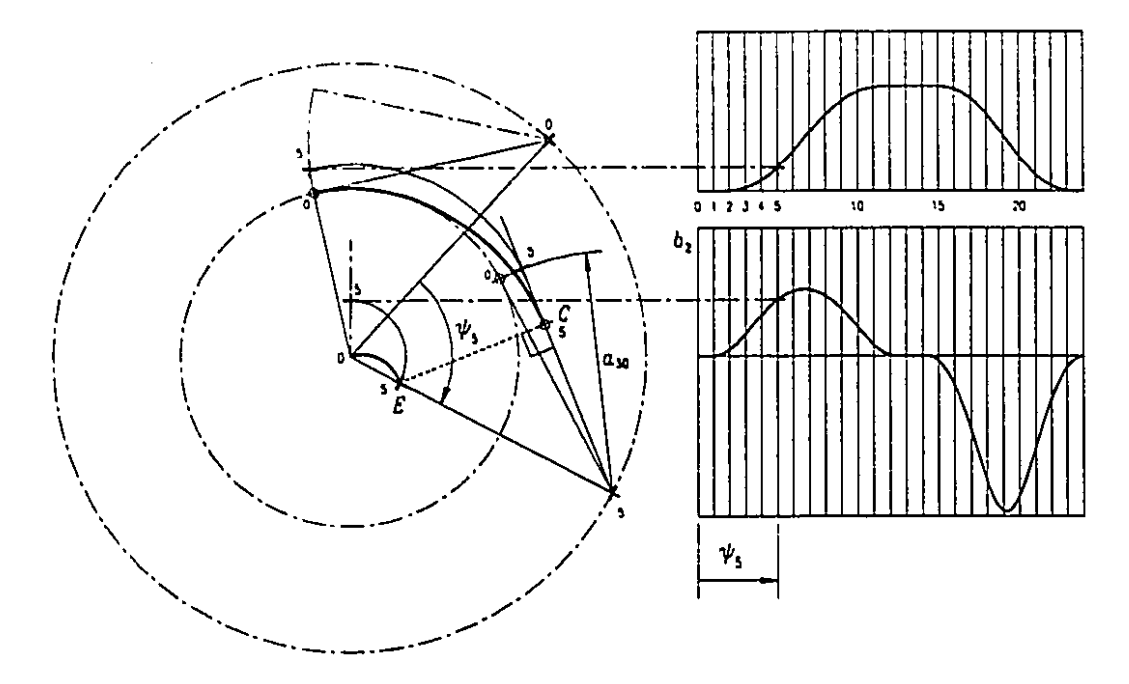


Figure E.7 Contact point for $\psi = \psi_5$ of the RHR mechanism

The reference value of a_3 is $a_{30} \equiv a_1 \cos \phi_0$, and is obtained as shown in Fig. E.6a. Thus, h_g is computed as

$$h_g = 2a_{30}\sin\frac{\Delta\phi}{2} \tag{E.8}$$

Shown in Fig. E.7 is the procedure to find the cam-follower contact point for $\psi = \psi_5$, where a_3 is variable. The profile thus resulting is designed with zero offset, i.e., with $a_4 = 0$, as shown in Fig. E.8.

If $a_4 \neq 0$, the profile is determined from that obtained with zero offset and auxiliary circles of radius a_4 as discussed in Section 3.4.1. The intersection of these circles with the dashed lines gives the points of the desired profile, as shown in Fig. E.9.

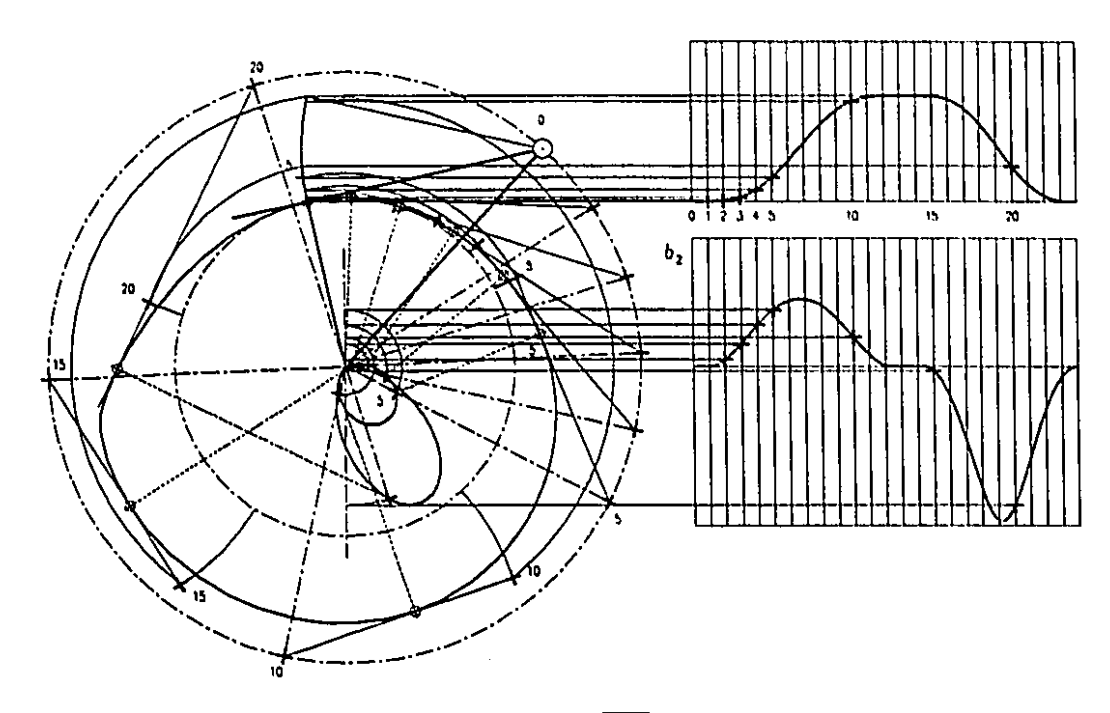


Figure E.8 Cam profile of the RHHR mechanism with $a_4=0$

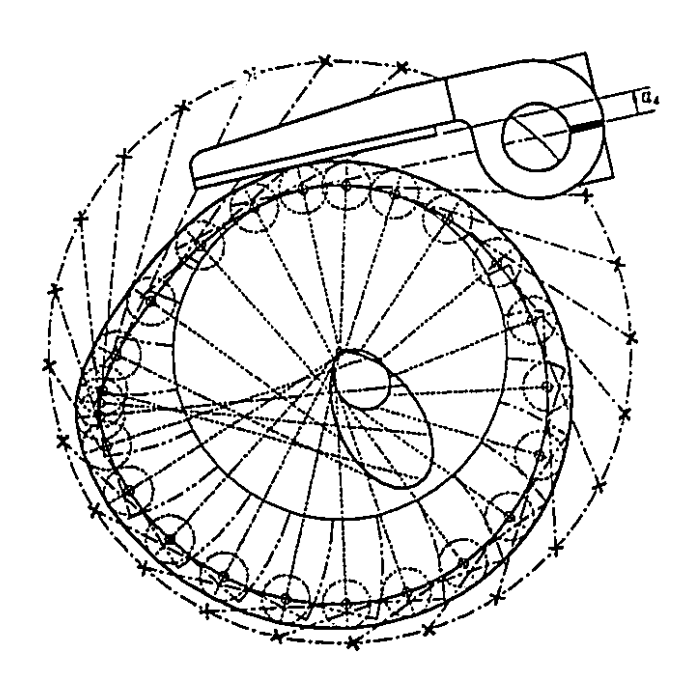


Figure E.9 Cam profile of the RHHR mechanism with $a_4 \neq 0$

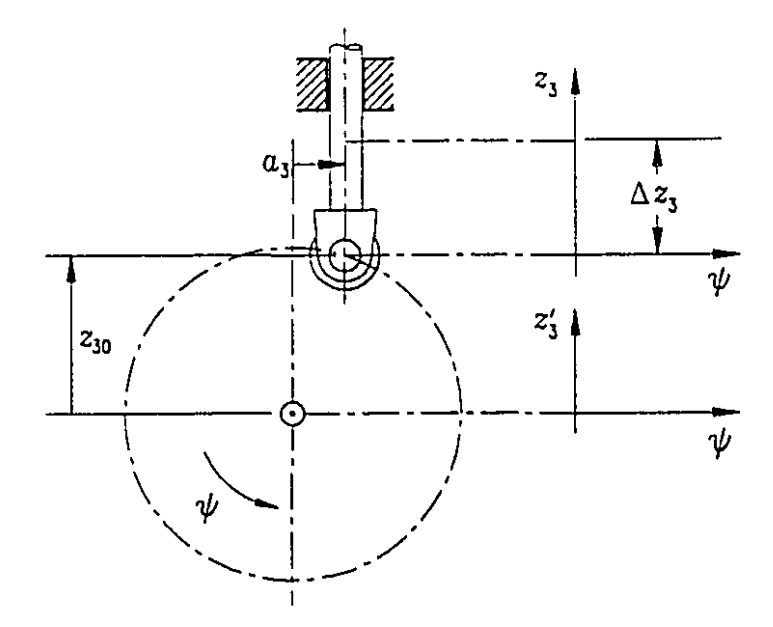


Figure E.10 RHRP mechanism layout

E.4 RHRP Mechanisms

The mechanisms to be discussed in this section, with $\alpha_1 = -\pi/2$, is shown in Fig. 3.7, the given parameters being shown in Fig. E.10. The ordinates of the two coordinate frames are parallel to the direction of motion of the follower. Moreover, according to eq.(2.21d), $b_2 = z_3'$.

Once the plots of z_3 and z_3' are obtained either graphically or numerically, their ordinates are projected onto line \mathcal{L} , as shown in Fig. E.11 for the value of $\psi = \psi_5$. The *i*-points from z_3 are rotated through the angle ψ_i , while the *i*-points from z_3' , are rotated through the angle $\psi_i + \pi/2$. Hence, the pitch curve of the RHRP mechanism and the cam profile of the RHP mechanism, respectively, are readily obtained.

The points of the cam profile are determined as the intersections of the circles of radius a_4 with segment EC', the profile thus obtained being shown in Fig. E.12.

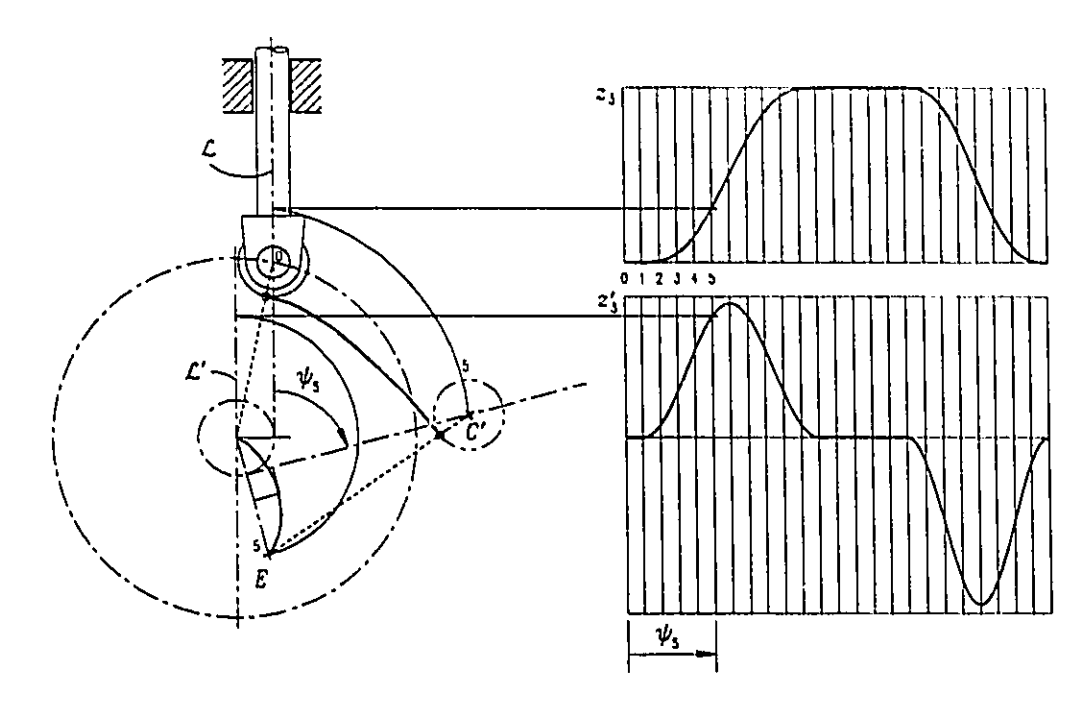


Figure E.11 Contact point for $\psi=\psi_5$ of the RHRP mechanism

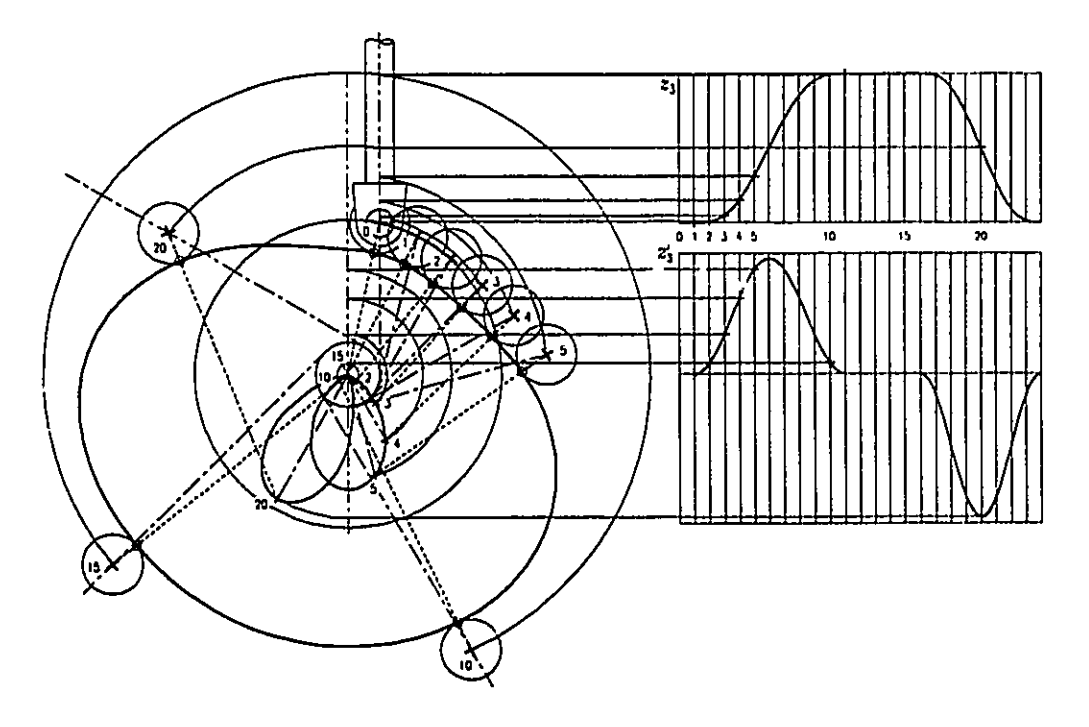


Figure E.12 Cam profile of the RHRP mechanism

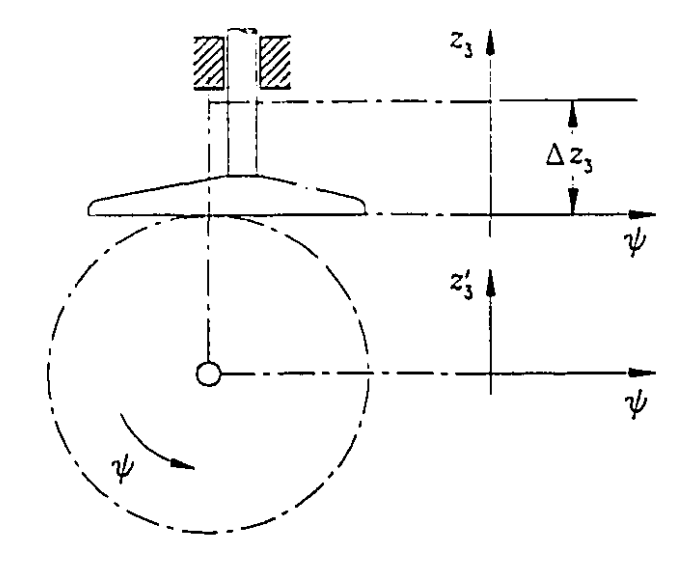


Figure E.13 RHHP mechanism layout

E.5 RHHP Mechanisms

The procedure to plot the cam profile points for the RHP mechanism is the same as that followed in Section E.4, the cam points of the RHHP mechanism being obtained likewise. The only difference here is that $a_3 = 0$ for $\psi = 0$, as shown in Fig. E.13, and, as discussed in Chapter 3, a_3 changes so that the pressure angle is zero; in other words, segment EF is always perpendicular to the face of the follower, as shown in Fig. E.14 for $\psi = \psi_5$. The profile obtained is shown in Fig. E.15.

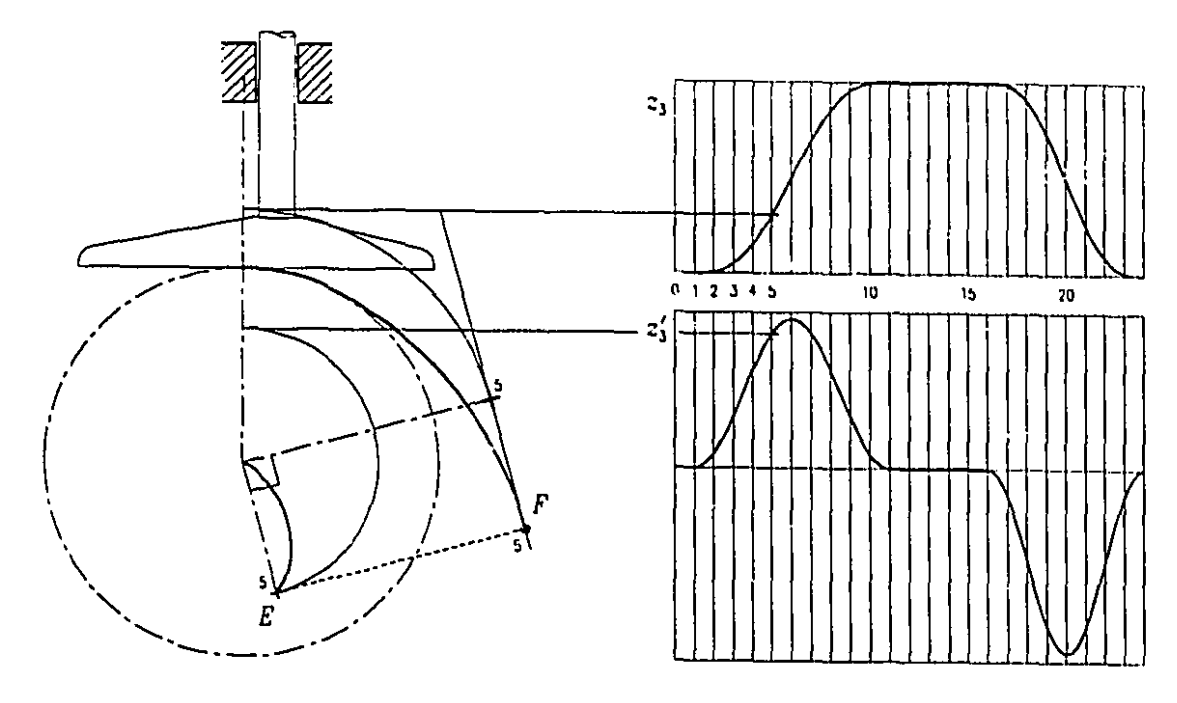


Figure E.14 Contact point for $\psi=\psi_5$ of the RHHP mechanism

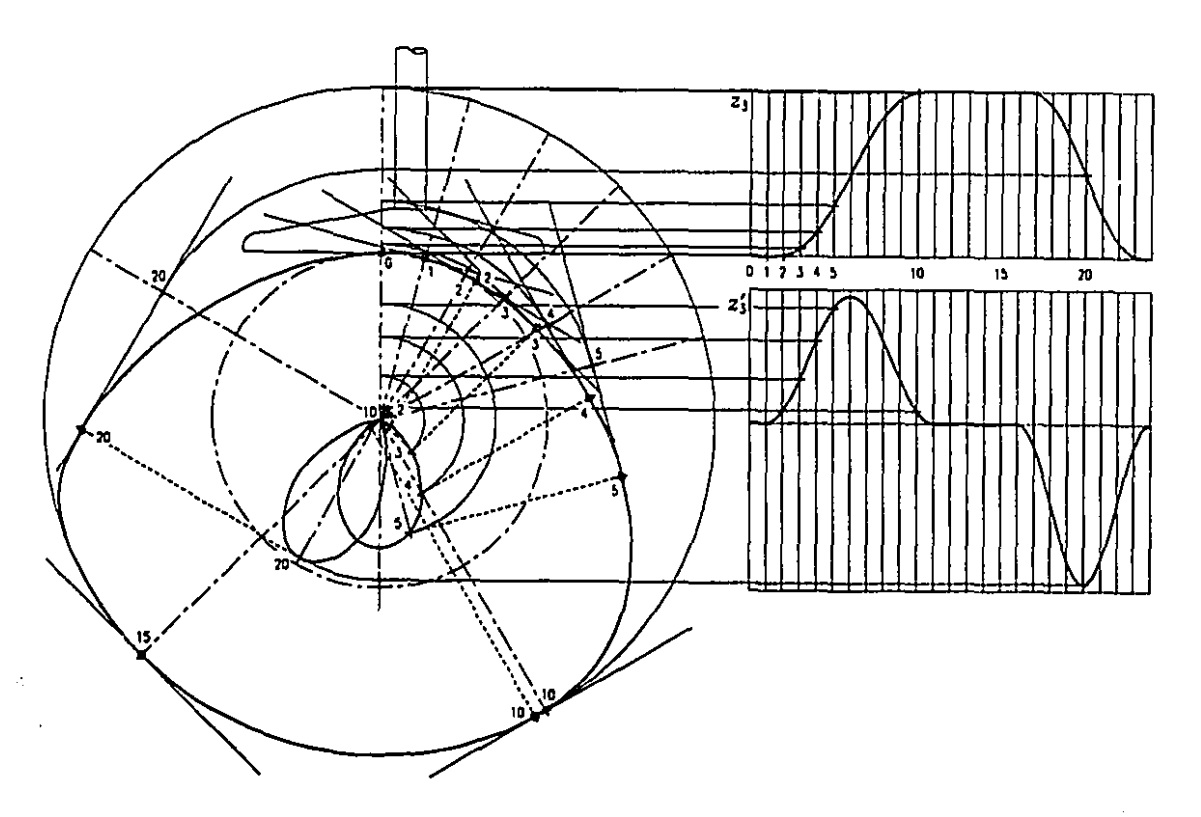


Figure E.15 Cam profile of the RHHP mechanism